


## AN ABSTRACT OF THE THESIS OF

Rudolph Stanley Paige for the Master of Science degree in  
Mechanical Engineering.

Date thesis is presented 3 May 1963

Title Effects of Gamma Radiation on Selected Single Crystals

Abstract approved 

Single crystals of Potassium Aluminum Sulfate Dodecahydrate (Potash Alum),  $\text{KAl}(\text{SO}_4)_2 \cdot 12\text{H}_2\text{O}$ , Potassium Ferricyanide (Red Prussiate of Potash),  $\text{K}_3\text{Fe}(\text{CN})_6$ , Potassium Sodium Tartrate Tetrahydrate (Rochelle Salt),  $\text{KNaC}_4\text{H}_4\text{O}_6 \cdot 4\text{H}_2\text{O}$ , Sodium Nitrate,  $\text{NaNO}_3$ , Potassium Chromium Sulfate Dodecahydrate (Chrome Alum),  $\text{KCr}(\text{SO}_4)_2 \cdot 12\text{H}_2\text{O}$ , and Sodium Chlorate,  $\text{NaClO}_3$ , were grown by the author and irradiated with  $\text{Co}^{60}$  gamma rays up to  $1.06 \times 10^9$  roentgens at  $14^\circ\text{C}$ . X-ray diffraction patterns were photographed using the single crystal Laue technique and Debye-Scherrer powder method before and after the specimens were irradiated. The Rochelle salt single crystal was decomposed by the gamma-rays which prevented post-gamma irradiation research on this sample. Spectrophotometer absorption recordings were made of all single crystals, except the Rochelle Salt, before and after gamma ray exposure. The single crystal of  $\text{NaClO}_3$  was checked for ionic conductivity as a function of temperature from liquid nitrogen temperature to room temperature

before and after irradiation on a vibrating reed electrometer. A variety of effects were noted in the specimens varying from decomposition to no observable changes.

The Potassium Sodium Tartrate Tetrahydrate single crystal decomposed, changed color and produced a different powder diffraction pattern. All of the single crystals specimens, except the Rochelle Salt and the Potash Alum, showed new color center development. Spectrophotometer absorption spectra disclosed new absorption peaks, absorption band broadening and in some samples bleaching of absorption peaks after gamma irradiation. The  $\text{NaClO}_3$  and  $\text{NaNO}_3$  Laue transmission x-ray patterns showed asterism caused by lattice disregistry within the single crystals. Powder patterns of the irradiated specimens show extra reflections and intensity variations in Bragg angle peaks. It is probable these extra reflections result from the scattering contributions from vacancies and interstitials located at preferred positions within the lattice.

Niether the powder sample nor the single crystal specimen of Potassium Aluminum Sulfate Dodecahydrate changed in color, shape, absorption spectra, lattice structure, x-ray patterns, or physical appearance. The absence of any effect in this specimen is both remarkable and difficult to explain. This specimen appears to be an exception to predictable damage expected in essentially ionic solids.

EFFECTS OF GAMMA RADIATION  
ON  
SELECTED SINGLE CRYSTALS

by

RUDOLPH STANLEY PAIGE

A THESIS

submitted to

OREGON STATE UNIVERSITY

in partial fulfillment of  
the requirements for the  
degree of

MASTER OF SCIENCE

June 1963

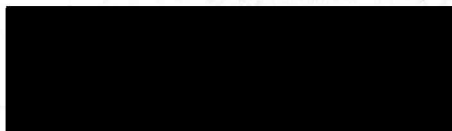
APPROVED:



---

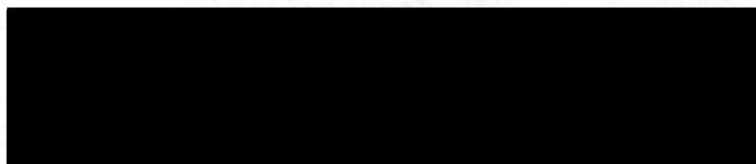
Associate Professor of Mechanical Engineering

In Charge of Major



---

Head of Department of Mechanical and Industrial  
Engineering



---

Dean of Graduate School

Date thesis is presented 3 May, 1963

Typed by Joan Shaw



## ACKNOWLEDGMENT

No serious undertaking can be accomplished by an individual without the encouragement, assistance, and understanding of others with whom he associates. Since I believe this to be true, I wish to take this opportunity to recognize the faculty members at Oregon State University and the staff members of the radiation facility at the Albany Division of the Bureau of Mines.

I wish to make special mention of Professor Edward A. Daly, whose unselfish guidance proved invaluable, Professor Olaf G. Paasche, whose many private discussions brought me new understanding of the field of materials, Professor Charles O. Heath, whose early encouragement and understanding gave me that extra motivation which we all seek when pressures are greatest, and of Dr. Allen B. Scott and Dr. Masamitsu Hirai, whose intimate knowledge and widely recognized research of color centers provided personal guidance and laboratory assistance for this research. Mr. Howard Poppleton and Mr. Steven Hill of the Bureau of Mines are hereby gratefully acknowledged and thanked for their assistance during irradiation of the specimens.

None of my studies nor this thesis would have been accomplished without the incomparable patience, understanding, kindness, tolerance, and personal assistance of my wife, Gerie. I humbly acknowledge and thank her for her continued encouragement to me and the

typing of many papers, including this thesis.

My thanks, also, to Joan Shaw, for the preparation of the final draft.

EFFECTS OF GAMMA RADIATION ON  
SELECTED SINGLE CRYSTALS

by

Rudolph Stanley Paige

TABLE OF CONTENTS

|      |  |     |
|------|--|-----|
| I.   | Introduction   | 1   |
| II.  | Current Concepts of the Effects of Gamma Radiation<br>in Ionic Solids  | 4   |
| III. | Gamma Irradiation Damage in Ionic Crystals                             | 9   |
|      | A. Production of Color Centers in Alkali Halides                       | 9   |
|      | B. Radiation Effects on Ionic Conductivity                             | 20  |
|      | C. Radiation Effects Observable by X-Ray Diffraction                   | 22  |
|      | D. Irradiation of Other Salts  | 27  |
| IV.  | Materials and Methods  | 29  |
|      | A. Crystal Selection and Growth  | 29  |
|      | B. Optical Absorption Spectroscopy and X-Ray<br>Diffraction Procedures | 42  |
|      | C. Gamma Irradiation Procedures and Facilities                         | 54  |
|      | D. Gamma-Ray Dosimetry   | 59  |
| V.   | Experimental Results and Specific Conclusions                          | 62  |
|      | A. Irradiation Effects on Potassium Sodium<br>Tartrate Tetrahydrate    | 63  |
|      | B. Irradiation Effects on Potassium Chromium<br>Sulfate Dodecahydrate  | 68  |
|      | C. Irradiation Effects on Sodium Chlorate                              | 77  |
|      | D. Irradiation Effects on Sodium Nitrate                               | 87  |
|      | E. Irradiation Effects on Potassium Ferricyanide                       | 95  |
|      | F. Irradiation Effects on Potassium Aluminum<br>Sulfate Dodecahydrate  | 98  |
| VI.  | General Summary  | 107 |
| VII. | Bibliography   | 111 |

## FIGURES

|     |   |     |
|-----|---|-----|
| 1.  | Models of Color Centers   | 15  |
| 2.  | (001) Plane of $\text{KNaC}_4\text{H}_4\text{O}_6 \cdot 4\text{H}_2\text{O}$  | 37  |
| 3.  | Cell Structure of $\text{NaClO}_3$  | 40a |
| 4.  | Gamma Irradiation Cell  | 56  |
| 5.  | Cobalt-60 Capsule Arrangement for Specimen Irradiation  | 58  |
| 6.  | Powder Diffraction Patterns of $\text{KNaC}_4\text{H}_4\text{O}_6 \cdot 4\text{H}_2\text{O}$<br>before and after Irradiation                      | 67  |
| 7.  | Optical Absorption Spectrum of Single Crystal of<br>$\text{KCr}(\text{SO}_4)_2 \cdot 12\text{H}_2\text{O}$ (Unirradiated)                         | 69  |
| 8.  | Optical Absorption Spectrum of Single Crystal of<br>$\text{KCr}(\text{SO}_4)_2 \cdot 12\text{H}_2\text{O}$ (Irradiated)                           | 71  |
| 9.  | Laue X-Ray Transmission Pattern of Single Crystal of<br>$\text{KCr}(\text{SO}_4)_2 \cdot 12\text{H}_2\text{O}$ before and after Gamma Irradiation | 72  |
| 10. | Powder Patterns of $\text{KCr}(\text{SO}_4)_2 \cdot 12\text{H}_2\text{O}$ before and after<br>Gamma Irradiation                                   | 73  |
| 11. | Optical Absorption Spectrum of Single Crystal of<br>$\text{NaClO}_3$ (Unirradiated)   | 78  |
| 12. | Optical Absorption Spectrum of Single Crystal of<br>$\text{NaClO}_3$ (Irradiated)   | 80  |
| 13. | Experimental Arrangement of Ionic Conductivity<br>Measurement   | 81  |
| 14. | Laue X-Ray Transmission Pattern of Single Crystal of<br>$\text{NaClO}_3$  | 84  |
| 15. | Powder Diffraction Patterns of $\text{NaClO}_3$ before and<br>after Irradiation   | 85  |

|     |  |     |
|-----|--|-----|
| 16. | Optical Absorption Spectrum of Single Crystal of $\text{NaNO}_3$ (Unirradiated)  | 88  |
| 17. | Optical Absorption Spectrum of Single Crystal of $\text{NaNO}_3$ (Irradiated)  | 89  |
| 18. | Laue X-Ray Transmission Pattern of Single Crystal of $\text{NaNO}_3$   | 91  |
| 19. | Powder Diffraction Patterns of $\text{NaNO}_3$ before and after Irradiation  | 93  |
| 20. | Optical Absorption Spectrum of Single Crystal of $\text{K}_3\text{Fe}(\text{CN})_6$  | 96  |
| 21. | Optical Absorption Spectrum of Single Crystal of $\text{K}_3\text{Fe}(\text{CN})_6$ (Irradiated)   | 97  |
| 22. | Laue X-Ray Transmission Pattern of Single Crystal of $\text{K}_3(\text{Fe}(\text{CN})_6)$ before and after Gamma Irradiation                   | 99  |
| 23. | Powder Diffraction Pattern of $\text{K}_3\text{Fe}(\text{CN})_6$ before and after Irradiation  | 101 |
| 24. | Optical Absorption Spectrum of Single Crystal of $\text{KAl}(\text{SO}_4)_2 \cdot 12\text{H}_2\text{O}$ (Unirradiated and Irradiated)          | 103 |
| 25. | Laue-X-Ray Transmission Pattern of Single Crystal of $\text{KAl}(\text{SO}_4)_2 \cdot 12\text{H}_2\text{O}$ before and after Gamma Irradiation | 104 |
| 26. | Powder Diffraction Patterns of $\text{KAl}(\text{SO}_4)_2 \cdot 12\text{H}_2\text{O}$ before and after Irradiation                             | 106 |



# TABLES

|       |   |     |
|-------|---|-----|
| I.    | Notations for Color Centers   | 14  |
| II.   | Positions and Parameters of Atoms in $\text{KAl}(\text{SO}_4)_2 \cdot 12\text{H}_2\text{O}$                                 | 34  |
| III.  | Positions and Parameters of Atoms in $\text{KNaC}_4\text{H}_4\text{O}_6 \cdot 4\text{H}_2\text{O}$                          | 38  |
| IV.   | Anion-Oxygen Bond Distance in $\text{KNaC}_4\text{H}_4\text{O}_6 \cdot 4\text{H}_2\text{O}$                                 | 39  |
| V.    | Electromagnetic Spectrum  | 44  |
| VI.   | X-Ray Powder Pattern Laboratory Data for Unirradiated $\text{KNaC}_4\text{H}_4\text{O}_6 \cdot 4\text{H}_2\text{O}$         | 65  |
| VII.  | X-Ray Powder Pattern Laboratory Data for Irradiated $\text{KNaC}_4\text{H}_4\text{O}_6 \cdot 4\text{H}_2\text{O}$           | 66  |
| VIII. | X-Ray Powder Pattern Laboratory Data for Unirradiated $\text{KCr}(\text{SO}_4)_2 \cdot 12\text{H}_2\text{O}$                | 74  |
| IX.   | X-Ray Powder Pattern Laboratory Data for Irradiated $\text{KCr}(\text{SO}_4)_2 \cdot 12\text{H}_2\text{O}$                  | 75  |
| X.    | X-Ray Powder Pattern Laboratory Data for Irradiated and Irradiated $\text{NaClO}_3$   | 86  |
| XI.   | X-Ray Powder Pattern Laboratory Data for Unirradiated and Irradiated $\text{NaNO}_3$  | 94  |
| XII.  | X-Ray Powder Pattern Laboratory Data for Unirradiated and Irradiated $\text{K}_3\text{Fe}(\text{CN})_6$                     | 100 |
| XIII. | X-Ray Powder Pattern Laboratory Data for Unirradiated and Irradiated $\text{KAl}(\text{SO}_4)_2 \cdot 12\text{H}_2\text{O}$ | 105 |

# EFFECTS OF GAMMA RADIATION ON

## SELECTED SINGLE CRYSTALS

### SECTION I

#### INTRODUCTION

The environmental conditions are to a large extent the controlling factor for the behavior of materials. A new and dynamic environment has been introduced by nuclear energy and space research, which has prompted a fresh approach to the study of the effects of nuclear radiation on materials. The interest in the effects of radiation on materials has captured the imagination and interest of the professionals as well as the laymen. Nuclear engineers, materials engineers, metallurgists, mechanical engineers, physicists and chemists are concerned with the phenomena associated with irradiation of materials by neutrons, gamma rays, fission fragments, alpha particles or other energetic particles for scientific and practical interests. Not only must scientists and engineers study the theoretical phenomena but he must also be prepared to apply theory to the practical application of material design and selection. Radiation damage has imposed an additional design parameter on the selection and use of materials in nuclear energy environments. This more imposing discovery brought about by the studies of the mechanism of radiation effects in solids focuses our attention on the uses

of radiation as a powerful tool to increase our knowledge of the physics of solids. New processes have been uncovered for the preparation of polymeric materials of commercial importance. Many of the studies of the effects of radiation are pointing the way to an entirely new field of organic synthesis. However, much of the information concerning the effects of radiation upon materials has been relatively unknown until after the 1955 Geneva Conference on the Peaceful Uses of Atomic Energy. It was this conference which gave the impetus for the release of information from AEC Laboratories, universities and other research institutions through unclassified scientific literature.

Much of the research up to date has centered upon the materials which have an immediate military or commercial value in the construction and operation of nuclear reactor, space vehicles, research laboratories or chemical processing facilities. Radiation effects on some materials have received limited research because the materials do not enjoy current commercial use.

One group of materials which deserves more research are the ionic solids which find use in high temperature ceramic materials. Many researchers have investigated the production of color centers in alkali halides. One method of producing these color centers is by exposing these crystals to electromagnetic radiation. This material is exceedingly simple in structure, from the standpoint of both lattice

and electronic systems. Moreover, the single crystals can be obtained with comparative ease in a state of purity and reasonable perfection. The simplicity of these crystal specimens provided an ideal material for study and research. The probability of understanding the phenomenon of the properties of this monovalent structure is both intriguing and inviting. Intensive interest has been stimulated by efforts of Pohl and Seitz (49, p. 459-461) through their pioneering research and reporting of the color center phenomena in alkali halides. The early work of these pioneers laid a solid foundation for other scientists to build upon. The effects noted in alkali halides by electromagnetic radiation was ideal to evaluate and interpret radiation effects in other material. It is the intent of this thesis to expand, in a small way, the knowledge gained from the alkali halide and project the effects noted in them to more complex ionic crystals. It is the primary purpose of this research to provide a broad survey of six different essentially ionic crystals. It is hoped this thesis will encourage others to narrow their research to provide a more thorough understanding of the properties of these materials. Not only is knowledge of this type necessary from a scientific viewpoint but also it is imperative to provide engineers with a practical knowledge which can be used in our space programs, nuclear power facilities, and our ever-growing technological industries.

## SECTION II

CURRENT CONCEPTS OF THE EFFECTS OF GAMMA RADIATION  
IN IONIC SOLIDS

Gamma-rays and x-rays, are highly penetrating electromagnetic radiation which produce ionization in all solids. It is instructive to note how these rays behave in their passage through matter. In their nomadic route through matter they lose their energy in three primary ways. The first, which is most significant for gamma rays of low energy and for absorbers of high atomic weight, is the photoelectric effect, whereby electrons are ejected from atoms or molecules encountered by the radiation. This process is of considerable interest in ionic crystal because ionic structures rely on their electronic stability to maintain their properties. The ejection of an electron from an atom position disturbs this equilibrium and starts a variety of latent potential forces into kinetic activity.

If  $\underline{E}$  is the energy of a photon, then in a photoelectric encounter an amount of energy  $\underline{P}$ , equal to the binding energy of the electron in the atom, will be required to remove the electron. The whole of the remaining energy which is  $E - P$  will be carried off by the electron in the form of kinetic energy. Using this hypothesis, Einstein deduced his photoelectric law:

$$\frac{1}{2} mv^2 = h\nu - P$$



This law states that the maximum kinetic energy  $\frac{1}{2}mv^2$  of the emitted electron is equal to the energy  $h\nu$  of the incident light quantum minus a quantity  $\underline{P}$  which represents the amount of work needed by the electron to get free of the atom. This law explains the experimental results which were observed when light rays interact with a metallic material. A summary of these results are as follows:

1. If a photon of a given frequency can liberate electrons from an atom, the electron current is proportional to the intensity of the light.

2. For a given metallic material, there is a smallest value of the frequency for which the incident light can liberate electrons; light of smaller frequency cannot eject electrons no matter how long it interacts with the material or how great is its intensity.

3. Light of frequency greater than this critical value causes the immediate emission of electrons; the time interval between the incidence of the light on the metallic material and the appearance of electrons is not more than  $3 \times 10^{-9}$  sec.

4. The maximum kinetic energy of the emitted electron is a linear function of the frequency of the light which causes their emission and is independent of the intensity of the incident light.

Though the word "light" has been used a more general work "photon" is applicable. The ejection of an electron by any electromagnetic ray, x-ray or gamma ray included, has the same general

validity. In this process, the photon is eliminated and results in a true absorption event.

The second major factor contributing to the loss of energy and absorption of gamma rays is the compton effect discovered by the American physicist A. H. Compton in 1923. He found that when electromagnetic waves fall on a material of low atomic weight the scattered radiation contains some rays of longer wave length than the incident rays. Since the scattering was produced by the electrons present in the atom it was concluded the interaction caused the loss in electromagnetic ray energy. The main features of compton scattering can be found in many references (24, p. 322-341). However, it will be useful to state some of the results obtained from them. The energy lost by a photon in a single compton scattering process can be obtained from the following equation.

$$\lambda - \lambda_0 = \frac{h}{m_0 c} (1 - \cos \phi)$$

In this equation  $\lambda_0$  is the wave length of the photon before collision,

$\lambda$  is the wave length after collision, and  $\phi$  is the angle between the initial and final direction of the photon. By substituting  $\lambda = \frac{c}{\nu}$ , multiply by Planck's constant  $h$  and by mathematical manipulation of the preceding equation, we can produce an equation which gives the energy of the scattered photon in terms of the initial energy and the scattering angle, namely,

$$h\nu = \frac{h\nu_0}{\frac{1 + h\nu_0}{m_0 c^2} (1 - \cos \phi)}$$

The recoiling electron has a kinetic energy given by

$$\begin{aligned} T &= h\nu_0 - h\nu \\ &= h\nu_0 (1 - \cos \phi) \frac{\frac{h\nu_0}{m_0 c^2}}{1 + \frac{h\nu_0}{m_0 c^2} (1 - \cos \phi)} \end{aligned}$$

The electron has the maximum kinetic energy when  $\cos \phi = -1$  or  $\phi = 180^\circ$ , the photon is scattered directly backward. The electron receives the least energy in a grazing collision.

It can be seen by these equations the incoming electromagnetic wave loses energy and thereby becomes susceptible to total absorption by further interactions with the material. The Compton scattering is not a pure absorption process alone but contributes to the scattering of the initial beam and reduces the final magnitude of a transmitted columnated beam.

The Compton effect plays a major role when the absorber is a material of high atomic number and the energy of the radiation is neither too high nor too low. Increase of the atomic number of the absorber increases the extent of absorption caused by the Compton effect.

The third popularly recognized electromagnetic ray interaction with matter is the formation of the positron-electron pair. For gamma rays of higher energy the photoelectric and Compton effects are not so important for their absorption, especially in elements of high atomic weight, as is the formation of positron-electron pairs. This

process requires that the electromagnetic rays possess a minimum energy of 1.02 Mev, and hence it can have no influence on radiation of less energy. As the energy of the gamma ray increases above the 1.02 Mev minimum pair production effect increases rapidly. The probability of pair formation increases with the square of the atomic number of the absorber. For absorbers of high atomic weight and gamma rays of high energy, pair production is the main cause of energy loss. The formulas for the probability of pair formation are more complicated than those for photoelectric absorption and Compton scattering and will not be written here.

The three processes mentioned above are the major mechanisms for the absorption of gamma rays by matter. The basic property of the absorption of gamma rays is the exponential decrease in the intensity of radiation as a homogeneous beam of gamma radiation passes through a thin slab of matter. When a beam of gamma rays of intensity  $I_0$  is incident on a slab of thickness  $\Delta X$ , the change in intensity of the beam as it passes through the slab is proportional to the thickness and to the incident intensity:

$$\Delta I = - I_0 \mu \Delta X$$

where the proportionality constant  $\mu$  is called the absorption coefficient. If the gamma ray photons all have the same energy,  $\mu$  is independent of  $X$ , and the integration of the previous equation yields

$$I/I_0 = e^{-\mu X}$$



This equation gives the intensity of radiation I after a beam of initial intensity  $I_0$  has traversed a thickness X of a given material. It should be noted these equations which describe the absorption of gamma radiation are the same as those for x-ray and those which describe light rays in the absorption spectroscopy mentioned in a later section. This result is not surprising because all of these rays are electromagnetic radiation. The discussion of the electromagnetic spectrum and the overlap of the arbitrary regions will be delayed until visible region absorption spectroscopy is discussed.

The three processes just described result either in the ejection of an electron or the formation of a positron-electron pair carrying a considerable amount of energy. It is these free electrons which it is believed cause the formation of color centers in ionic crystals.

### SECTION III

#### GAMMA IRRADIATION DAMAGE IN IONIC CRYSTALS

##### A. Production of Color Centers In Alkali Halides

Gamma-rays produce ionization in all solids, and this is their most important effect. During the ionization process, primary electrons are produced and cause further ionization and excitation in the medium as a secondary process. Atomic displacements and decomposition of molecules are important results of irradiation, because of



interaction between the energetic electrons and atoms. Atomic displacements in crystalline materials produce interstitials and vacancies in the lattice and have important consequences on the properties of the crystals. In metals, ionization produced by radiation is very rapidly neutralized by the conduction electrons, and no structural changes result from this process. In ionic crystals there is no so-called "electron cloud" as in metallic solids to neutralize the ionization caused by electromagnetic radiation.

Varley (60, p. 130-143), Seitz (51, p. 7-94) and numerous other researchers have made extensive investigations of the alkali halide crystals. We will use the knowledge gained from the study of alkali halide to compare the effects which occurred in the semi-ionic crystals used for this thesis. Although many properties of ionic crystals are appreciably structure sensitive and are influenced significantly by lattice defects, complications associated with the influence of energetic photons of these properties make it difficult to separate for isolated examination those effects specifically caused by fast particles such as neutrons, betas, or photons.

Effects of high energy gamma rays ( $>1$  Mev) are similar to that of fast electrons. On the other hand, effects of high energy particle radiation are similar to those of low energy electromagnetic radiation (37, p. 29).

Alkali halides crystallize in simple structures of high symmetry

since the packing of ions in these crystals is dictated almost entirely by the requirements of electrostatic forces and the relative size of the ions. This type of binding leads to considerably greater freedom of lattice defects which provide no directional bonds to be ruptured and reformed when these entities migrate. Consequently, these crystals may have extensive disorder without showing very large structural effects. The effects of disorder are moderated to a large extent by clustering and recombination of defects during and after irradiation provided this can take place near or above room temperature. Moreover, lattice strains associated with defects can be compensated by relaxation of neighboring atoms or ions.

The alkali halides are insulators with an energy gap of the order of 10 ev. Therefore their optical spectra, corresponding to the transition of an electron from the valence band to the conduction band, lay in the ultraviolet wave length. One or more peaks due to absorption by excitons are found on the long wave length side of the ionization levels. The exciton bands correspond to the transition of a halide ion to an excited state, with the excitation traveling through the crystal. When alkali halide crystals are exposed to x-rays or gamma rays, or are bombarded by electrons or heavy particles, new absorption bands appear. Some of these bands are due to holes or electrons trapped at imperfections in the crystal and are usually referred to as color center bands. The color centers containing trapped electrons are called

electron-excess color centers, while those containing trapped holes are hole-excess color centers. In addition to bombardment there are other methods to color alkali halide crystals. They may be colored by adding suitable chemical impurities, such as transition element ions having excited energy levels separated from the ground state by an optical frequency. It is also possible to color the crystals by introducing a stoichiometric excess of the cation or anions.

When the crystal is colored we say it possesses color centers. Actually a color center is a lattice defect which absorbs light. The simplest type of color center is one called an F center. R. W. Pohl named these from the German Farbzentren (color center). From the foregoing remarks it becomes self-evident we may use optical absorption spectra as a powerful tool to measure the production of lattice defects in ionic crystals which may be produced by irradiation. As this thesis continues, we will use this knowledge to study gamma ray damage in more complex ionic specimens. However, to return to alkali halides, it should be noted many types of centers other than F centers have been reported and to some extent their nature and composition understood. It is both instructive and practical to discuss the F center in detail while an introductory knowledge of the other models is adequate for our query. F centers are believed to be formed by electromagnetic rays when the photon frees an electron from one of the inner shells of an atom of the lattice and subsequently, this electron

becomes trapped in a lattice. The most apparent trapping positions are the vacancies in the negative ion lattice, according to de Boer (52, p. 133). It has been concluded from investigations of photoconductivity that such is the case. Seitz concludes the F centers are electrons trapped in vacant halogen-ions sites. In addition to this simple model, there are other possible electron traps in colored alkali halide crystals. They can be interstitial ions, vacancies, clusters of interstitial ions or of vacancies or both, impurities, and possibly dislocations. The center, which includes both the trap and trapped electron, may be electrically neutral or it may be charged. It is of practical value to have a mental image of the more common color center models currently accepted, as shown by Table I and Figure 1. (52, p. 133).

The notations used in Table I give all the physical information which usually defines the physical model; namely, the charge of the ions which are missing and the lattice sites from which they have been removed, the kind and number of trapped particles, and the charge and number of the added ions. The additional ions are assumed to fit somehow into the existing vacancies, if any. If no vacancies exist, the added ions occupy interstitial sites. The information is presented in the following table, under the title of "Designation:" (missing ions/trapped or missing particles/added ions).



Table I

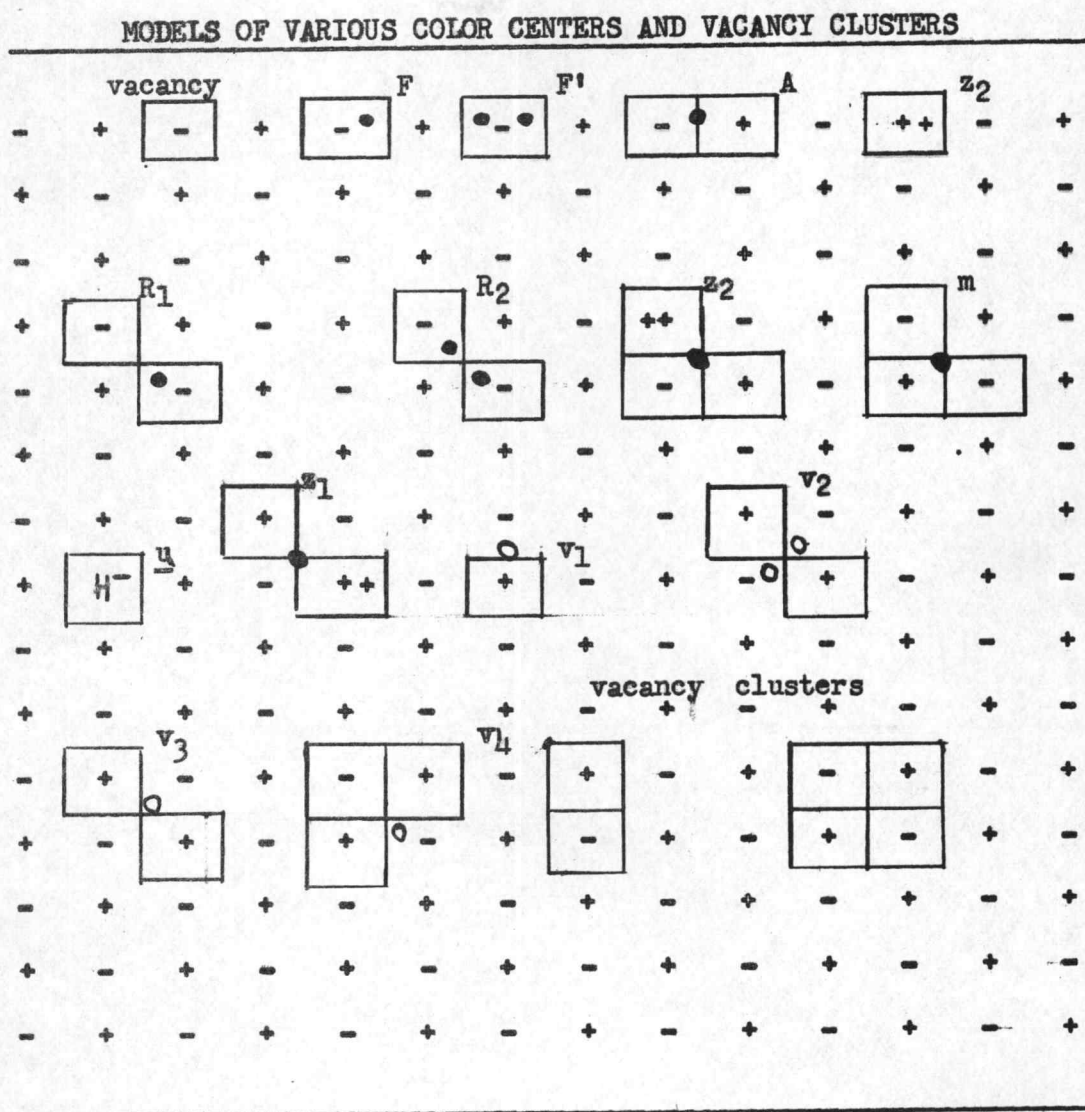
## NOTATION FOR THE MORE COMMON COLOR CENTERS (52)

| Designation                          | Usual Name  | Absorption<br>bands<br>attributed to it |
|--------------------------------------|---|---|
| ( - / e / )                          | de Boer or vacancy<br>model of $\overline{F}$ center (50) | F                                       |
| ( - / 2d / )                         | F' center (50)  | F'                                      |
| ( $\overline{-}$ - / e / )           | $F_2$ center (19)   | $R_1$ (?)                               |
| ( $\overline{-}$ - / 2e / )          | $F_2$ center (19)   | $R_2$                                   |
| ( $\overline{+}$ - / e / )           | M center (Seitz) (50)                                     | $R_1$ (?)<br>M (?)                      |
| ( / e / P )                          | Interstitial H atom (11)                                  | $U_2$                                   |
| ( / e / + )                          | Interstitial model of<br>$\overline{F}$ center (50)       | F (?)                                   |
| ( + / e / $M^{++}$ )                 | $Z_1$ center (Seitz) (50)                                 | $Z_1$ (?)                               |
| ( $\overline{+}$ + / e / $M^{++}$ )  | $Z_2$ center (Seitz) (50)                                 | $Z_2$ (?)                               |
| ( $\overline{+}$ + / 2e / $M^{++}$ ) | $Z_3$ center (Seitz) (50)                                 | $Z_3$ (?)                               |
| ( / 2e / P )                         | Interstitial hydride ion (11)                             | $U_1$                                   |
| ( / 2e / P )                         | Substitutional hydride<br>ion (11)                        | U                                       |
| ( + / -e / )                         | $V_1$ center (Seitz) (50)                                 | $V_1$                                   |
| ( $\overline{+}$ + / -2e / )         | $V_2$ center (Seitz) (50)                                 | $V_2$                                   |
| ( $\overline{+}$ + / -e / )          | $V_3$ center (Seitz) (50)                                 | $V_3$                                   |
| ( $\overline{+}$ + / -e / )          | $V_4$ center (Seitz) (50)                                 | $V_4$                                   |

KEY: P, proton e, electron -, halide ion; +, alkali ion;  
 $M^{++}$ , doubly charged positive ion; (?), assignment in doubt.



Figure 1



As it is believed that the excess alkali atoms fit into an alkali halide crystal in normal alkali ion lattice positions, a corresponding number of negative ion vacancies must be created in the process. A negative ion vacancy in an otherwise periodic lattice behaves electrostatically like a positive charge, so that an electron moving about a negative ion vacancy resembles qualitatively a hydrogen atom. We identify an F center with an electron bound to a negative ion vacancy, the electron being provided by the ionization of an alkali atom on entering the lattice.

The F band absorption is characteristic of the crystal and not of the alkali metal used in the vapor; that is, the band in Potassium Chloride is the same whether the crystal is heated in Potassium or Sodium vapor.

It is found by chemical analysis that crystals colored additively contain a stoichiometric excess of alkali metal atoms, the excess commonly being of the order of  $10^{-16}$  to  $10^{-19}$  per cubic centimeter. It is found further that the integrated absorption under the F band corresponds quantitatively to that expected theoretically based on the known amount of excess alkali metal.

Colored crystals are less dense than uncolored crystals which is in agreement with the elementary picture that the introduction of vacancies should lower the density. This would weigh against an interpretation of the F center as an electron bound to an interstitial

alkali ion.

Crystals with F centers can be bleached by illumination with light absorbed in the F band, and illumination in any part of the band cleaches the whole band. This proves that the F centers in any crystal are all similar. The bleaching is attributed to the ionization of the F center and is accompanied by photoconductivity; that is, the crystal becomes conducting during irradiation. The width of the band may be accounted for by the thermal motion of the ions.

The  $F'$  centers are produced by irradiating, at not too high a temperature, a crystal already colored by F centers with light that is absorbed by the F centers. A broad band on the red side of the F band is produced in this way, and the intensity of the F band is decreased to a corresponding extent. The new band is called the  $F'$  band. It is found that two F centers are destroyed for each incident quantum, suggesting that one F center is ionized by the incident radiation and the electron thus liberated is then captured by another F center to form an  $F'$  center consisting of an anion vacancy with two bound electrons. It is also found that the displacement range of the photoelectrons is inversely proportional to the concentration of F centers; this fact supports the assumption that the photoelectrons are trapped by F centers to produce  $F'$  centers. It is found further that  $F'$  centers may be destroyed by irradiating the crystal with light absorbed by the  $F'$  band, and the original F center appear again in the process.



If crystals containing F centers are irradiated with light in the F band, there is a suitable temperature range in which coagulation occurs. The final products of the coagulation are colloidal particles of alkali metal. Some products of coagulation in the  $R_1$ ,  $R_2$ , and  $M$  bands lying in the red and infrared have been reported by A. B. Scott, et al. (47, 48, 57).

It is a natural thought that by heating a crystal in halogen vapor to introduce a stoichiometric excess of halogen it should be possible to produce a whole new series of centers which are the antimorphs of the centers produced by excess alkali metal atoms. The new centers should contain holes instead of electrons, because a halogen atom has a deficit of one electron with respect to the ion; the hole will be attracted by a cation vacancy just as an excess electron is attracted to an anion vacancy.

A series of absorption bands in the ultraviolet region is introduced in this way; the bands are known as V bands.  $V_1$  is assumed to be the antimorph of the F center.  $V_1$ ,  $V_3$  are antimorphs of the R centers and  $V_4$  to antimorph of the M center. The identification of the  $V_1$  center above with the  $V_1$  band is uncertain, as the spin resonance results of Kaenzig (22) suggest that a center having the symmetry of the  $V_3$  center produces the  $V_1$  band.

The V bands may also be produced by x-ray or particle irradiation. It is clear from consideration of charge conservation that some

type of hole center must be produced to accompany the F centers created by irradiation.

The actual mechanism of defect production by photons is not clearly understood. Setiz's model essentially suggests the following sequence of events. Excitons and electrons and holes are produced by the absorption of x-rays which later recombine and give up their energy in disturbed regions in the crystal. If this energy release takes place in the vicinity of a dislocation jog, then vacancies of both signs may "boil off" from the lattice discontinuities.

Studies of extensive exposure of color alkali halides to x-ray produces a greater concentration of F centers than can be accounted for by the concentration of anion vacancies initially present (42). Also, careful density measurements show x-radiation produces a small but measurable density decrease. Exposure to x- and gamma-radiation markedly changes mechanical and plastic properties of these materials (12). These observations reinforce the theory proposed by Seitz that defect introduction is caused by the electromagnetic radiation.

More recently Varley (59) has proposed a theory of multiple ionization to explain defect generation. He theorizes briefly as follows. If an anion is stripped of two or more electrons by an energetic photon, as in an Auger Cascade, then it will be in a highly unstable electronic state by virtue of the crystal potential. Moreover, if the time required for the anion to recapture its electrons is long compared to its



vibrational period (approximately  $10^{-13}$  seconds), then it will be forced from its equilibrium position into an interstitial site from there it can meander through the crystal a neutron atom. As long as the ejected atom remains in an interstitial site it will not have an aggressive tendency to attract another electron. The vacant lattice site may capture an electron for form an F center. At sufficiently high temperature the interstitial halogen may migrate through the lattice until it recombines with the F center or until it becomes trapped at some lattice discontinuity such as a dislocation or in a cation vacancy. The halogen atom in essence acts as a positive hole. In summary, the Varley mechanism requires:

1. the lattice be largely ionic,
2. the cross section for multiple ionization be sufficiently large,
3. the recombination time for electrons and stripped atoms be long enough to allow ejection (approximately  $10^{-13}$  seconds),
4. the ejected atom go far enough to be stable against immediate return upon neutralization.

Although Varley's original theory was constructed upon purely univalent ionic solids, such as the alkali halides, it is plausible these conditions could be satisfied in many materials.

#### B. Radiation Effects On Conductivity

The electrical conductivity in the alkali halides is ionic and

occurs by the motion of positive ion vacancies. At low temperatures in extrinsic or structure sensitive range the conductivity is a function of cation vacancies, either "frozen in" the crystal or as a result of divalent cation impurity. At high temperatures on the other hand, the conductivity is intrinsic, i. e., it depends on the concentration of cation vacancies generated thermally by an equilibrium process which is independent of the past history of the specimen. Since it has been theorized that high energy radiation causes more defects we could expect a conductivity increase in the extrinsic range to be the primary radiation effect. However, this is not the case. Mapother (29) has reported the cation diffusion coefficient in the extrinsic range has decreased by a factor of three in a NaCl crystal exposed to x-rays. This same behavior has been reported by others (51, 54, 2, 8) in both NaCl and KCl. The first experiments which showed the influence of nuclear irradiation were reported by Nelson, Proull and Caswell (38). They concluded that gamma ray irradiation decreased the conductivity while long neutron irradiation increases the conductivity. Several suggestions have been proposed by Seitz and Sproull to explain decrease in conductivity. They suggest that cation vacancies capture the positive holes thereby neutralizing them and make them unavailable for charge transport. However, these explanations do not appear to be conclusive according to Billington (3, p. 270-279) who points out Mapother's observation that x-irradiation decreases the cation

diffusion coefficient which implies the V center is less mobile than the unoccupied vacancy. Billington further suggests there are two objections to this interpretation. First simple V centers are believed to be unstable at room temperature in both KCl and NaCl and, secondly, most of the decrease apparently occurs as a result of relaxation after removing the ionizing radiation. At this time, there is no clear explanation for the conductivity in ionic crystals due to irradiation. This points out the need for aggressive research in this area to provide a reasonable interpretation of these phenomena.

It is desirable at this point to mention that the changes and differences observed in alkali halides have also been noted in other crystals, some of which have combined covalent and ionic bonding. For example, the optical behavior of MgO has been reported by Boyd et al. and by Nelson and Pringsheim (3, p. 279-283). Levy and Dienes (27) have investigated Corundum ( $\alpha$ -Al<sub>2</sub>O<sub>3</sub> or sapphire). Extensive investigations have been conducted on fused silica, quartz, and diamonds (17, 46, 13, 34-36, 39, 40, 26-28).

#### C. Radiation Effects Observable by X-Ray Diffraction (9)

One of the earliest research tools used to evaluate the effects of irradiation on crystalline materials was x-ray diffraction. Much of the understanding gained by the author of the effects of irradiation was as a direct result of the study of diffraction photographs of single

crystals and powder specimens which were used for this thesis research. Lattice changes or imperfections can be identified by displaced, weakened, broadened or extension of characteristic Bragg reflections. All materials do not show the effects of irradiation in the same way. Metals show the least effect, while ionic and covalent crystals are more strongly affected. The greater ease with which displaced atoms anneal at ordinary temperature in metals explains the difference in observed defects in diffraction patterns. In the case of organic crystals, the patterns show a disruptive influence due to cleavage or cross linking produced by irradiation. Generally speaking, current literature has reported significant changes in x-ray patterns are due to heavy particle irradiation only. However, we will note significant asterism in some of the single crystal Laue patterns prepared for this thesis. The production of vacancies in a crystalline material always reflects a decrease in crystal density whether or not stable interstitials are produced concurrently. Lattice vacancies known as Schottky defects lowers the density of the crystal because the net result of their production is an increase in the volume of the specimen with no increase in mass. The production of Frenkel defects does not, at least to the first order, change the volume of the crystal and so the density remains unchanged.

An interstitial atom in an otherwise perfect lattice can weaken a reflection by diffracting an out of phase ray which annuls another ray.



On the other hand, a vacancy in a perfect crystal acts as an extra scattering center since it is not available to annul a similarly phased ray in another plane, i. e., destructive interference is absent.

Bragg's Law,  $\lambda = 2d \sin \theta$ , states the essential condition which must be met if diffraction is to occur. Essentially at scattering angles other than the Bragg angle the scattering of the perfect crystal lattice vanishes, while the imperfections remain. Using this simple fact, an analysis of diffraction patterns will show an increase in background scattering between Bragg angle peaks. The approximate background scattering intensity to a first approximation can be calculated from the following equation proposed by Dienes and Vineyard (10, p. 107-117):

$$I = (n_i + n_v) f^2$$

where  $n_i$  are the interstitials,  $n_v$  are the vacancies and  $f$  is the atomic structure factor. Of course, the Bragg peaks will be reduced in intensity by a corresponding amount. Antal, Weiss and Dienes used the scattering of very slow neutrons to determine defect concentrations of interstitials and vacancies in much the same way as stated above. In ionic crystals both interstitials and vacancies produce an identifiable change in lattice constants, i. e., size and shape of the lattice cell. In ionic crystals, vacancies cause the neighboring atoms to move outward rather than inward as generally expected. The absence of the electrostatic force provided by the vacancy explains this



behavior. However, there is no conclusive evidence in current literature to reinforce this hypothesis (23). It is this author's opinion that a concentration of defects of interstitials and vacancies produce mosaic, bent or polygonized structure within an otherwise perfect lattice structure. This results in non-ideal diffraction pattern which could be shown as asterism in a single crystal Laue pattern, a broadening of Bragg peak lines, and increased background intensity in powder patterns. In addition to variation in the intensity, the size and shape of Laue transmission "spots" and the width of the powder diffraction peaks the lattice size and shape are affected by irradiation. Both vacancies and interstitials can be expected to produce change in lattice parameters although the latter would provide more obvious effects than the former. The average increase of lattice parameter have been observed in a number of irradiated materials by measuring the shift in the position of x-ray reflections. These effects have been noted in ionic solids and solids with combined covalent and ionic bonding. The effects have been due to irradiation by combined gamma ray and heavy particle irradiation. Crawford and Wittels (8) reported lattice expansion in zircon ( $\text{ZrSiO}_4$ ), beryl ( $\text{Be}_3\text{Al}_2\text{Si}_6\text{O}_{18}$ ), chrysoberyl ( $\text{BeOAl}_2\text{O}_3$ ), phenacite ( $2\text{BeO} \cdot \text{SiO}_2$ ) and other naturally found minerals. Diamond, silicon carbide, quartz, magnesium oxide, spinel, and sapphire were investigated by Primak and co-workers (43) who reported lattice expansions particularly in the first three

materials. Although it has been stated previously that metals anneal out defects, Simmons and Balluffi (53) have reported lattice parameter increase in copper single crystals. However, this was noted at low temperature ( $12^{\circ}\text{K}$ ) with bombardment by 12 Mev deuterons. When the specimen was warmed to room temperature a negligible amount of lattice expansion was noted. The significant fact to be noted here is that interstitials must have been present to cause lattice expansions in the metals, vacancies could not have produced an expansion.

Huang (21) among others (58, 31, 6, 12, 4) has treated the problem of x-ray reflections produced by lattice defects. He has itemized three specific effects which he has incorporated into an empirical formula. First, he notes there is a reduction in the intensity of the Bragg reflections; second, there is a slowly varying background scattering; and, finally, he notes a characteristic diffuse scattering in the vicinity of the Bragg direction. This "Huang effect" has immediate application to analysis of radiation damage in solids. The theory is inconclusive at best due to limited experimental evidence; however, as an approximation it provides a starting point for analysis. The absence or concealment of the effects are not conclusive for mitigating radiation damage. There are experiments which presently emphasize the limitation of the Huang effects. Crawford and Wittels (8, vol. 7, p. 654-665) reported the effects on a reactor exposed zircon crystal

at Oak Ridge. Laue transmission photographs show a progressive disappearance of higher angle reflections, a broadening of inner reflections and a pronounced small angle region reflections caused by mosaic blocks within the crystal lattice approaching three degrees disorientation. This effect is contrary to isolated atomic centers of strain which are the basis for the Huang model. Heavy irradiation cannot be expected to satisfy the Huang approximation. X-ray diffraction, as with all tools, has its boundaries of limitations; used within these borders it provides part of the insight into understanding solid state problems but used with other tools it adds to broadening the spectrum of understanding of the fringes of the unknown.

#### D. Irradiation of Other Salts

In addition to the alkali halides other salts have been investigated in a very limited degree. Gilliland and Yockey (16, p. 367-374) have recently reported thermoluminescence studies of the gamma ray irradiation of Rochelle Salt and Guanidine Aluminum Sulfate Hexahydrate. Glow peaks were noted for that latter salt with none for the former. Rochelle Salt and certain other salts are known to decompose when exposed to ionizing radiation. Allen and Ghormley (1, p. 208-209) studied Barium Nitrate and found it decomposed during irradiation, releasing nitrite ions and oxygen. Sodium Nitrate, Potassium Nitrate and Potassium Chlorate also were found to decompose and evolve gas,

as reported by Hennig, Lees and Matheson (18, p. 664-668). It has been clearly concluded the decomposition results from electronic ionization and excitation rather than from displaced atoms. The Sodium Nitrate has also been investigated by Pringsheim (44, p. 369-375) who correlated optical properties with decomposition. He found two absorption bands, one at 345 millimicrons and another a color center band which is continuous with a peak near 335 millimicrons. The color center band is identified with  $\text{NO}_2^-$  ions since the same band appeared upon adding  $\text{NaNO}_2$  to the melt.

Rosenwasser, Dreyfus and Levy (46, p. 184-190) found gamma rays produce an absorption band at 3600 Angstroms and poorly defined bands at 6600 Å and 7600 Å that decay at room temperature in Sodium Oxide.



## SECTION IV

## MATERIALS AND METHODS

A. Crystal Selection and Growth

Monoatomic ionic crystals are probably the easiest to understand from a bonding standpoint. The alkali halide structure, because of its simplicity, has provided a foundation for the explanation of the principal bonding forces of ionic crystals. The current concept of ionic formation is that the structures are made up of atoms or groups of atoms that either lack electrons or have a surplus over the number necessary for electroneutrality. The probability of ionic formation of some elements is based upon the stability of certain electronic configurations. For example, the closed-shell grouping of eight outer electrons appears to be the most stable arrangement. Elements with more or less than this in their outer shells have an affinity for or against electrons in attempting to assume a closed shell configuration. A measure of the ease of ionization of an atom is the "ionization potential" which is the energy which must be supplied to the atom to remove an electron from a normal state in the atom. The valence of an atom in usual chemical reactions can be traced to ionization potential energies necessary to remove the most loosely bound electrons.

Study of the periodic table shows the positive ions consist of the



first three columns of the periodic table, the transition elements, and the rare earth elements. In addition to the individual atoms certain groups of atoms function as ions such as  $\text{CN}^-$ ,  $\text{NO}_3^-$ ,  $\text{CO}_3^{-2}$  and  $\text{ClO}_3^-$  to form ionic crystals. Within the molecules the atoms probably have covalent bonding with the total atom complex showing an excess or deficiency of electrons which establishes its valency. The general configuration of the ionic structure maintains its stability by having each ion surrounded by as many ions of opposite charge as possible. The principal attractive force between ions of opposite sign is the electrostatic or coulombic force. The repulsive force in ionic crystals arises from the interaction of the electron clouds surrounding an atom. The other energy terms for ionic solids are the dipole - dipole, dipole - quadripole, quadripole - quadripole, and zero-point energy terms. The total lattice energy as computed theoretically from the preceding energy terms are in remarkable agreement with measured values as compared by Seitz (49). This agreement helps to support the present concept of ionic solids. It is the apparent accuracy and simplicity of this model which prompted the author to select ionic materials for this thesis. Additionally, the binding is of a nature which is highly susceptible to ionizing gamma-radiation which was available for research. Ionic crystals reflect lattice structure damage when observed through many laboratory measuring devices. For the most part, the structures of the crystals will be described

using the codification established by the Strukturbericht (14).

All single crystal specimens used in this research were grown by the author, using the supersaturated solution technique described by Holden (20) and Buckley (5). The method for growing water soluble crystals makes use of their solutibility temperature relationship. Seeds are placed in a vessel which contains a supersaturated solution of the crystal desired at about 40° C. Salt comes out of the solution and is deposited on the seed surface, thus reducing the degree of supersaturation. To maintain it in a growing condition, the temperature is reduced a fraction of a degree per day, the supersaturation level is maintained and the crystal continues to grow. When it reaches room temperature, the crystal may be removed or the process can be repeated.

A total of six single crystal specimens were selected for experimentation. All six have similarities and still possess differences which provide an opportunity to observe the effect of ionizing radiation. The crystals did not possess elements which contained hazards of induced radioactivity. All specimens were of a predominantly ionic structure which again influenced their selection for experimentation. Three samples were mixed crystals of the double salt configuration. The preceding information is mentioned to establish selection criteria and similarity of a general nature existing between specimens. To acquaint the reader with the individual character of each specimen

used, each will be discussed separately.

The first crystal to be discussed is Potassium Aluminum Sulfate Dodecahydrate ( $\text{KAl}(\text{SO}_4)_2 \cdot 12\text{H}_2\text{O}$ ). This is a double salt which belongs to the cubic system of the crystallographic classification. It is a colorless crystal of essentially ionic bonding. Before discussing its structure, it should be pointed out that the penta-atomic divalent radical  $\text{SO}_4^{-2}$  acts as a stable grouping. The sulfur atom has a high ionization potential and tends to form covalent bonds that are inherently stronger than ionic bonds. The radical as a whole tends to act as a charged ion and the identity of the elements making up the radical is lost. Although this is a member of the cubic system we cannot visualize a lattice structure as ordered as the alkali halides because of the nonsphericity of the radical complexes. The nonsphericity of the radical and the deviation from simple "CsCl or NaCl" type structure cause polarizations of the ions. Polarization is remotely related to magnetic and electric phenomena but in the structural sense relates to the distortion of the spherical field of an ion. Large loosely bound ions are the most readily polarized radicals. On the other hand, the ions that cause the polarization are usually small ions of high charge. In the present discussion of the double compound of Potassium Aluminum Sulfate Dodecahydrate, the complexity of the structure is further magnified by the molecules of hydration. A pair of sulfate ions gains one of its four electrons from a potassium atom and three from an

aluminum atom, leaving a potassium ion with a plus one charge, and an aluminum ion with the unusually large charge of plus three. The majority of the alums, commonly designated as the alpha alums are typified by  $\text{KAl}(\text{SO}_4)_2 \cdot 12\text{H}_2\text{O}$ . The alums provide a large series of crystals in which small trivalent metal atoms are enveloped by six octahedrally coordinated  $\text{H}_2\text{O}$  molecules. The position and parameters for typical alums which have been studied in detail are listed by Wyckoff (63, 64). Table II shows the positions and parameters of the atoms in alpha alum  $\text{KAl}(\text{SO}_4)_2 \cdot 12\text{H}_2\text{O}$ ;  $a_0 = 12.133 \text{ \AA}$ . The structure can be visualized as a super lattice on the Cesium Chloride structure arrangement. To do this, no distinction is drawn between uni- and tri-valent metal atoms. The plus charge metal atoms and the divalent sulfate ions are distributed similarly to the Cesium and Chloride ions of  $\text{CsCl}$ . The alternation of the different metal atoms explains the double-length large cell of the alums. In all known cases, six water molecules are closely coordinated with the small trivalent metal ion. The distribution of the other six depends on the size of the univalent cations. In the case of  $\text{KAl}(\text{SO}_4)_2 \cdot 12\text{H}_2\text{O}$ , this univalent cation is also surrounded by six octahedrally distributed water molecules which is typical of alpha alum. The aluminum atom of the  $\text{Al}(\text{H}_2\text{O})_6$  coordinate complex is so small that contact can occur between its water molecules but the central Potassium ion of the  $\text{K}(\text{H}_2\text{O})_6$  octahedron complex is too big to have such contact. In Potash alum,

Table II Positions and Parameters of Atoms in  $\text{KAl}(\text{SO}_4)_2 \cdot 12\text{H}_2\text{O}$ 

| ATOM                 | POSITION** | X    | Y    | Z    |
|----------------------|------------|------|------|------|
| K                    | b          | 1/2  | 1/2  | 1/2  |
| Al                   | a          | 0    | 0    | 0    |
| S                    | c          | 0.31 | 0.31 | 0.31 |
| O (1)                | c          | 0.24 | 0.24 | 0.24 |
| O(2)                 | d          | 0.30 | 0.27 | 0.43 |
| H <sub>2</sub> O (1) | d          | 0.04 | 0.13 | 0.30 |
| H <sub>2</sub> O (2) | d          | 0.02 | 0.02 | 0.16 |

\*\* a - 000 F. C.

b - 1/2 1/2 1/2 F.C.

c -  $\pm$  (u u u; u + 1/2, 1/2 - u,  $\bar{u}$ ;  $\bar{u}$ , u + 1/2, 1/2 - u;  
1/2 - u, u, u + 1/2)d - (x y z ; z x y; y z x; x + 1/2, 1/2 - y,  $\bar{z}$ ;  $\bar{z}$ , x + 1/2,  
1/2 - y; 1/2 - y,  $\bar{z}$ , x + 1/2,  $\bar{x}$ , y + 1/2, 1/2 - z; 1/2 - z,  
 $\bar{x}$ , y + 1/2; y + 1/2, 1/2 - z,  $\bar{x}$ ; 1/2 - x,  $\bar{y}$ . z + 1/2;  
z + 1/2, 1/2 - x,  $\bar{y}$ ; y, z + 1/2, 1/2 - x)



Al - H<sub>2</sub>O bond is 1.98 Å and K - H<sub>2</sub>O bond is 2.94 Å.

The second double salt used for this thesis was Potassium Chromium Sulfate Dodecahydrate, another pseudomorph of alpha alum using a chromium atom in place of the aluminum. This specie has all of the structural quality mentioned previously except for color.

"Chrome alum" is purple in color due to the presence of chromium. It is instructive to mention at this point the use of the words "mixed crystals" is misleading since it suggests a mixture rather than a solution. A better term would be a "solid solution," since there is a molecular dispersion rather than the chunk the previous term implies. The alpha alums are soluble in each other in any amount with the same atomic arrangement, and their molecules have approximately the same size and shape. Noting this striking similarity it would be reasonable to predict similar effects due to gamma ray irradiation. It shall be noted later this is not the case.

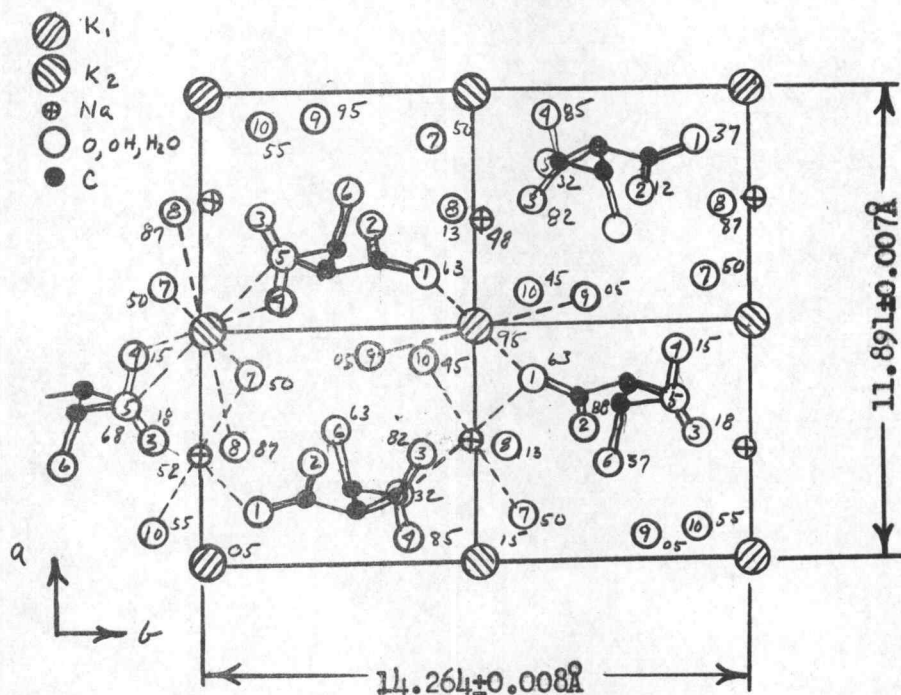
The third double salt referred to previously was K·Na·C<sub>4</sub>·H<sub>4</sub>O<sub>6</sub>·4H<sub>2</sub>O, Rochelle Salt. This essentially ionic crystal behaves like an intermediate solid solution in that there is a possibility of dissolving excess K or Na ions into the structure while still maintaining its compound characteristics. The crystal structure of Rochelle Salt was first determined by Beevers and Hughes in 1941 (33, p. 20-24). The cell dimensions determined by them are as follows:

$$\begin{aligned} a &= 11.93 \text{ \AA} \\ b &= 14.30 \text{ \AA} \\ c &= 6.17 \text{ \AA} \end{aligned}$$

The structure is most easily seen in projection on the (001) plane shown in Figure 2. The tartrate ions lie inclined to this plane and some of their atoms overlap in projection. All sodium ions are in equivalent positions and have the same arrangement of six nearest "oxygen" (which include hydroxyl groups and water molecules under the term "oxygen") neighbors lying roughly at the corners of an octahedron. Of the two different potassium ions,  $K_1$  has four near oxygen neighbors only (the next nearest being at more than 3.2 Å distance), while  $K_2$  has eight. The atomic parameters according to Beevers and Hughes are given in Table III.

There are three possible hydrogen bonds in the structure, between the oxygen molecule 1 and the water molecule 10, between the water molecule 10 and the water molecule 9, and between the water molecule 9 and the oxygen 2. The distance between the successive molecules are 1 to 10, 2.59 Å; 9 to 10 is 2.86 Å; and 9 to 2 is 3.02 Å. The bond with the shortest distance is 1 to 10 and it is the motion of the hydrogen nucleus along this bond that causes ferroelectricity in Rochelle Salt according to the analysis of Mason (30). This bond lies nearly along the x-axis which is the ferroelectric axis of the crystal. In addition to possessing piezoelectric properties, Rochelle Salt is a transparent, colorless crystal belonging to the orthorhombic system

Figure 2



Rochelle Salt: projection of structure on 001.

Figures beside atoms give height above plane  $z = 0$  in hundredths of cell edge, which can be converted into Angstrom units when multiplied by  $c/100$ .

Dotted lines show environment of representative atoms within the cell. (30, p. 22)

Table III (33, p. 21)

Atomic parameters in (orthorhombic) Rochelle Salt expressed as hundredths of the cell edge. These were originally measured in sixtieths of the cell edge; hence, there is a rounding-off error in the second figure.

Crystallographically equivalent positions are:

$$x, y, z; 1/2 + x, 1/2 - y, z; 1/2 - x, 1/2 + y, z; x, y, z.$$

| Atom                 | Parameters |    |    |
|----------------------|------------|----|----|
|                      | x          | y  | z  |
| K <sub>1</sub>       | 0          | 0  | 05 |
| K <sub>2</sub>       | 0          | 50 | 15 |
| Na                   | 23         | 99 | 52 |
| O(1)                 | 12         | 10 | 37 |
| O(2)                 | 22         | 20 | 12 |
| O(3)                 | 23         | 40 | 82 |
| O(4)                 | 06         | 37 | 85 |
| OH(5)                | 16         | 36 | 32 |
| OH(6)                | 29         | 24 | 63 |
| H <sub>2</sub> O(7)  | 40         | 08 | 50 |
| H <sub>2</sub> O(8)  | 25         | 05 | 87 |
| H <sub>2</sub> O(9)  | 44         | 30 | 05 |
| H <sub>2</sub> O(10) | 42         | 40 | 45 |
| C(1)                 | 15         | 18 | 28 |
| C(2)                 | 12         | 28 | 42 |
| C(3)                 | 17         | 27 | 65 |
| C(4)                 | 15         | 35 | 80 |



in crystallography. This crystal was selected for experimentation since it could be grown to a large size without difficulty and it possesses piezoelectric properties.

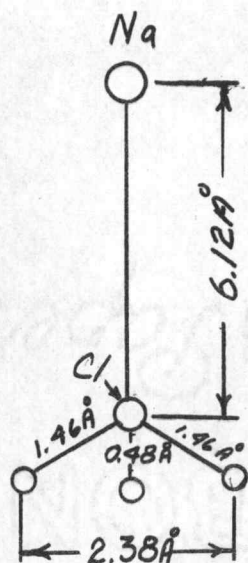
The distances between cations and oxygen are shown in Table IV, below:

Table IV

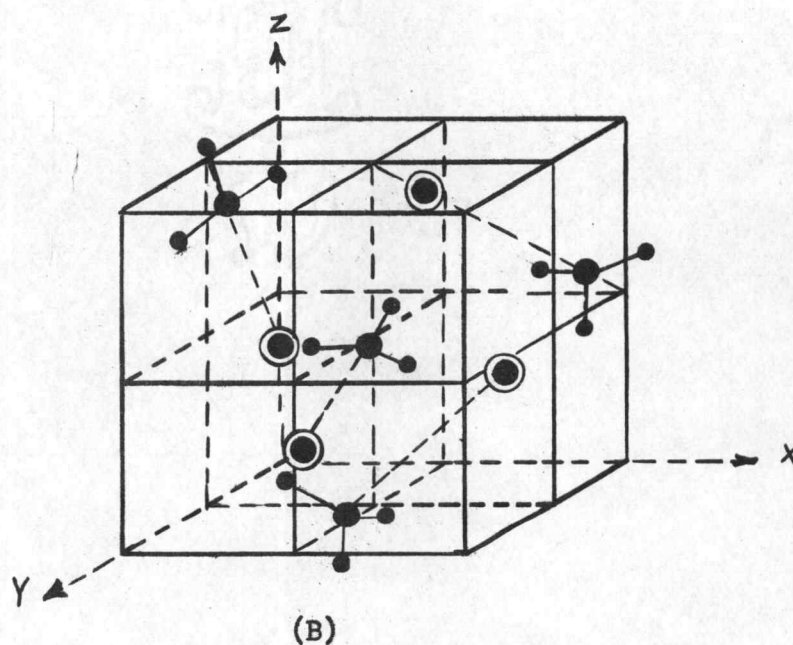
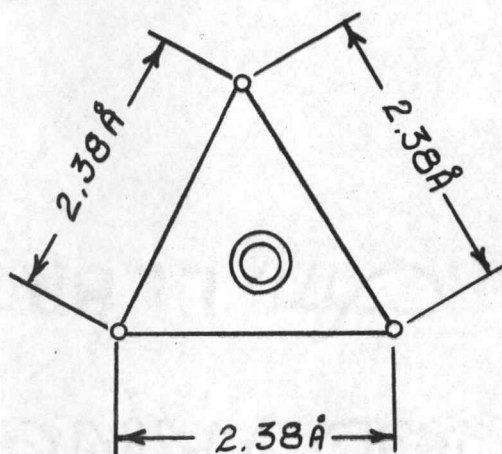
|               | A    |              | A    |
|---------------|------|--------------|------|
| $K_1 - O(1)$  | 2.79 | $Na - O(1)$  | 2.29 |
| $K_1 - O(9)$  | 3.01 | $Na - O(10)$ | 2.31 |
| $K_1 - O(8)$  | 3.29 | $Na - O(8)$  | 2.34 |
| $K_1 - O(10)$ | 3.52 | $Na - O(7)$  | 2.39 |
|               |      | $Na - O(3)$  | 2.49 |
| $K_2 - O(4)$  | 2.75 | $Na - O(5)$  | 2.52 |
| $K_2 - O(7)$  | 2.75 |              |      |
| $K_2 - O(5)$  | 2.96 |              |      |
| $K_2 - O(8)$  | 3.07 |              |      |

Another crystal which was selected because it possessed piezoelectric properties was Sodium Chlorate,  $\text{NaClO}_3$ . According to the arbitrary classification in Strukturbericht, this is an  $\text{ABX}_3$  compound. The  $\text{BX}_3$  ion in these compounds are of two types of structure. The first type,  $\text{CO}_3^{-2}$  and  $\text{NO}_3^-$  radicals are planer, with the C and N being found at the center of the triangle formed by the oxygen atoms. This will be discussed further when the fifth crystal used for this research, namely  $\text{NaNO}_3$ , is considered. The second type of  $\text{BX}_3$  radical is the pyramidal placement of the B atom into the oxygen triangle as found in Sodium Chlorate. The  $\text{ClO}_3^-$  radical has this structure. It is believed this structure is derived from a tetrahedral placement of  $\text{O}^{-2}$  ions with one of the ions removed and the three remaining bonds being directed to the central atom at the same angle as in the tetrahedral bonding. X-ray crystal structure studied show that Sodium Chlorate has four molecules per unit cell. Each molecule consists of three oxygen atoms arranged in the form of an equilateral triangle with a separation of 2.38 Å between oxygen centers as shown in Figure 3. The chlorine is located at a distance of 0.48 Å above the plane of the oxygen atoms in a line through the center of gravity of the oxygen. The sodium lies above the chlorine at a distance of 6.12 Å. Sodium Chlorate is colorless and belongs to the cubic system with lattice constant  $a = 6.57$  Å. Sodium Nitrate was mentioned as belonging to the  $\text{ABX}_3$  compounds possessing a planar tetra-atomic

Figure 3



(A)



(B)

- (A) Position of sodium, chlorine and three oxygen atoms in sodium chlorate.
- (B) Location of molecules in unit cell for sodium chlorate (30, p. 191).

univalent ion which is the  $\text{NO}_3^-$  radical.  $\text{NaNO}_3$  belongs to the hexagonal system and is a colorless ionic compound. This crystal is more difficult to grow than the crystals mentioned previously. The range of supersaturation within which it grows is very narrow; therefore, it is quite sensitive to temperature changes. The crystal is double refractory similar to the mineral calcite. The lattice structure is similar to Sodium Chloride; however, in place of the spherical chloride ions, this crystal has flat nitrate ion. The four atoms constructing a nitrate ion are all in the same plane with the Nitrogen in the center and surrounded by three oxygen atoms, N - O distance is 1.25 Å roughly pictured as a triangular block. The blocks are arranged in a parallel planes and the cubic structures of the Sodium Chloride is broadened, in the plane of the blocks into a rhombohedral structure. As in Sodium Chloride, the electrostatic forces exerted by the positively charged sodium ions and the negatively charged nitrate ions have caused each of them to collect their opposites around them and to push their fellows away. The rhombohedral planes are electrically neutral in Sodium Nitrate.

This crystal shows a pronounced rhombohedral cleavage. The axes of this cleavage rhombohedron are those of a large tetramolecular pseudo-cell which expresses the Na-Cl structural characteristics.

The sixth crystal to be used in this research was a red crystal of the monoclinic system named Potassium Ferricyanide,



$K_3Fe(CN)_6$ . This crystal presented the greatest difficulty to grow due to its sensitivity to temperature change. Structure Reports (62) provides the following description of  $K_3Fe(CN)_6$ . It is monoclinic,

$$\begin{aligned} a &= 7.04 \text{ \AA} \\ b &= 10.44 \text{ \AA} \\ c &= 8.40 \text{ \AA} \\ B &= 107 \frac{1}{2}^\circ \end{aligned}$$

The  $CN^-$  ion groups are assumed to be situated in such a way that the Fe atom is surrounded by 6  $CN^-$  groups in an approximately octahedral configuration. The interatomic distances are Fe - CN = 2.4 - 2.6 Å and C - N = 1.0 - 1.2 Å.

The atomic positions

$$\begin{aligned} 2Fe \text{ in } 2(a): & 0, 0, 0; 0, \frac{1}{2}, \frac{1}{2} \\ 2KI \text{ in } 2(c): & 0, 0, \frac{1}{2}; 0, \frac{1}{2}, 0 \\ 4KII \text{ in } 4(3): & (X, Y, Z, \cdot X, \frac{1}{2} - Y, \frac{1}{2} + 2) \\ & \text{with } X = \frac{1}{2} \\ & Y = \frac{1}{2} \\ & Z = \frac{1}{8} \end{aligned}$$

KI has an approximately octahedral environment of six  $CN^-$  groups, but around KII there are six  $CN^-$  groups in a configuration approaching a trigonal prism. Every  $CN^-$  group has one Fe and three K neighbors.

## B. Optical Absorption Spectroscopy and X-Ray Diffraction Procedures

The science of spectroscopy dates back to Newton's discovery in 1672 that the amount of refraction undergone when light is passed through a prism varies with the color of the light. The search

conducted in this thesis relied heavily on electromagnetic spectrum to investigate the damage effects in the crystal mentioned in the preceding section. Two different radiation regions were used from the spectrum. They were the optical rays, which include infrared wave lengths, the visible rays and ultra violet rays, and the x-rays which include gamma rays. Although these regions are arbitrary and overlapping, it is convenient to identify them in Table V for future reference.

In this section, we shall discuss spectrophotometer and x-ray techniques used for the investigation of the specimens. A model DK-1 Beckman recording spectrophotometer with a Beckman DU Monochromator was used to identify the absorption spectra of the single crystal. The light source is a tungsten filament lamp or a hydrogen discharge tube, depending on the spectral region under investigation. The nature of light absorption will be reviewed to support the theoretical basis of the results obtained before and after irradiation.

When energy is absorbed by a medium, it may be used up mainly in three ways: it may be re-emitted at a different (usually longer) wave length, and this phenomenon is called fluorescence if the emission stops as soon as the irradiation ceases or phosphorescence if the emission continues after the irradiation ceases; it may bring about photochemical changes (usually irradiation with rays of wave lengths within the absorption band); or, as happens most commonly, it

Table V

## ELECTROMAGNETIC SPECTRUM

| Frequency<br>$10^n$ -cps | *Wave<br>Length,<br>m | Type of Radiation    | Typical Source                  |
|--------------------------|-----------------------|----------------------|---------------------------------|
| n = 23                   | $10^{-15}$            | Cosmic photons       | Astronomical                    |
| 22                       | $10^{-14}$            | v-rays               | Radioactive Nuclei              |
| 21                       | $10^{-13}$            | v-rays, x-rays       |                                 |
| 20                       | $10^{-12}$            | x-rays               | Atomic inner shell              |
| 19                       | $10^{-11}$            | Soft x-rays          | Electron impact on<br>a solid   |
| 18                       | $10^{-10}$            | Ultraviolet, x-rays  | Atoms in sparks                 |
| 17                       | $10^{-9}$             | Ultraviolet          | Atoms in sparks<br>and arcs     |
| 16                       | $10^{-8}$             | Ultraviolet          | Atoms in sparks<br>and arcs     |
| 15                       | $10^{-7}$             | Visible spectrum     | Atoms, hot bodies,<br>molecules |
| 14                       | $10^{-6}$             | Infrared             | " " "                           |
| 13                       | $10^{-5}$             | Infrared             | " " "                           |
| 12                       | $10^{-4}$             | Far infrared         | " " "                           |
| 11                       | $10^{-3}$             | Microwaves           | Electronic devices              |
| 10                       | $10^{-2}$             | Microwaves, radar    | " "                             |
| 9                        | $10^{-1}$             | Radar                | " "                             |
| 8                        | $10^0$                | TV, FM radio         | " "                             |
| 7                        | $10^1$                | Shortwave radio      | " "                             |
| 6                        | $10^2$                | AM radio             | " "                             |
| 5                        | $10^3$                | Longwave radio       | " "                             |
| 4                        | $10^4$                | Induction heating    | " "                             |
| 3                        | $10^5$                | Induction heating    | Electronic devices              |
| 2                        | $10^6$                | Elec. power, heating | Rotating mach.                  |
| 1                        | $10^7$                | Elec. power, heating | Rotating mach.                  |
| n = 0                    | $10^8$                | Elec. power          | Commutated DC                   |
| 0 cps                    | Infinity              | Direct current       | Generators,<br>Batteries        |

\*  $f\lambda = 3 \times 10^8$  m/sec = velocity of propagation; where  $f$  = frequency, cps;  $\lambda$  = wave length, m.

may be converted into increased vibration of the atoms.

According to the Bohr theory, the excitation of an atom (by some process providing energy, such as heating, or subjection to an electric discharge - x-ray, light, etc.) involves an absorption of energy by the atom and causes one or more of the planetary electrons to be displaced from inner to outer orbits. When these excited atoms revert to normal, with the return of the electrons to their original orbits, the energy absorbed in the excitation process is emitted in the form of light. The Bohr theory, however, goes much further than this. It postulated that the electron orbits of an atom are limited in the sense that only orbits of certain precise energy characteristics are available to the electrons. It is this grafting of quantized energy levels to the Rutherford atom that provides the clue to the line-nature of atomic spectra. For, given that the atom can exist only in certain states of precise energy,  $E_1, E_2, E_3, \dots, E_n$ , it follows that an excitation of the atom involves an energy change of precise value viz.,  $(E_n - E_m)$ , where  $E_n$  is the energy of the initial, and  $E_m$  that of the final state of the atom. The Bohr theory relates this energy change to the frequency of the absorbed or emitted radiation by the equation

$$(E_n - E_m) = h\nu_{nm}$$

where  $\nu_{nm}$  is the frequency corresponding to the transition n to m.

Thus, each transition corresponds to the emission of monochromatic radiation, which, when multiplied millions of times by



repetition in other atoms, is seen as light and as a single spectral line. Since the wave length or frequency of these lines can be measured with accuracy, they provide useful tools for the exploration of atomic structure, and have been intensively investigated.

When atoms are activated by heat or electric energy, their electrons are raised through one or more steps of a possible series of energy levels,  $E_1$ ,  $E_2$ ,  $E_3$ , etc., which may be stable or may revert to a lower level, or even to the ground state, with consequent liberation of energy. For every drop in energy level, e.g.,  $E_3$  to  $E_2$ , the energy difference is emitted in the form of monochromatic radiation of frequency  $\nu$  such that  $E_3 - E_2 = h\nu$ , where 'h' is Planck's constant.

When light passes through an absorbing medium containing atoms, e.g., mercury vapor, the converse of this emission process takes place, and in raising the energy levels of the mercury atoms, monochromatic radiation is absorbed. This causes gaps in the spectrum of the original light source, which take the form of absorption lines exactly complementary to the observed emission lines when the same atom radiates energy.

The absorption of energy by molecules is a much more complicated process, but even here, if the compound is in the vapor state at low pressure, the absorption spectrum will consist of a series of separate lines. In solid or in liquid state, owing to the close packing

of the molecules, this selective absorption of monochromatic radiation is lost, and broad bands of absorption result.

The total energy of a molecule is made up of binding energy and kinetic energy, and may be represented by:

$$E = E_{\text{electronic}} + (E_{\text{vibrational}} + E_{\text{rotational}})$$

The electronic binding energy is usually by far the largest term. Changes in the electronic energy usually require larger changes in total energy and is associated with the absorption bands in the visible and ultra violet regions. Changes in the energy of vibrations of the atomic nuclei are associated with absorption bands situated in the near infrared region. The smallest energy changes commonly observed in a molecule are those associated with transitions from one rotational state to another, and the absorption bands resulting from rotational changes only are situated in the far infrared beyond 20 microns.

It may be of value here to consider the energy changes which give rise to absorption in these spectral regions. Thus absorption in the far ultra violet region at wave lengths near 150 millimicrons and below, involves energy changes of about 185 kcal. per molecule or more. Changes of this type are not electronic transitions but consist of the complete removal of electrons (photo ionization) and the rupture of covalent bonds. For absorption to occur at the limit of the quartz ultra violet region (200 to 220 millimicrons), the energy change of the

electronic transition must be between about 120 and 140 kcal. per molecule. At the edge of the visible spectral region (400 millimicrons) the energy requirement is between 60 and 70 kcal. per molecule and absorption at 1 and 20 (associated with vibrational and rotational changes) corresponds to about 25 kcal. per molecule and one kcal. per molecule, respectively. Note that  $1 \text{ ev/molecule} = 23.05 \text{ kcal./molecule}$ .

If the energy changes in molecules were electronic only, the absorption spectra would consist solely of lines, but for every electronic change there occurs simultaneous vibrational and rotational changes, so that the number of absorption lines is very large, and lines pack together, forming bands. Thus the absorption spectra of vapors and gaseous compounds under low pressure show broad bands of absorption, although, with spectroscopes of high resolving power, these bands can be shown to possess fine structure. In the simple cases this fine structure can be analyzed, and each line related to some particular energy transition (electronic, vibrational, and rotational) in the molecule.

When matter in the atomic state is suitably excited, it can emit light which, when passed through a prism, gives a line spectrum consisting of a series of lines which are actually more or less widely spaced images of the slit of the spectroscope.

When simple elements in the gaseous state are excited by

electrical means, it is observed that they glow and emit radiation in the form of light, varying somewhat in color with the nature and intensity of the mode of excitation. Different elements so excited give colors that can usually be differentiated simply by visual inspection. When the emitted light is examined in a spectroscope, the spectra are found to consist of series of lines situated in various parts of the spectrum, and each series is quite characteristic of the element producing it. The wave lengths of the lines in these line spectra can be accurately measured and provide a certain means of identification of the emitting elements. This is the basis of emission spectroscopy as an analytical tool. The phenomenon is not confined to matter existing normally in gaseous form for even metals, when introduced into an electric spark, emit their own characteristic radiations.

The spectrum of the simplest element, hydrogen, was studied by Balmer in 1885. He showed that the wave lengths of the most intense lines could be expressed by the simple formula:

$$\lambda = Km^2 / (m^2 - 2^2)$$

where K is a constant and m is one of a series of whole numbers, 3, 4, 5, 6, etc. This series of lines in the hydrogen spectrum is known as the Balmer series, and the formula holds for each of the thirty lines (approximately) in the series which have been detected so far. Balmer's formula is more often stated in terms of wave numbers



( $\nu = 1/\lambda$ ), and then becomes

$$1/\lambda = N(1/2^2 - 1/m^2)$$

where N is a constant ( $109677.7 \text{ cm}^{-1}$ ).

The constant N is known as Rydberg's constant. It was found by Rydberg to be characteristic of the series of lines in the hydrogen spectrum and also to occur in similar formula defining the lines in the spectra of other elements.

By taking the difference of any two of the "spectral terms"  $N/1^2$ ,  $N/2^2$ ,  $N/3^2$ ,  $N/4^2$ , etc. It is possible to obtain the frequency of any particular line of the hydrogen spectrum. Since related formulae, using the same constant, reproduce lines in the spectra of other elements as well as hydrogen, it is clear that there must be some fundamental relation between spectral lines and atomic structure. These line spectra are now known to be characteristic of matter in the atomic state and are frequently called atomic spectra.

Molecules, on the other hand, when similarly caused to emit light, yield a band spectrum that can be recognized on sight as quite different from an atomic line spectrum. The band spectrum consists of a series of lines that come more and more closely together as the wave lengths of the lines increase; they then appear to be continuous, and finally suddenly disappear altogether. At longer wave lengths, another series of lines may then be observed, first wide apart, but approaching more and more closely before disappearing again. Each

converging series of lines is a distinct band and can be accurately measured. The complete absorption or emission spectrum of any one molecule usually consists of a group of such bands.

The great complexity of the electronic spectra of polyatomic molecules in general, even in the gaseous state, makes the complete mathematical interpretation of their spectra so difficult as to be almost impossible at the present time.

Before considering the physical shape and arrangement of the crystals in the spectrophotometer, a discussion of Lambert's law of light absorption is in order. It states that the proportion of light absorbed by a transparent medium is independent of the intensity of the incident light and that each successive unit layer of the medium absorbs an equal fraction of the light passing through it. Mathematically this leads to the expression which is essentially the same as that describing x-ray and gamma ray absorption.

$$I = I_0 e^{-\alpha d}$$

or  $\log_e$

$$\log_e \frac{I_0}{I} = \alpha d$$

where:

$I_0$  = intensity of the incident light

$I$  = intensity of the transmitted light

$d$  = thickness of the layer in cm

$\alpha$  = absorption coefficient of the medium

$$\alpha = 2.3026 K.$$

The term optical density is synonymous with absorbance which is mathematically stated as

$$\text{optical density} = \log_{10} \frac{I_0}{I} = K_d$$

With the preceding as a background, the physical laboratory techniques required to measure absorption data will now be considered. The crystals which were grown assumed various shapes as influenced by their characteristic growth habits. Some were shaped like cubes while other took the shape of an octahedron, etc. The spectrophotometer had a holder which could accommodate a specimen  $7\text{mm}^2$  and approximately 4mm thick. All of the original crystals were cut and wet polished to fit the holder. This size crystal was ideal for Laue x-ray diffraction work also. Optical absorption spectra were taken before and after x-ray and gamma irradiation. Results of this data will be discussed in Section V. After recording absorption spectra of the single crystal Laue diffraction photographs were taken. In this method a beam of white radiation, the continuous spectrum from an x-ray tube, is allowed to fall on a fixed single crystal. The wavelength of the beam is variable and the specimen is fixed. The Bragg angle is therefore fixed for every set of planes in the crystal, and each set picks out and diffracts that particular wave length which satisfies the Bragg law. It is fundamental in x-ray analysis that diffraction can occur only when the Bragg law,  $\lambda = 2d \sin \Theta$ , is satisfied.

Although there are two variations of the Laue method, the transmission method was preferred for this research due to the light elements contained in the samples. In the transmission method, the specimen is placed between the x-ray source and a flat film permitting the beam to be transmitted through the crystal. The beam is diffracted and forms an array of spots, generally ellipses, on the film. The spots lying on any one curve are reflections from planes belonging to one zone. The positions of the spots on the film depends on the orientation of the crystal relative to the incident beam, and the spots themselves become distorted and smeared out if the crystal has been bent or twisted in any way. Although the main use of the Laue method is the determination of crystal orientation and the assessment of crystal perfection, only the latter was used for this report. The Laue method was not enough to determine crystal damage from gamma-irradiation, therefore, the powder method was also used to supplement it. Some of the grown crystals which were not shaped for spectrophotometer use were ground to a very fine powder. In the powder method, a monochromatic beam was used to produce powder patterns by the Debye-Scherrer method. The method was selected to determine changes in lattice parameters or changes in atom location as reflected by intensity changes or diffraction line width. A NORELCO x-ray unit was used for the diffraction work.



### C. Gamma Irradiation Procedure and Facilities

One of the byproducts of nuclear fission has been the development of radioactive isotopes, some of which emit short wave length, very high energy electromagnetic radiations called gamma rays. Thus, a relatively compact, low cost and reliable source of large quantities of gamma radiation has become available.

The ability of gamma radiation to penetrate deeply into matter is advantageous because it permits the gamma energy to be imparted through the process containers. The rate of applying energy can be controlled closely. Gamma radiation below 2 Mev does not transmute matter or leave residual radioactivity.

As mentioned previously, interaction of matter with ionization radiation, of which gamma rays are one type, results in the liberation of orbital electrons. These electrons form the chemical bonds between the atoms of most materials, liquids, gaseous, and solid. Chemical bonds may be formed or broken and free radicals and other excited states created. By controlling the chemical and physical environment during the transition period of chemical instability brought about by gamma irradiation, it may be possible to influence the direction or rate of process reactions.

To obtain this radiation, the cobalt 60 high level gamma irradiator facility at the Bureau of Mines, Albany Metallurgy Research

Center, Albany, Oregon, was used. The facility, licensed by the Atomic Energy Commission (AEC) was designed and constructed by the Bureau's Division of Minerals. A cobalt 60 source of not less than 100,000 curies was furnished by the Atomic Energy Commission under a letter of agreement to do minerals research.

The arrangement of the cell in which irradiation tests were made is shown in Figure 4. Its inside dimensions are 12 feet high and 8 by 12 feet in plan. The 48-inch thick walls are of high density concrete. Storage for the gamma radiation source is provided in a water-filled well, 17 feet deep and six feet in diameter.

The gamma irradiation is provided by 24 cobalt 60 capsules, each irradiated to about 4200 curies. The capsules are about five inches long and  $3/4$  inches in diameter. The cobalt 60 is encapsulated in an inner jacket of welded aluminum. The individual irradiation source capsules are arranged variously in different source holders to achieve selected irradiation or flux intensity patterns. The source holder is 15 inches in diameter and 30 inches high, and when fully loaded will yield a gamma flux of about  $10^6$  roentgens an hour. By arranging the source capsules more compactly, an intensity of about  $10^7$  roentgens an hour can be obtained. For the crystals used in this research, the compact arrangement for maximum intensity was used.

The gamma source is raised from or lowered into the water (mean temperature  $14^{\circ}\text{C}$ ) filled storage well by an elevator operated

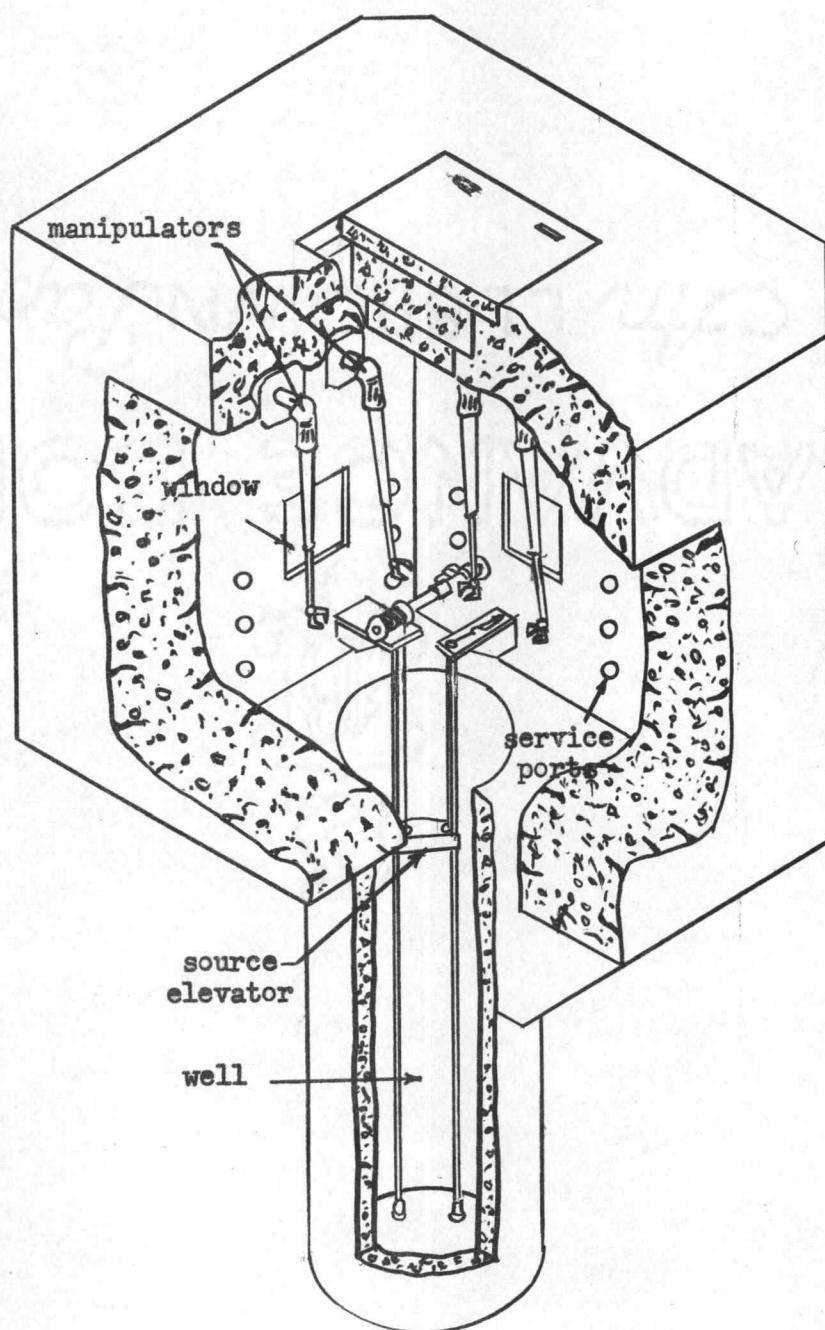


Figure 4 - Gamma Irradiation Cell

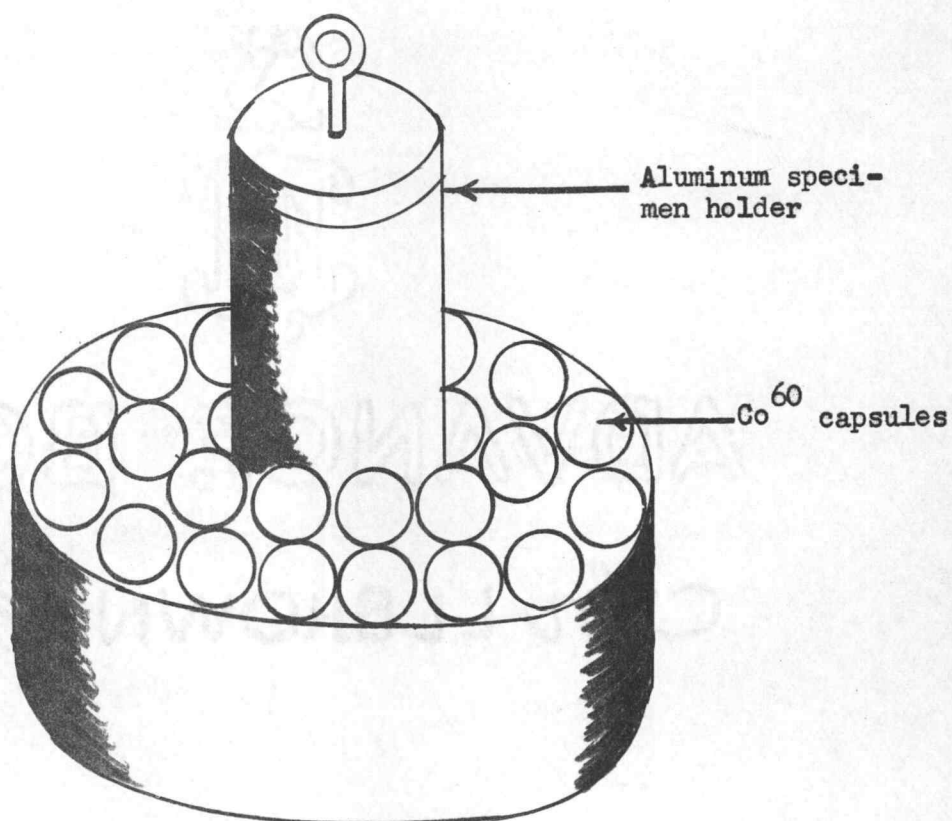
remotely from outside the cell. When the source is at the bottom of the well the radiation at the surface of the water is virtually background. Personnel may enter the cell safely and can manipulate the submerged source capsules or source holder with long-handled grappling tools.

The interior of the cell can be viewed from outside its walls through two heavy-density, oil-filled glass windows. Mercury vapor lamps inside the cell provide illumination. Manipulators are installed inside the cell to operate controls, re-arrange apparatus, alter the gamma source capsule arrangement, or carry out other internal mechanical activities.

Each of the pre-shaped single crystals which were used for absorption readings, and the powder samples used for x-ray diffraction patterns were placed in laboratory specimen bottles, and sealed with wax. These bottles (2cm in diameter and 8 cm high) were placed in a sealed aluminum can 7.2 cm in diameter, 18 cm high with a wall thickness of approximately 0.5cm. All six samples were irradiated in the aluminum can at the same time. The powder samples were wrapped in aluminum foil to prevent them from contaminating the single crystal. In each of the six laboratory bottles were placed the same kind of material which composed both the single crystal and powder sample. The water tight aluminum can was lowered into the well of the gamma irradiator shown in Figure 4. Figure 5 shows the



Figure 5



The capsules are 5 inches long and  $\frac{3}{4}$  inches in diameter. The cobalt-60 is encapsulated in an inner packet of welded stainless steel and an outer jacket of welded aluminum. The arrangement shown yields a gamma flux of approximately  $10^7$  roentgens per hour.

general configuration of the cobalt capsules and the position of the aluminum can. The specimens were left in that position for 64 hours and 20 minutes. Immediately following removal from the gamma irradiator, the sealed aluminum sample container was delivered to the Spectrophotometer at Oregon State University. The samples were removed from the aluminum can under dark room conditions to prevent optical bleaching of the specimens. The specimens were maintained at a temperature of  $14^{\circ}\text{C}$  while in the water during irradiation; however, when removed for spectrophotometer reading, some thermal bleaching could have occurred. When the aluminum sample can was opened, a pungent odor was noted. Pressure had apparently changed within the container since a hissing sound could be heard when the top was loosened. Each single crystal specimen was removed from the inner glass sample bottle and optical density measurements were repeated on the same Beckman spectrophotometer used for measurements before gamma irradiation. Report of specific results will be reported in the next section.

#### D. $\gamma$ -Ray Dosimetry

Although specific gamma absorption value could not be determined for each sample irradiated, dose rate determinations were made for the total dose received inside of the aluminum can. To determine the gamma ray dose rate inside of the aluminum can, the

following procedure was used. The aluminum sample holder used for the test specimen was filled with glass wool and in the center was placed a dosimeter vial. The aluminum can was lowered into the bottom of the irradiator well into the  $\text{Co}^{60}$  capsule holder in the same position as when the crystals were irradiated. The aluminum can assembly was left in position for 7.5 minutes, then removed quickly. This procedure was followed twice.

A ceric sulfate solution was used as a chemical dosimeter. The reaction which takes place is a reduction of ceric to cerous ion. The yield is independent of concentration from  $3.2 \times 10^{-2}$  to approximately  $10^{-5}$  M. The yield has also been shown to be independent of energy from about 100 kv x-rays to 2 Mev gamma rays. Dose rates seem to have no effect on the yield from approximately 1/2 r/sec to approximately 500 r/sec. The dose was determined with a ferrous sulfate actinometer using 15.4 mm/1/1,000 rep for the oxidation yield prepared by the Albany Metallurgy Research Center Laboratory.

A weighed quantity of ceric sulfate (reaction grade) was added to 0.8N sulfuric acid and then diluted to volume with 0.8N  $\text{H}_2\text{SO}_4$ . The exact concentration to be used depends upon the total dose to be measured.

Since the cerous ion concentration is determined by difference, it is advantageous to start with a low initial ceric ion concentration. Experience has shown that a concentration change of 30% or more

gives excellent results. The concentration was determined volumetrically against sodium oxalate.

Ceric ion has an absorption maximum at 320 millimicrons in  $\text{H}_2\text{SO}_4$  solution. The absorption maximum is not a broad one and is therefore sensitive to wave length setting. This maximum should be determined for the instrument to be used. The slit width used was 0.5mm. Quartz cells and a hydrogen lamp were used for all determinations. In this case, the ceric ion concentration was determined before and after irradiation and the cerous ion concentration was obtained by difference. A curve of optical density vs ceric ion concentration was used. The concentration is expressed in micromoles per liter. The careful preparation of this calibration curve was the key to the successful use of ceric sulfate as a dosimeter.

The ceric sulfate reduction yield is based upon the ferrous sulfate oxidation yield. If ceric sulfate and ferrous sulfate are subjected to the same irradiation (same energy, dose rate and total dose) and the amount of iron oxidized is compared to amount of cerium reduced, one finds that approximately six times as much iron has reacted as cerium.

Below are the results for the two trial dosimeter vials used in this experiment:



| Dosimeter # | Starting Soln $\mu$ M/l | After Rad* $\mu$ M/l | <sup>+4</sup> Ce Yield $\mu$ M/l | Dose Rate $\times 10^7$ R/HR |
|-------------|-------------------------|----------------------|----------------------------------|------------------------------|
| Ce - 121    | 7600                    | 2360                 | 5240                             | 1.63                         |
| Ce - 122    | 7600                    | 2410                 | 5190                             | 1.62                         |

Sample calculations:

$$\text{Dose rate } \phi = \frac{\text{Ce yield}^{\supset +4}}{\text{**G-factor} \times \text{time}} = \frac{\frac{\mu\text{M/l}}{1000 \text{ RADS}}}{\text{(HRS)}} = \text{RADS/HR.}$$

$$\phi = \frac{(5240)}{(2.58)} / 1000 \times \frac{7.5}{60} = 1.63 \times 10^7 \text{ RADS/HR}$$

\*Ce<sup>+4</sup> con'c determined with Beckman DU Spectrophotometer

\*\* G-factor for ceric sulfate dosimeter = 2.58  $\mu$  M/l  $\cdot$  1000 RAD

Using these dose rate values over a period of 64 hours and 20 minutes, which was the exposure time of the crystals, gives a total dosage of  $1.06 \times 10^9$  roentgens.

## SECTION V

### EXPERIMENTAL RESULTS AND SPECIFIC CONCLUSIONS

Since there are six different materials being reported upon, each one will be discussed separately in this section. As mentioned in the previous section, all specimens received the same experimental processing. It should be noted that an important part of the experimental procedure was the careful exposure of each different

specimen to identical environments. Extreme precautions were taken to reproduce identical events for each specimen, particularly during the irradiations sequence. It was intended to have variability of specimens rather than environmental elements.

#### A. Irradiation Effects on Potassium Sodium Tartrate Tetrahydrate

The first material to be discussed is Potassium Sodium Tartrate Tetrahydrate ( $\text{KNaC}_4\text{H}_4\text{O}_6 \cdot 4\text{H}_2\text{O}$ ). Coolidge and Moore (16, p. 367) reported the decomposition of Rochelle Salt which was exposed to x-rays as evidenced by evolution of gas bubbles when the crystal was warmed to melting. Decomposition was also reported by Zheludev, et al., (16, p. 367). They determined decomposition when irradiated with  $10^5$  r/hr resulting in the emission of gases ( $\text{H}_2$ ,  $\text{CO}$ ,  $\text{CO}_2$ ,  $\text{CH}_4$ ) in amounts of five molecules per 100 ev in addition to change in piezoelectric effects.

For a thorough presentation of the properties and history of Rochelle Salt, the reader should consult the book by W. P. Mason (30). With these reports as a background, it is not surprising to report the crystals of Rochelle Salt were decomposed when removed from the specimen bottle after receiving over a billion roentgen of gamma irradiation. Physical examination of the resulting powder showed a change in color from a dry white powder to a yellow wet paste. The single crystal absorption spectra could not be repeated to

compare its optical absorption curve with the unirradiated specimen. When the glass specimen bottle was opened, an odor could be detected which the author assumes was the emission of gases previously reported by Zheludev. No efforts were taken to collect or analyze gases evolved by the specimens. Single crystal Laue x-ray diffraction photograph could not be repeated due to decomposition of the single crystal. However, the powder specimen which was wrapped in aluminum foil was still intact which permitted a repeat of the powder diffraction photographs.

On the following pages in Tables VI and VII, the powder diffraction laboratory data sheets show the relative intensity of Bragg angle diffraction peaks before and after irradiation. It will be noted that the intensities and "d" spacings are significantly different. To show this change more clearly, Figure 6 shows positive prints of the diffraction patterns before and after irradiation. This change in lattice parameters should be expected based upon the work of Zheludev, who confirmed the loss of molecules from the structure. No attempt was made to analyze the crystal structure during this research sequence due to the complexity and difficulty of such a task. It is interesting to note Rochelle Salt was the only specimen used in this experiment which decomposed, although it possessed structural features found in some of the other crystals in the experiment. For example, the sodium chlorate crystal shows piezoelectric properties but it remained

Table VI

## X-RAY LABORATORY DATA

|  |  |
|--|--|
| Target: CU                                     | Camera: Debye-Scherrer   |
| KV: 35   | Specimen: $\text{KNaC}_4\text{H}_4\text{O}_6 \cdot 4\text{H}_2\text{O}$                                  |
| MA: 18   | Sample Prep: Mortar and pestle   |
| Time: 1.2 hrs.                                 | crushed powder of $\text{KNaC}_4\text{H}_4\text{O}_6 \cdot 4\text{H}_2\text{O}$ , mixed with Duco cement |
| Camera Constant                                | thinned with acetone.  |
| Right Zero = 319.75                            | Condition: Unirradiated  |
| Left Zero = $\frac{93.40}{226.35}$             | Lattice Type: Orthorombic  |
| Corrected R = $\frac{224.94 \text{ R}}{\pi r}$ | Lattice Parameters   |
| = $\frac{0.994 \text{ R}}{}$                   | a = 11.93 A.   |
|  | b = 14.30 A.   |
|  | c = 6.17 A.  |

| Relative Intensity | Reading mm | Net R mm | Corrected R mm | Sin $\Theta$ | Planar Spacing "d" A. |
|--------------------|------------|----------|----------------|--------------|-----------------------|
| W                  | 74.35      | 19.05    | 18.90          | 0.13156      | 5.8430                |
| VS                 | 72.40      | 21.00    | 20.80          | 0.14470      | 5.3124                |
| W                  | 68.30      | 25.10    | 24.90          | 0.17296      | 4.4444                |
| S                  | 66.80      | 26.60    | 26.40          | 0.18464      | 4.1632                |
| S                  | 63.10      | 30.30    | 30.10          | 0.20859      | 3.6852                |
| S                  | 62.35      | 31.05    | 30.80          | 0.21337      | 3.6027                |
| W                  | 57.85      | 35.55    | 35.30          | 0.24395      | 3.1511                |
| S                  | 55.55      | 37.85    | 37.60          | 0.25949      | 2.9623                |
| W                  | 54.20      | 39.20    | 38.90          | 0.26825      | 2.8656                |
| VS                 | 51.55      | 41.85    | 41.50          | 0.28569      | 2.6907                |
| VS                 | 48.35      | 45.05    | 44.70          | 0.30702      | 2.5037                |
| W                  | 46.20      | 47.20    | 46.90          | 0.32160      | 2.3902                |
| M                  | 44.20      | 49.20    | 48.90          | 0.33479      | 2.2961                |
| M                  | 43.00      | 50.40    | 50.00          | 0.34202      | 2.2475                |
| W                  | 41.65      | 51.75    | 51.40          | 0.35119      | 2.1888                |
| W                  | 40.70      | 52.70    | 52.30          | 0.35706      | 2.1529                |
| M                  | 37.95      | 55.45    | 55.00          | 0.37461      | 2.0520                |
| W                  | 36.40      | 57.00    | 56.60          | 0.38494      | 1.9969                |
| VW                 | 34.10      | 59.30    | 58.90          | 0.39971      | 1.9231                |
| VW                 | 31.70      | 61.70    | 61.30          | 0.41501      | 1.8522                |
| VW                 | 29.90      | 63.50    | 63.10          | 0.42641      | 1.8027                |
| VW                 | 28.20      | 65.20    | 64.80          | 0.43712      | 1.7586                |



Table VII

## X-RAY LABORATORY DATA

Target: CU  
 KV: 35  
 MA: 18  
 Time: 2.0 hours

Camera Constant

Right Zero = 316.00

Left Zero = 89.55

$r = 226.45$

Corrected R = 224.94 R

$\pi r$

= 0.994 R

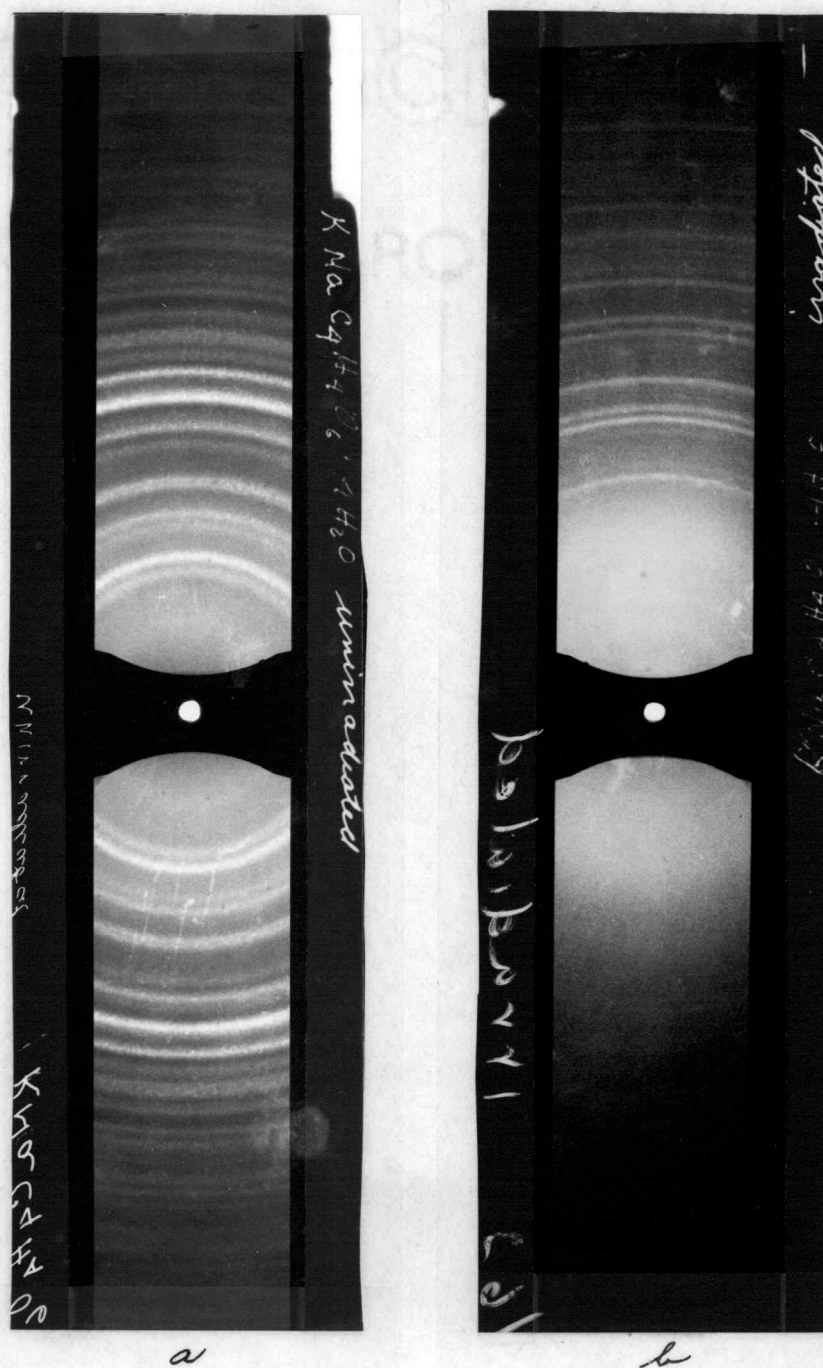
Camera: Debye-Scherrer  
 Specimen:  $\text{KNaC}_4\text{H}_4\text{O}_6 \cdot 4\text{H}_2\text{O}$   
 Sample Prep: Mortar and pestle  
 crushed powder of  $\text{KNaC}_4\text{H}_4\text{O}_6 \cdot 4\text{H}_2\text{O}$  mixed with Duco cement  
 thinned with acetone.

Condition: Irradiated

Lattice Type: Unconfirmed

| Relative<br>Intensity | Reading<br>mm | Net<br>R<br>mm | Corrected<br>R<br>mm | Sin $\Theta$ | Planar<br>Spacing<br>"d" A. |
|-----------------------|---------------|----------------|----------------------|--------------|-----------------------------|
| M                     | 58.20         | 31.35          | 31.10                | 0.21542      | 3.5684                      |
| VVW                   | 56.60         | 32.95          | 32.70                | 0.22631      | 3.3967                      |
| VVW                   | 52.20         | 37.35          | 37.00                | 0.25545      | 3.0092                      |
| VS                    | 50.65         | 38.90          | 38.60                | 0.26623      | 2.8874                      |
| S                     | 49.10         | 40.45          | 40.10                | 0.27631      | 2.7820                      |
| VVW                   | 47.15         | 42.40          | 42.10                | 0.28970      | 2.6534                      |
| S                     | 45.45         | 44.10          | 43.80                | 0.30104      | 2.5535                      |
| W                     | 39.50         | 50.05          | 49.70                | 0.34005      | 2.2605                      |
| M                     | 37.45         | 52.15          | 51.80                | 0.35380      | 2.1727                      |
| M                     | 32.60         | 56.95          | 56.50                | 0.38430      | 2.0003                      |
| VW                    | 30.70         | 59.85          | 59.40                | 0.40291      | 1.9079                      |
| VW                    | 28.70         | 60.85          | 60.40                | 0.40929      | 1.8781                      |
| VVW                   | 26.30         | 63.25          | 62.80                | 0.42452      | 1.8108                      |
| VVW                   | 22.70         | 67.85          | 67.40                | 0.45337      | 1.6955                      |
| VVW                   | 20.35         | 69.20          | 68.70                | 0.46144      | 1.6659                      |
| VVW                   | 12.50         | 77.05          | 76.50                | 0.50904      | 1.5101                      |

Figure 6

Powder Patterns of  $\text{KNaC}_4\text{H}_4\text{O}_6 \cdot 4\text{H}_2\text{O}$ 

- (a) Shows powder sample unirradiated,
- (b) Same powder sample irradiated with  $\text{Co}^{60}$  gamma rays.

in its original crystalline structure. The alums are double salts like Rochelle Salt but they retained original crystal properties.

B. Irradiation Effects on Potassium Chromium Sulfate Dodecahydrate

The second crystal to be discussed is the double salt, Potassium Chromium Sulfate Dodecahydrate ( $\text{KCr}(\text{SO}_4)_2 \cdot 12\text{H}_2\text{O}$ ). This material, as mentioned previously, was purple colored in its natural growth form. After irradiation, it appeared to darken and become more opaque. The general macroscopic appearance of the specimen such as size and shape did not change. A polished specimen, measuring 7 mm square and 4 mm thick, was placed in the DU Beckman spectrophotometer before and after irradiation with gamma rays. Figure 7 shows the optical density vs. wave length before gamma irradiation with the incident light transmitted through the 7 mm thickness of the crystal. Small absorption peaks can be observed in the infrared region at 1000 millimicrons and at 1250 millimicrons. A rather narrow, high intensity absorption peak was also measured at 330 millimicrons. In the short wave ultra violet region, general absorption occurs. After the crystal received gamma irradiation, its greatly increased absorption properties prevented the measurement of light transmittance by the spectrophotometer. The crystal was thinned by wet polishing the specimen to a thickness of 1.75 mm. The final specimen measured 7 mm square with a thickness of 1.75 mm.

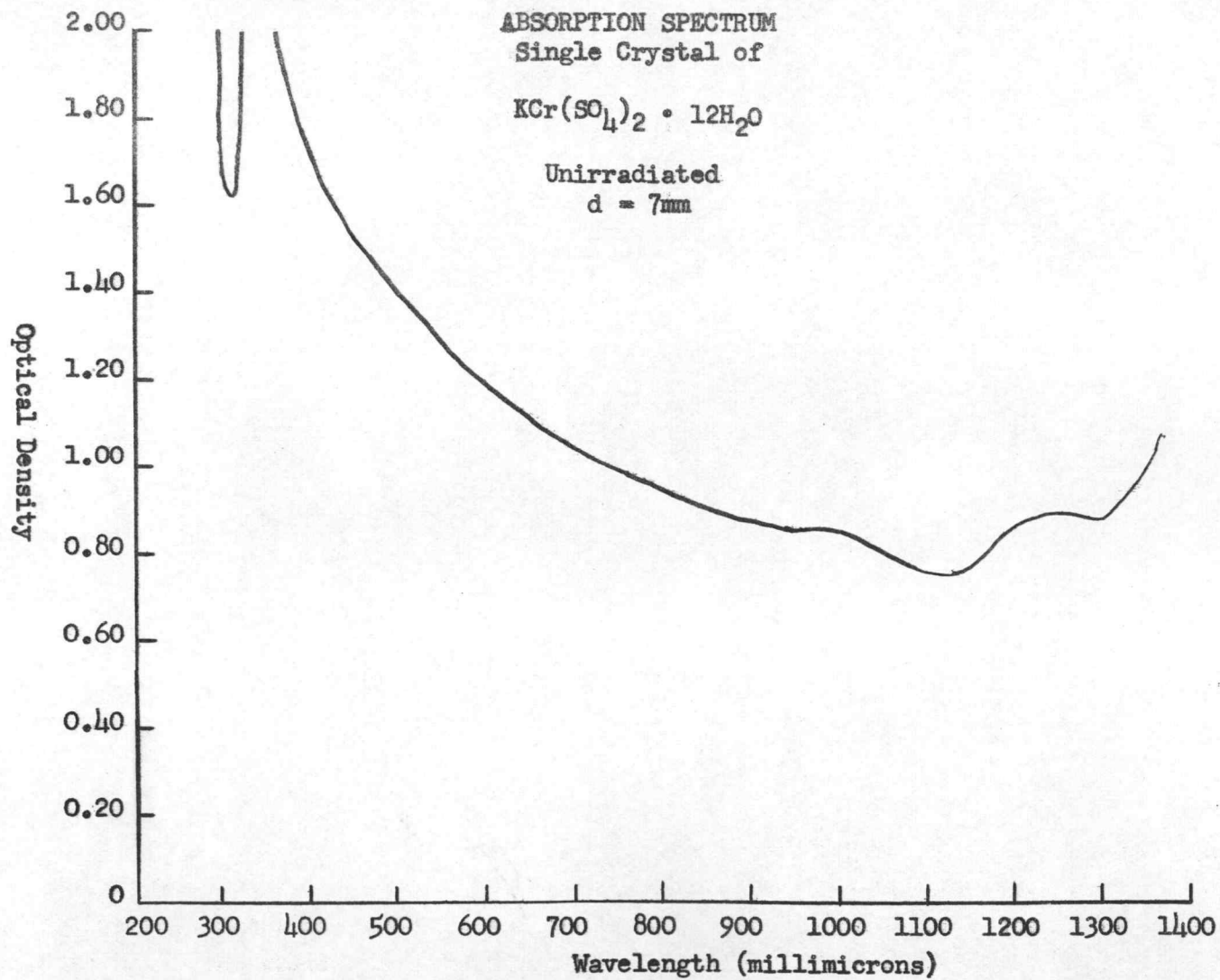


Figure 7



The light waves were transmitted through the thinned dimension which produced the absorption spectra noted in Figure 8. Here again it will be noted that the absorption peaks at 1000 millimicrons and 1250 millimicrons are present. However, absorption starts at 750 millimicrons which causes a disappearance of the 330 millimicrons band. The gamma irradiation has produced a broad absorption band starting in the visible range. This indicates lower energy absorption centers have been produced and are present in the crystal, probably as trapped electrons in lattice defects.

Visual inspection of the crystal showed a significant darkening of the crystal. Other macroscopic physical properties which could be judged by visual observation appeared unchanged.

The crystal was then analyzed by x-ray diffraction techniques. Figure 9 shows the Laue transmission patterns before and after gamma irradiation. Although there is a slight change in the orientation of the crystal with reference to the x-ray beam, the pattern does not show crystal distortions or change. Figure 10 shows the powder diffraction pattern of the specimen before and after gamma exposure. Table VIII and IX provide the powder pattern laboratory data to determine the planar spacings shown by the Bragg angles. Both the powder pattern photograph and the data support the probability of structural change within the crystal. In view of the optical absorption data, the transmission patterns and the powder patterns, it appears a uniform

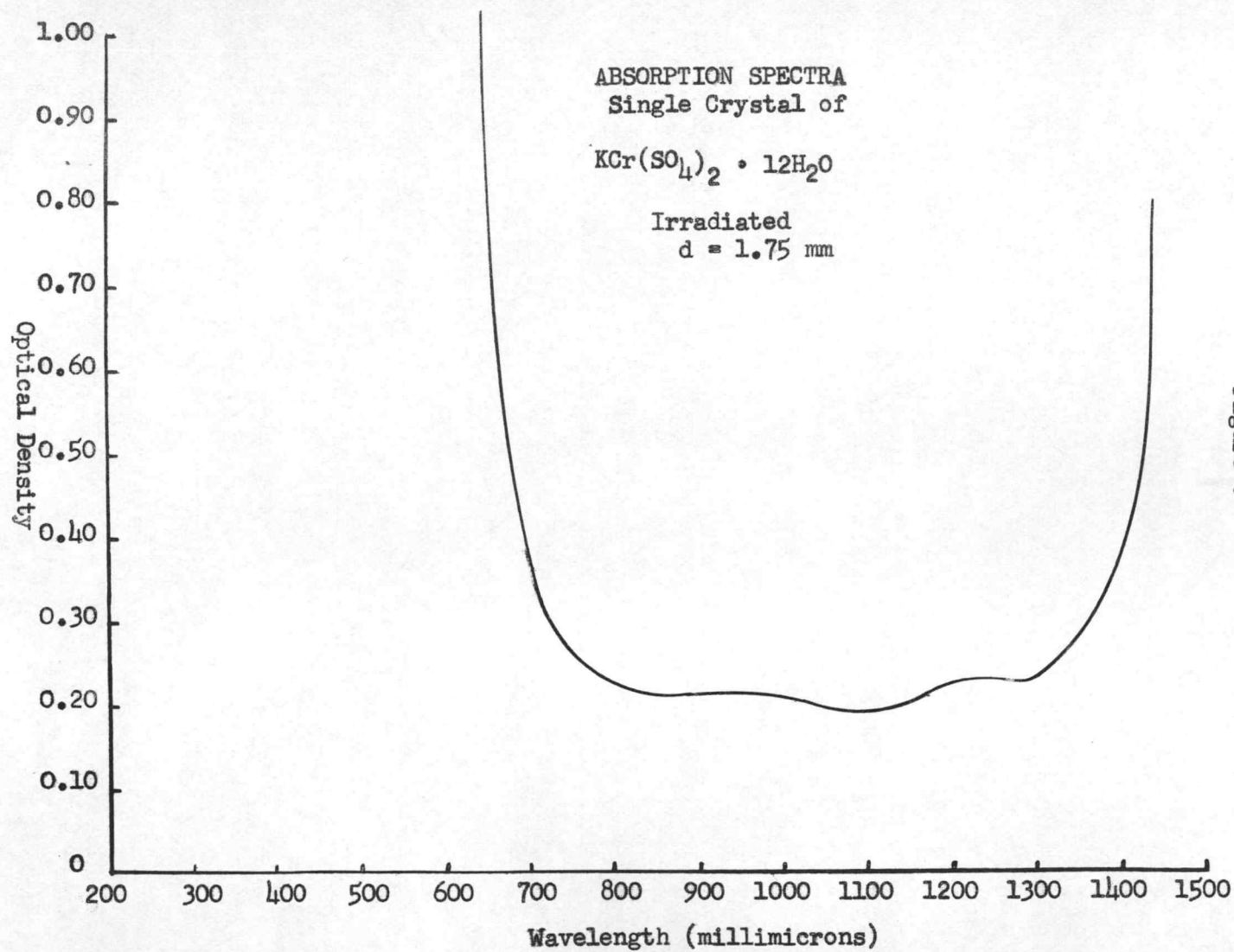
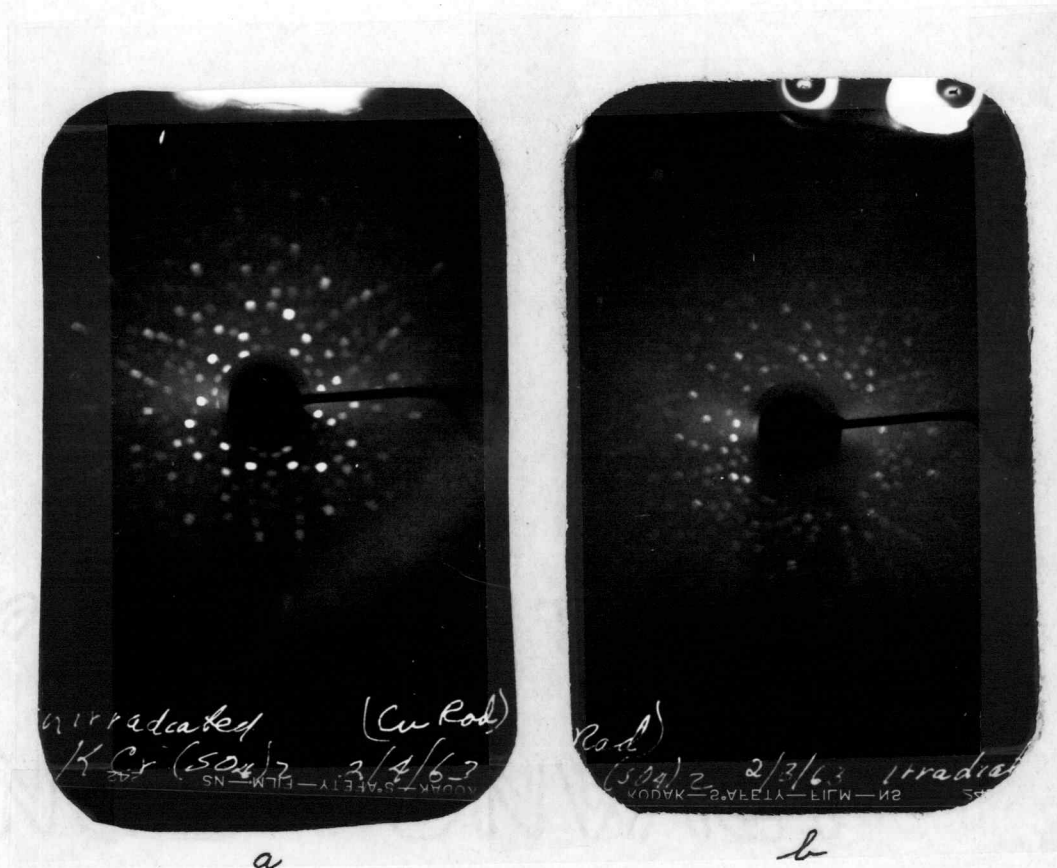


Figure 8

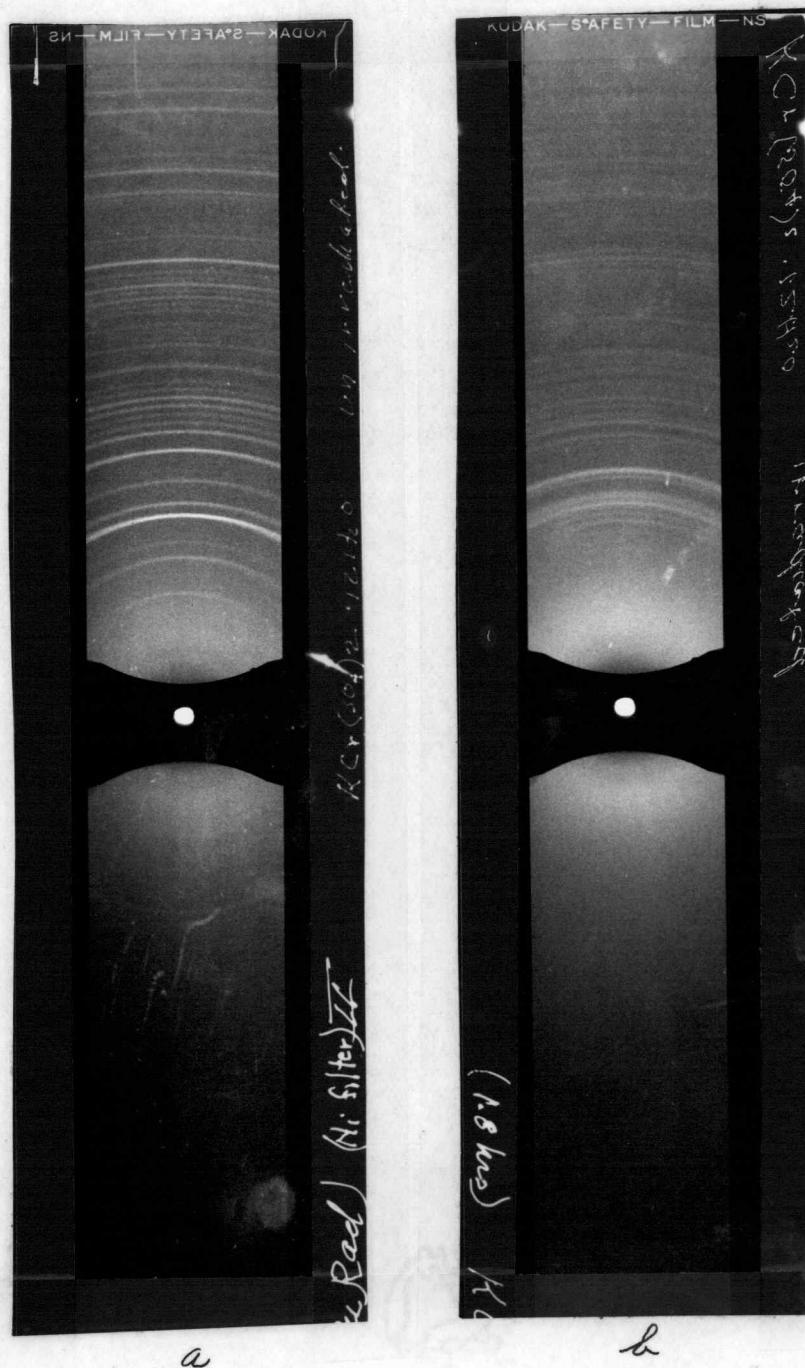
Figure 9



Laue X-Ray Transmission Photograph  
Single Crystal of  $\text{KCr}(\text{SO}_4)_2 \cdot 12\text{H}_2\text{O}$

- (a) Unirradiated, and
- (b) Irradiated with gamma rays from  $\text{Co}^{60}$ .

Figure 10



Powder Patterns of  $\text{KCr}(\text{SO}_4)_2 \cdot 12\text{H}_2\text{O}$

- (a) Shows powder sample unirradiated,
- (b) Same powder sample irradiated with Co<sup>60</sup> gamma rays.

ADVANCE BOND



Table VIII

## X-RAY LABORATORY DATA

|  |  |
|--|--|
| Target: CU                             | Camera: Debye-Scherrer   |
| KV: 35                                 | Specimen: $\text{KCr}(\text{SO}_4)_2 \cdot 12\text{H}_2\text{O}$   |
| MA: 18                                 |  |
| Time: 1.8 hrs.                         | Sample Prep: Mortar and pestle<br>crushed powder of $\text{KCr}(\text{SO}_4)_2 \cdot 12\text{H}_2\text{O}$ , mixed with Duco cement<br>thinned with acetone. |
| Camera Constant                        | Condition: Unirradiated  |
| Right Zero = 317.35                    | Lattice Type: Cubic  |
| Left Zero = 90.35                      |  |
| $r = 227.00$                           |  |
| Corrected R = $\frac{224.94}{\pi r}$ R | Lattice parameter  |
| $= 0.992$ R                            | $a = 12.133 \text{ \AA}$ .   |

| Relative Intensity | Reading mm | Net R mm | Corrected R mm | Sin $\Theta$ | Planar Spacing "d" A. |
|--------------------|------------|----------|----------------|--------------|-----------------------|
| M                  | 69.30      | 21.05    | 20.85          | 0.14470      | 5.3124                |
| W                  | 67.15      | 23.20    | 23.00          | 0.15988      | 4.8080                |
| S                  | 63.65      | 26.70    | 26.45          | 0.18327      | 4.2102                |
| S                  | 61.95      | 28.40    | 28.18          | 0.19492      | 3.9437                |
| S                  | 55.10      | 35.25    | 34.95          | 0.24124      | 3.1865                |
| M                  | 52.60      | 37.75    | 37.40          | 0.25814      | 2.9778                |
| W                  | 51.50      | 38.85    | 38.55          | 0.26556      | 2.8946                |
| W                  | 50.25      | 40.10    | 39.75          | 0.27362      | 2.8094                |
| M                  | 49.20      | 41.15    | 40.70          | 0.28100      | 2.7421                |
| W                  | 48.20      | 42.15    | 41.80          | 0.28769      | 2.6720                |
| VW                 | 46.95      | 43.40    | 43.00          | 0.29571      | 2.5995                |
| VW                 | 46.00      | 44.35    | 43.95          | 0.30171      | 2.5479                |
| VW                 | 44.10      | 46.25    | 45.85          | 0.31432      | 2.4456                |
| VW                 | 42.25      | 48.10    | 47.65          | 0.32623      | 2.3563                |
| VW                 | 41.30      | 49.05    | 48.65          | 0.33282      | 2.3097                |
| VW                 | 39.40      | 50.95    | 50.50          | 0.34530      | 2.2262                |
| VW                 | 38.40      | 51.95    | 51.50          | 0.35184      | 2.1848                |
| VW                 | 35.90      | 54.45    | 54.00          | 0.36812      | 2.0882                |
| VW                 | 33.35      | 57.00    | 56.50          | 0.38430      | 2.0003                |
| VW                 | 31.90      | 58.45    | 57.50          | 0.39073      | 1.9673                |
| W                  | 30.15      | 60.20    | 59.70          | 0.40482      | 1.8989                |
| VVW                | 28.10      | 62.25    | 61.70          | 0.41755      | 1.8410                |
| VVW                | 18.50      | 71.85    | 71.20          | 0.47685      | 1.6120                |
| VVW                | 10.25      | 80.10    | 79.40          | 0.52636      | 1.4604                |
| VVW                | 7.70       | 82.85    | 81.80          | 0.54053      | 1.4221                |

Table IX

## X-RAY LABORATORY DATA

|                                    |   |
|------------------------------------|---|
| Target: CU                         | Camera: Debye - Scherrer  |
| KV: 35                             | Specimen: $\text{KCr}(\text{SO}_4)_2 \cdot 12\text{H}_2\text{O}$                                  |
| MA: 18                             | Sample Prep: Mortar and pestle  |
| Time: 1.8 hrs.                     | crushed powder of $\text{KCr}(\text{SO}_4)_2 \cdot 12\text{H}_2\text{O}$ , mixed with Duco cement |
| Camera Constant                    | thinned with acetone.   |
| Right Zero = 316.87                | Condition: Irradiated   |
| Left Zero = 90.25                  |   |
| $r = 226.62$                       | Lattice Type: Unconfirmed.  |
| Corrected R = $\frac{224.94}{r}$ R |   |
| $= 0.993$ R                        |   |

| Relative Intensity | Reading mm | Net R mm | Corrected R mm | Sin $\Theta$ | Planar Spacing "d" A. |
|--------------------|------------|----------|----------------|--------------|-----------------------|
| VW                 | 65.30      | 24.95    | 24.75          | 0.17159      | 4.4799                |
| VW                 | 64.30      | 25.95    | 25.95          | 0.17846      | 4.3074                |
| S                  | 63.10      | 27.15    | 26.95          | 0.18670      | 4.1173                |
| M                  | 61.95      | 28.30    | 28.10          | 0.19492      | 3.9437                |
| S                  | 59.60      | 30.65    | 30.45          | 0.21064      | 3.6494                |
| VS                 | 58.75      | 31.50    | 31.25          | 0.31610      | 3.5571                |
| W                  | 55.00      | 35.25    | 35.00          | 0.24192      | 3.1775                |
| S                  | 54.30      | 35.95    | 35.70          | 0.24666      | 3.1164                |
| S                  | 52.50      | 37.75    | 37.50          | 0.25882      | 2.9700                |
| S                  | 51.20      | 39.05    | 38.75          | 0.26690      | 3.8801                |
| S                  | 50.30      | 39.75    | 39.45          | 0.27161      | 2.8302                |
| S                  | 49.40      | 40.85    | 40.55          | 0.27899      | 2.7553                |
| W                  | 47.25      | 43.00    | 42.70          | 0.29371      | 2.6172                |
| VW                 | 45.40      | 44.85    | 44.50          | 0.30570      | 2.5146                |
| VW                 | 43.20      | 47.05    | 46.70          | 0.32039      | 2.4001                |
| M                  | 38.80      | 51.45    | 51.10          | 0.34923      | 2.2011                |
| W                  | 32.50      | 57.75    | 57.35          | 0.38945      | 1.9738                |
| W                  | 31.80      | 58.45    | 58.05          | 0.39394      | 1.9513                |
| W                  | 31.10      | 59.15    | 58.75          | 0.39843      | 1.9293                |
| W                  | 30.10      | 60.15    | 59.70          | 0.40482      | 1.8989                |

crystallographic change has occurred which has changed the optical density of the specimen and produced color centers. The powder diffraction line positions, grouping and number, suggest the probability of a cubic or hexagonal structure. No attempt was made by the author to analyze the structure for this research thesis. The increased absorption in the crystal suggests the presence of color centers similar to those reported in the alkali halides. The absorption band starting at 750 millimicrons corresponds to the energy region approximately 1.75 to 2.75 ev, expected for trapped electrons in the alkali halides. If we make this assumption, then it can be concluded the gamma photons have ionized electrons within the crystal which have assumed positions in a lattice defect, or have combined with a positive hole. An electron is said to be trapped when it assumes a metastable position with potential energy between the conduction state and ground state. Electrons may become trapped in a number of ways, such as in vacancies, lattice imperfections or impurities. There is a characteristic energy which is required to activate an electron to free it from the trapped position. When an electron is released back into the conduction band it may become trapped again or it may return to the ground state, yielding a quantum of light.

The Laue transmission photograph indicates there has not been extensive crystal displacement which could have caused lattice disorientation or warping. However, the powder patterns shows a change

in planar spacing and probable atomic displacement. The new line positions can be caused by new lattice geometry brought about by different atom positions or the loss of atoms from the crystal. The change in line intensities indicates a change in atom location or possibly the loss of atoms. The new crystal structure is uniform and continues with normal perfection characteristics as indicated by the Laue pattern. From this it can be concluded the gamma irradiation has produced a change in the crystal structure by causing a displacement of atoms and possibly the decomposition of molecules. Both of these events produce vacancies and interstitials which change the properties of the crystal and furnish traps for electrons. There is an excellent probability the density has decreased, hardness has increased and electronic properties have changed. Each of these properties should be investigated to support the reported data. Further research is planned by the author on these properties for the materials used in this report.

### C. Irradiation Effects on Sodium Chlorate

The results of the optical absorption spectra for  $\text{NaClO}_3$  before gamma irradiation are shown in Figure 11. In the infrared region absorption peaks can be observed at 2600 millimicrons, 1925 millimicrons and 1425 millimicrons. No other significant absorption variations were noted until typical end absorption started in the ultra



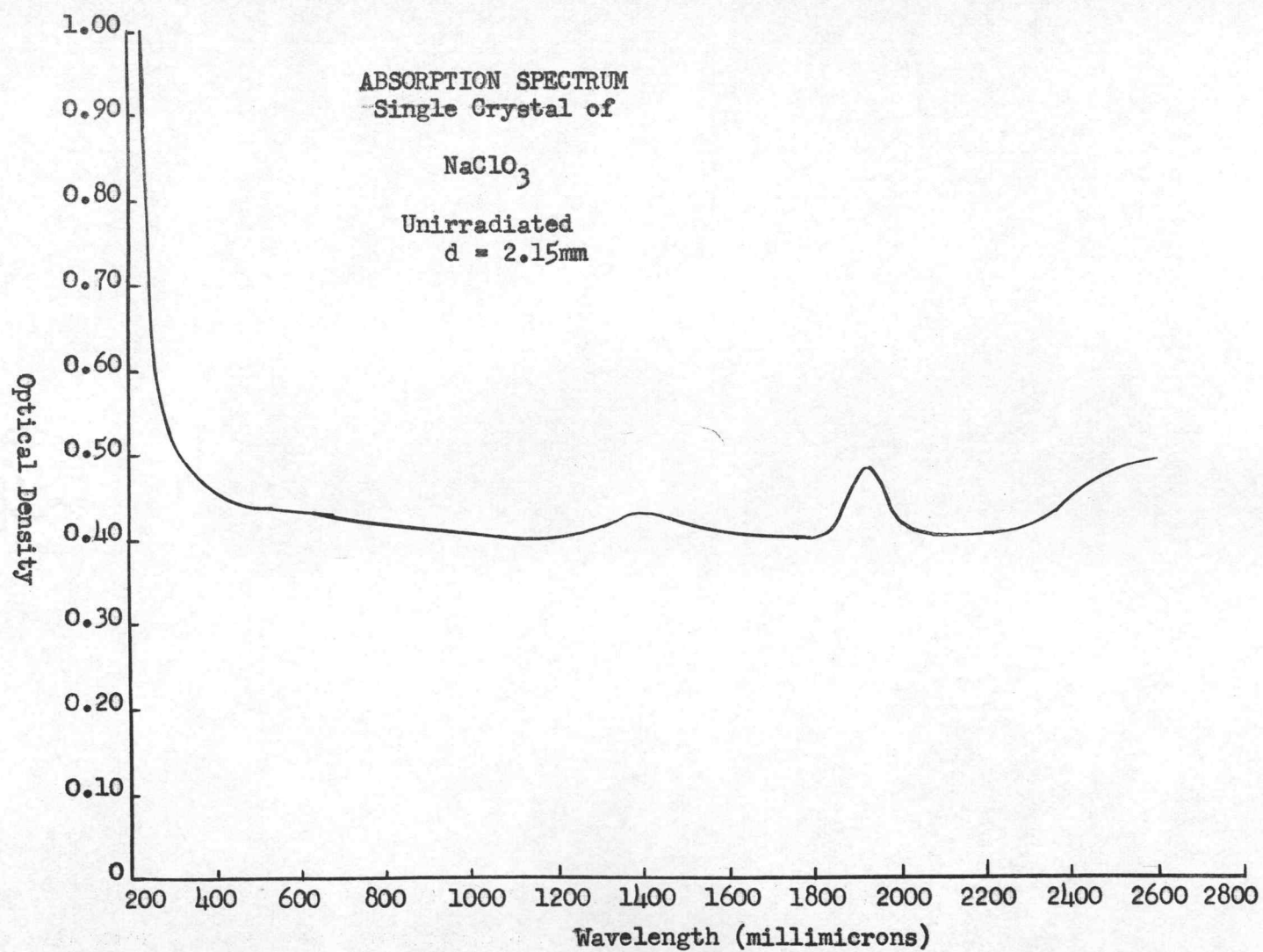


Figure 11

violet region. Figure 12 shows the same crystal after exposure to over  $1.06 \times 10^9$  roentgens of ionizing gamma radiation. The peaks at 2600 millimicrons, 1925 millimicrons and 1425 millimicrons have been flattened. End absorption begins at 900 millimicrons as a result of irradiation. This absorption appears to have been caused by the development of color centers in the crystal. Visual inspection of the specimen discloses a change from a clear transparent crystal to a yellow colored crystal. The single crystal of  $\text{NaClO}_3$  was cut and wet polished in the same way as the other crystal specimens to provide a transmission thickness of 2.15 mm for both readings. The specimen was 7 mm square to fit in spectrophotometer apparatus. Since Sodium Chlorate has piezoelectric properties ionic conductivity was measured as an added bonus item to investigate during this experiment. This phase of experimentation is reported at this time without preliminary discussion since it was an unscheduled addition to this single specimen for general knowledge rather than a preplanned sequence of this thesis. The results noted may provide some information for others investigating this crystal.

A stainless steel cryostat shown in Figure 13 was part of the laboratory equipment used as a sample holder capable of holding the sample at any desired temperature from  $200^\circ\text{C}$  to  $-180^\circ\text{C}$ . The cryostat was mounted in the sample chamber of the spectrophotometer. The crystal was mounted on a copper block having a square hole

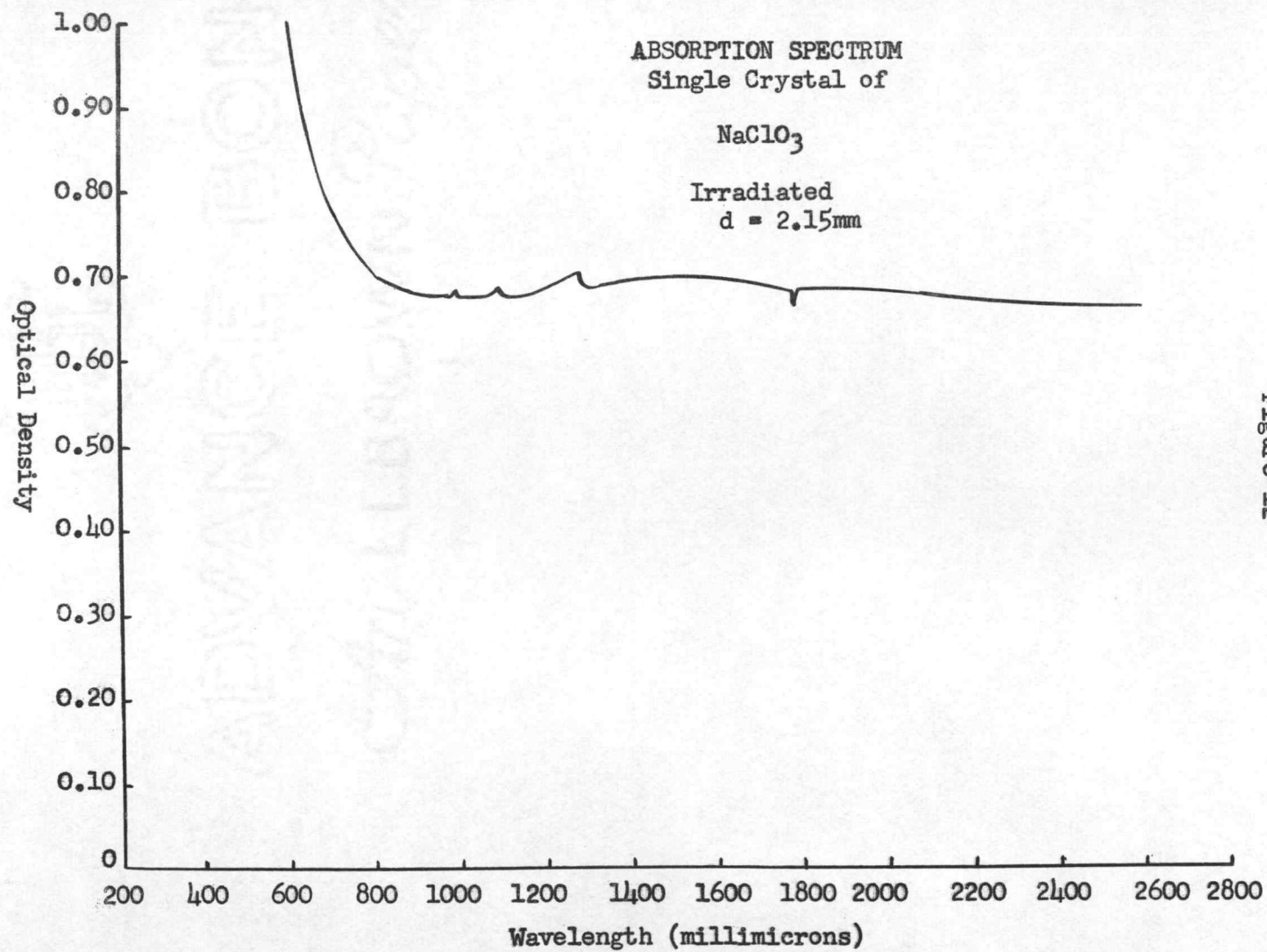
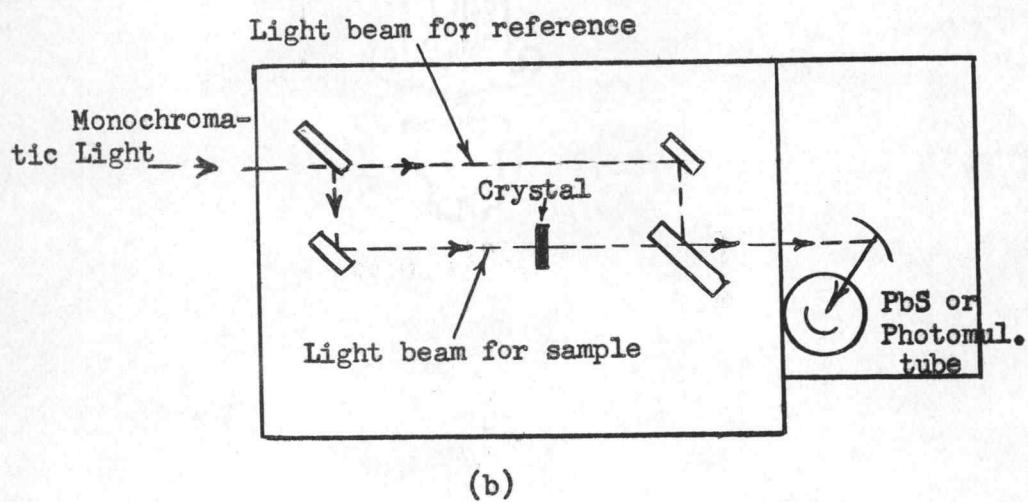
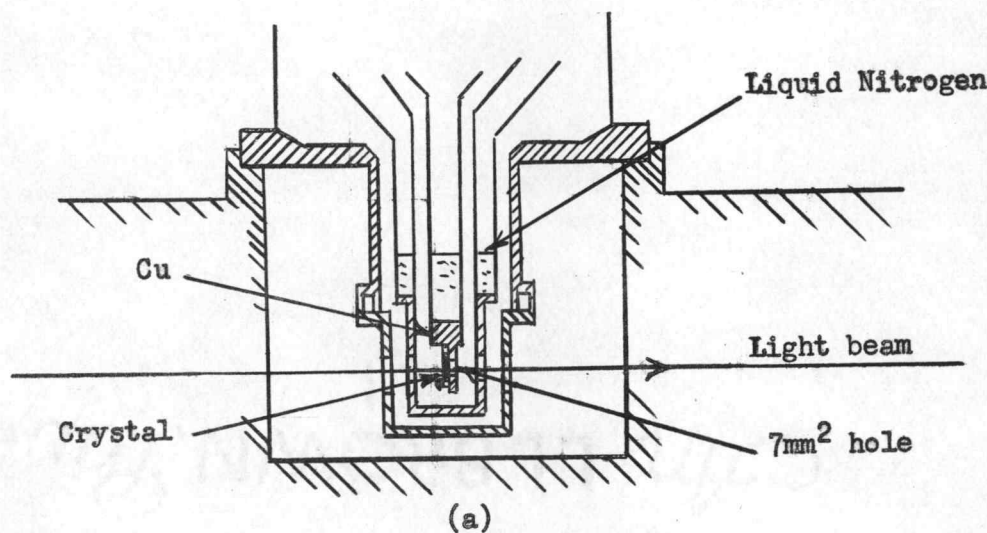


Figure 12

Figure 13



Experimental arrangement. (a): Sample holder

(b): Path of measuring and reference light beams.

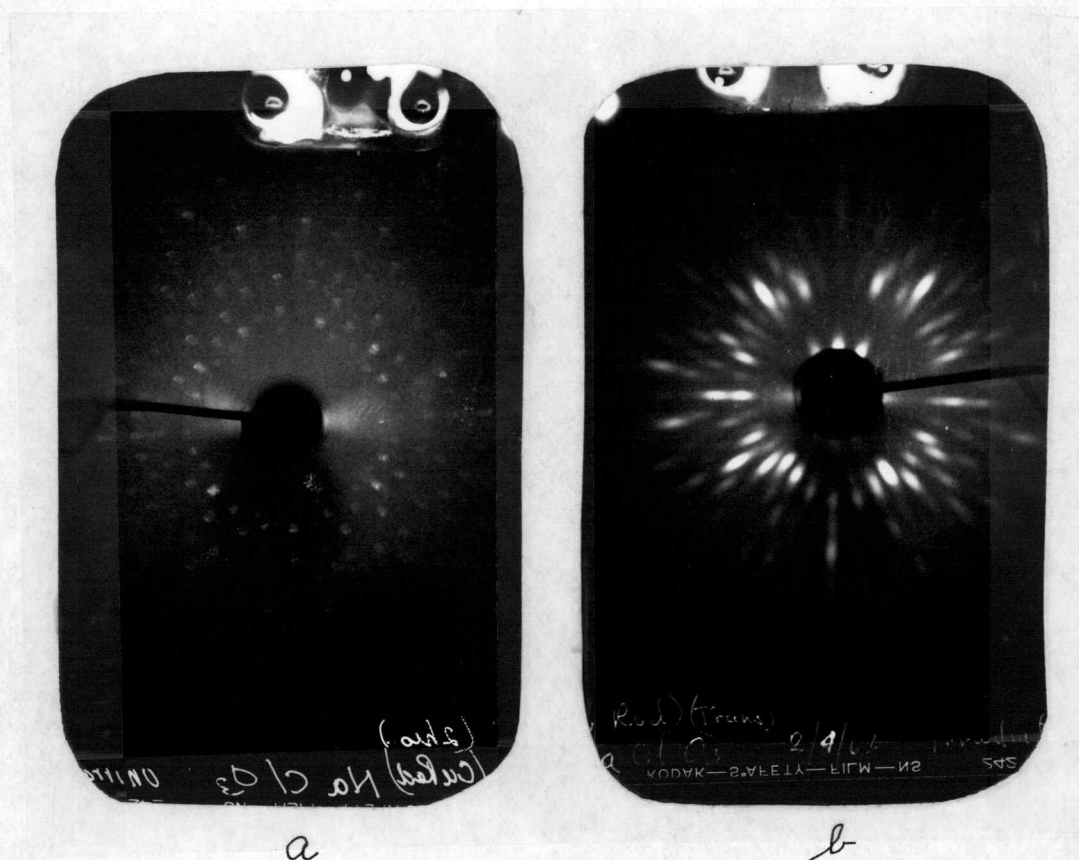


7 X 7mm<sup>2</sup> area for the conductivity measurements. The temperature of the crystal was measured by a copper-tungsten thermocouple which was attached at the bottom of the copper block. The ionic conductivity measurements were carried out at liquid nitrogen temperature under approximately  $10^{-3}$  mm hg vacuum and recorded on a Cary 31 vibrating reed electrometer. Before irradiation of the specimen, there was no change in the ionic conductivity with an increase in temperature. Measurements were taken at approximately 30°C intervals from -180°C to room temperature. The same crystal under the same experimental condition after gamma irradiation was again checked for conductivity. As before, readings were taken from -180°C to room temperature at the same temperature intervals. After irradiation, there was a uniform increase in ionic conductivity. This ionic conductivity is not in agreement with previously stated investigations by Nelson and Sproull on alkali halides. Ionic conductivity is an indication of the presence and mobility of positive ion vacancy. On the basis of ionic conductivity studies and density measurements, it is generally believed that in pure alkali halides the most common lattice vacancies are Schottky defects. From the results of this experiment showing a positive change in ionic conductivity in the specimen after gamma exposure should suggest the production of positive ion vacancies.

The crystal was further investigated by Laue x-ray transmission

and powder technique as had the other specimens. Figure 14 shows the Laue transmission patterns before and after gamma irradiation. It should be noted a rather dramatic change has taken place within the crystal to produce distortion of the Laue spots. This elongation, usually referred to as asterism, is evidence of lattice bending, polygonization or mosaic distortion. The probable cause and changes within the lattice have been discussed previously on page 23 of this thesis. These Laue photographs add further evidence to the optical absorption spectra, ionic conductivity and color change of the crystal to suggest the probability of the production of lattice defects similar to those reported in pure alkali halides. The powder diffraction patterns can be seen in Figure 15 and the calculated data is shown in Table X. The line locations and "d" spacings were the same before and after gamma irradiation. This shows that the lattice parameters and crystal shape and general atom orientation have not been changed. The line intensities and identification of (h k l) planes were compared and agreed with those reported by Frevel (41, p. 81). There was a noticeable decrease in over all line intensity in the back reflection region of the irradiated powder pattern. This is an indication of a change in atoms position such as interstitials. In the forward reflection region of the powder pattern, there was a general increase of line intensity which could indicate lattice vacancies. The conclusion stated for the previous specimen can also be applied to this crystal.

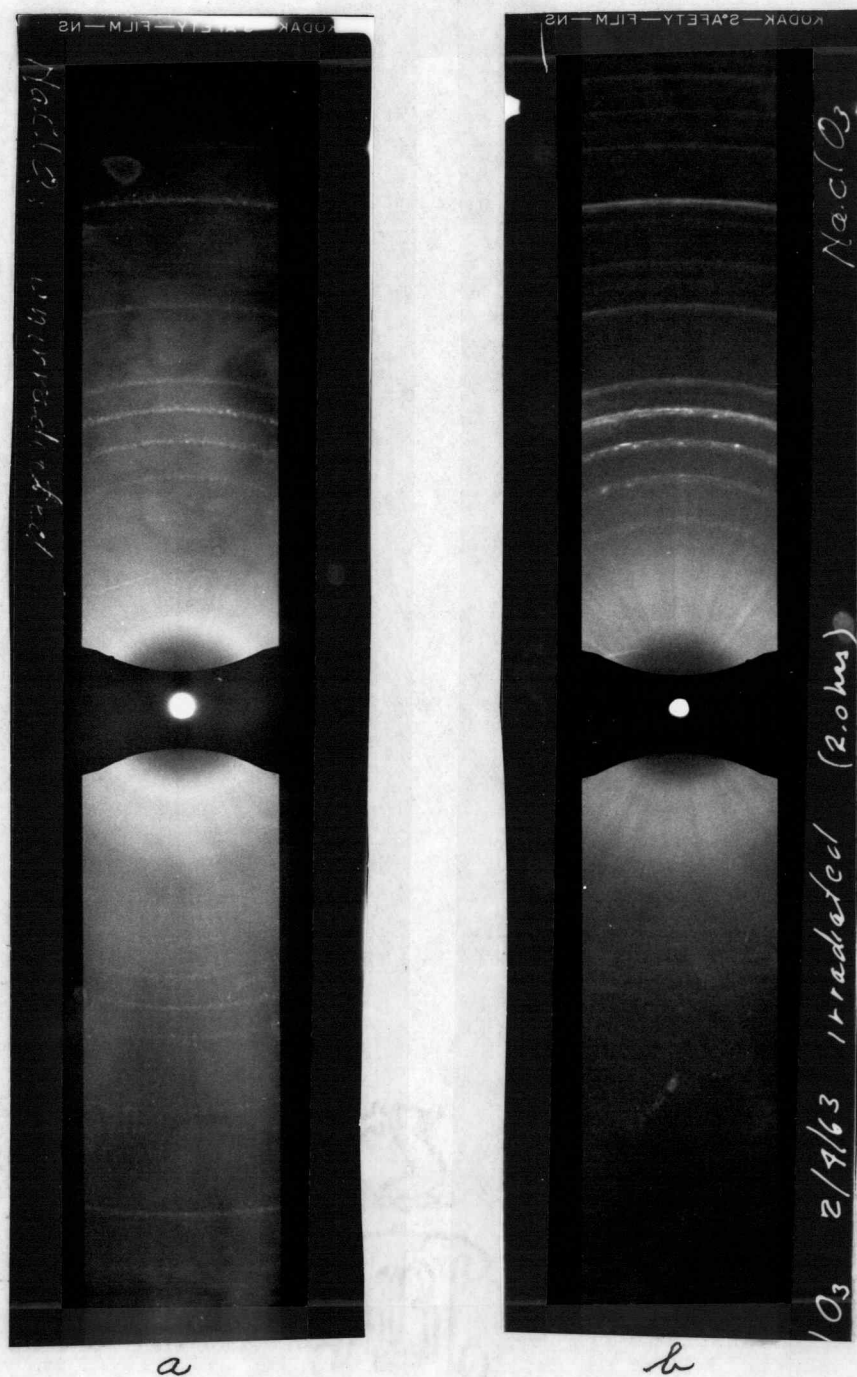
Figure 14



Laue X-Ray Transmission Photograph  
Single Crystal of  $\text{NaClO}_3$

- (a) Unirradiated, and
- (b) Irradiated with  $1.06 \times 10^9$  roentgens of gamma rays.

Figure 15

X-Ray Diffraction Powder Pattern of  $\text{NaClO}_3$ 

- (a) Shows powder sample unirradiated,
- (b) Same powder sample irradiated with gamma rays.



Table X

## X-RAY LABORATORY DATA

|  |   |
|--|---|
| Target: CU                             | Camera: Debye - Scherrer  |
| KV: 35                                 | Specimen: NaClO <sub>3</sub>  |
| MA: 18                                 |   |
| Time: 1.2 hrs.                         | Sample Prep: Mortar and pestle<br>crushed powder of NaClO <sub>3</sub> , mixed<br>with Duco cement thinned with<br>acetone. |
| Camera Constant                        | Condition: Irradiated and Unirradi-<br>ated pattern readings are the<br>same.   |
| Right Zero = 322.10                    |   |
| Left Zero = 95.20                      |   |
| $r = 226.90$                           |   |
| Corrected R = $\frac{224.94}{\pi r}$ R | Lattice Type: Cubic   |
| = 0.992 R                              | Lattice Parameter<br>$a = 6.57 \text{ \AA}$ .   |

| Relative Intensity | Reading mm | Net R mm | Corrected R mm | Sin $\Theta$ | Planar Spacing "d" A. |
|--------------------|------------|----------|----------------|--------------|-----------------------|
| M                  | 70.00      | 25.20    | 25.00          | 0.17365      | 4.4267                |
| M                  | 64.65      | 30.55    | 30.20          | 0.20938      | 3.6731                |
| S                  | 59.80      | 35.40    | 35.10          | 0.24260      | 3.1686                |
| VS                 | 55.85      | 39.35    | 39.00          | 0.26892      | 2.8585                |
| S                  | 51.95      | 43.25    | 42.90          | 0.29504      | 2.6054                |
| W                  | 42.10      | 53.10    | 52.60          | 0.35902      | 2.1411                |
| VVW                | 39.15      | 56.05    | 55.60          | 0.37849      | 2.0310                |
| VVW                | 36.45      | 58.75    | 58.30          | 0.39587      | 1.9418                |
| VVW                | 33.65      | 61.55    | 61.10          | 0.41374      | 1.8579                |
| VW                 | 31.10      | 64.10    | 63.60          | 0.42957      | 1.7895                |
| S                  | 28.50      | 66.70    | 66.20          | 0.44589      | 1.7240                |
| W                  | 21.20      | 74.00    | 73.40          | 0.49030      | 1.5628                |
| W                  | 18.90      | 71.30    | 75.60          | 0.50362      | 1.5263                |
| VW                 | 16.50      | 78.70    | 78.00          | 0.51803      | 1.4839                |
| VVW                | 14.40      | 80.80    | 80.10          | 0.53051      | 1.4490                |
| VW                 | 12.15      | 83.05    | 82.30          | 0.54347      | 1.4144                |
| VVW                | 10.00      | 85.20    | 84.40          | 0.55572      | 1.3832                |

#### D. Irradiation Effects on Sodium Nitrate

The fourth crystal which will be discussed is Sodium Nitrate,  $\text{NaNO}_3$ . Figure 16 shows the spectrophotometer absorption pattern before irradiation with gamma rays. Two significant absorption bands can be observed at approximately 2600 millimicrons and 2400 millimicrons followed by a series of narrow bands at 2200 millimicrons, 2050 millimicrons and 1975 millimicrons. A broad absorption zone of low intensity should be noted between 1100 millimicrons and 1900 millimicrons. Finally, the typical end absorption noted in all the other crystals starts at approximately 600 millimicrons with no transmission in the ultra violet region. The  $\text{NaNO}_3$  single crystal was cut and wet polished to fit the spectrophotometer. The absorption was recorded after transmission through 3mm of the single crystal. The crystal was transparent and colorless during the first optical density measurement prior to exposure to gamma rays. Figure 17 shows the optical density as a function a wave length after the crystal specimen was irradiated. The same transmission thickness was used as before for absorption measurements. The high intensity narrow absorption bands in the infrared region at 2600 millimicrons and 2400 millimicrons were again recorded with essentially the same relative intensity as originally. The other three lower intensity peaks at 2200 millimicrons, 2050 millimicrons, and 1975 millimicrons were also reproduced

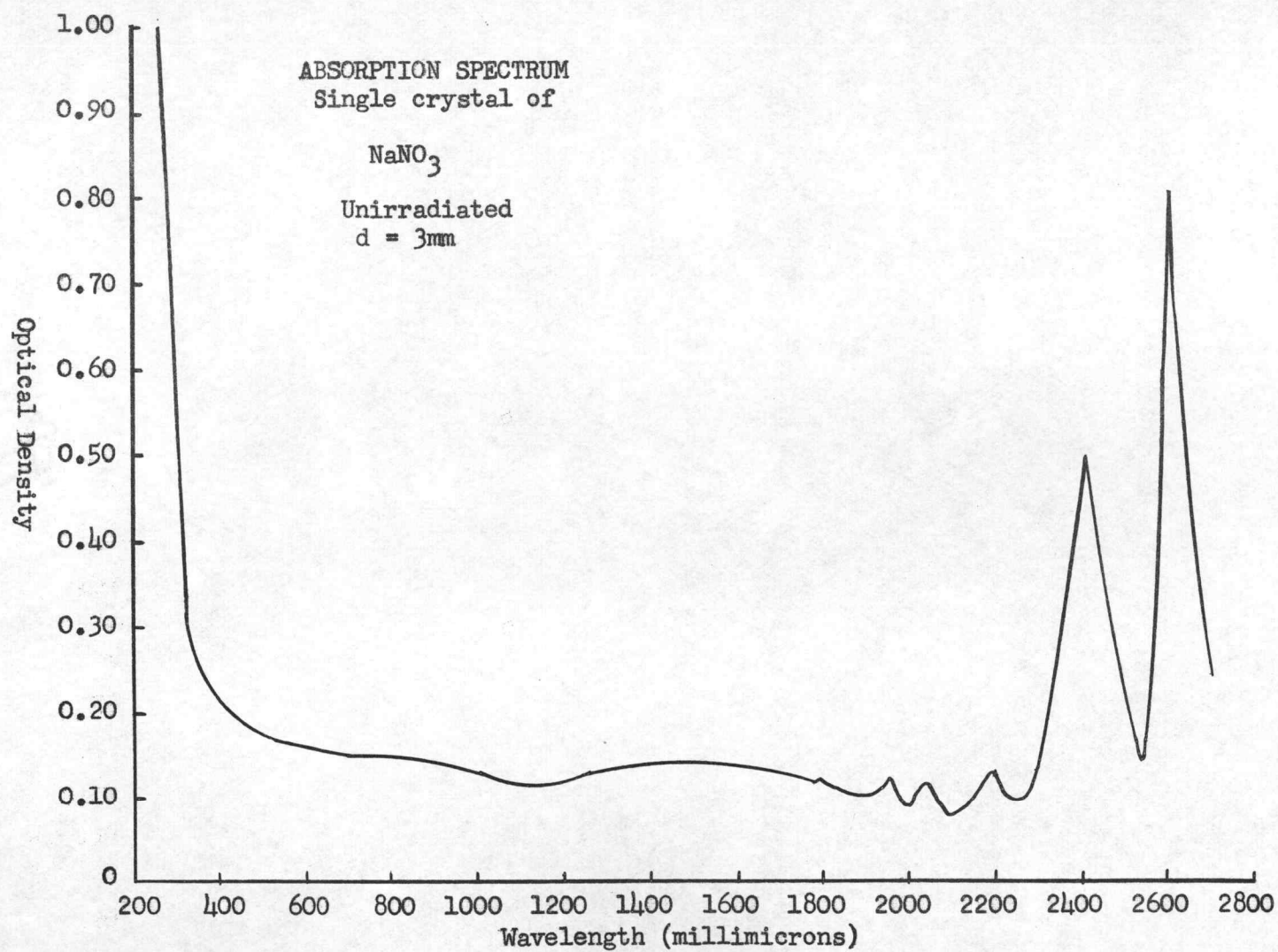


Figure 16

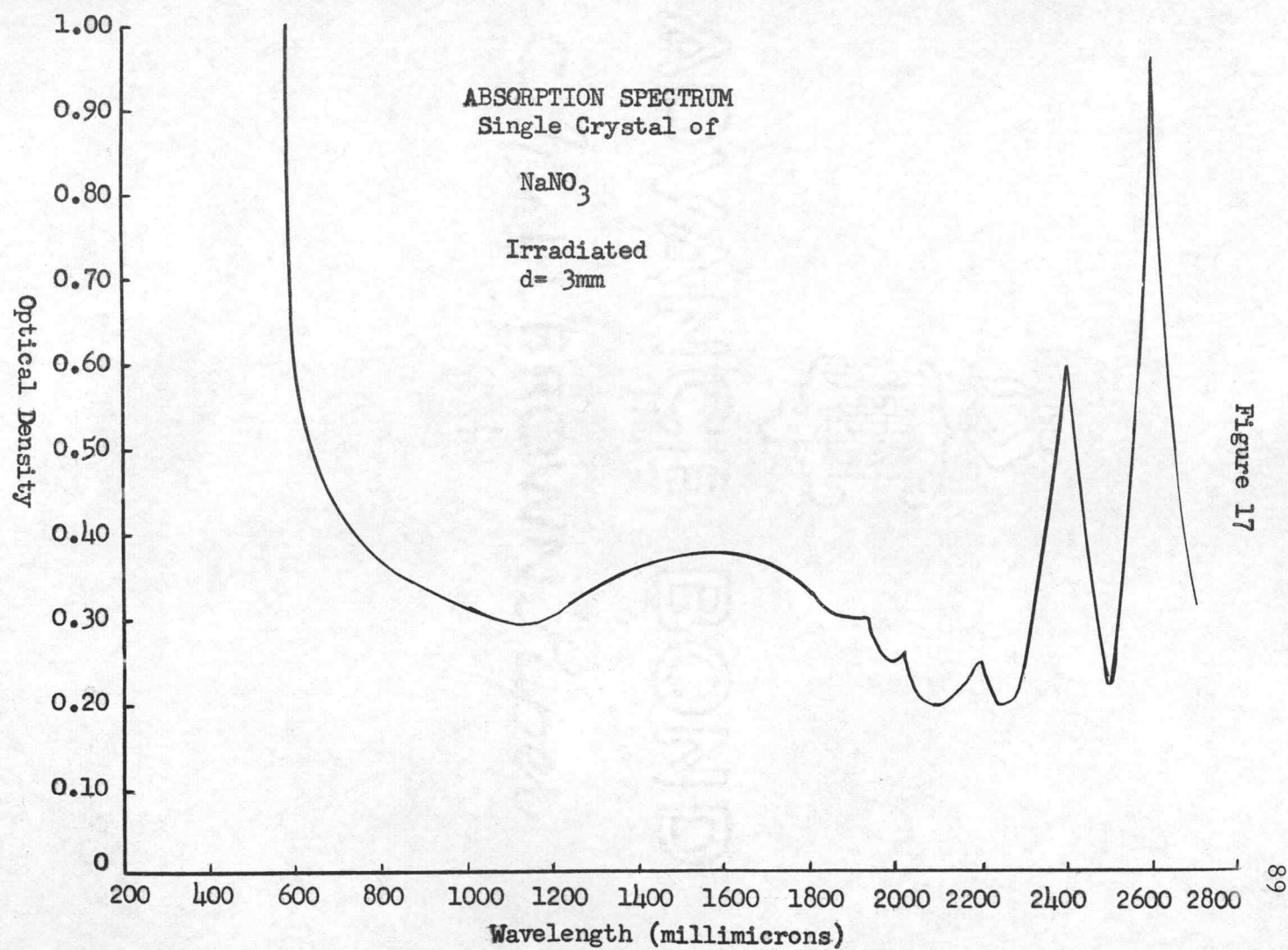
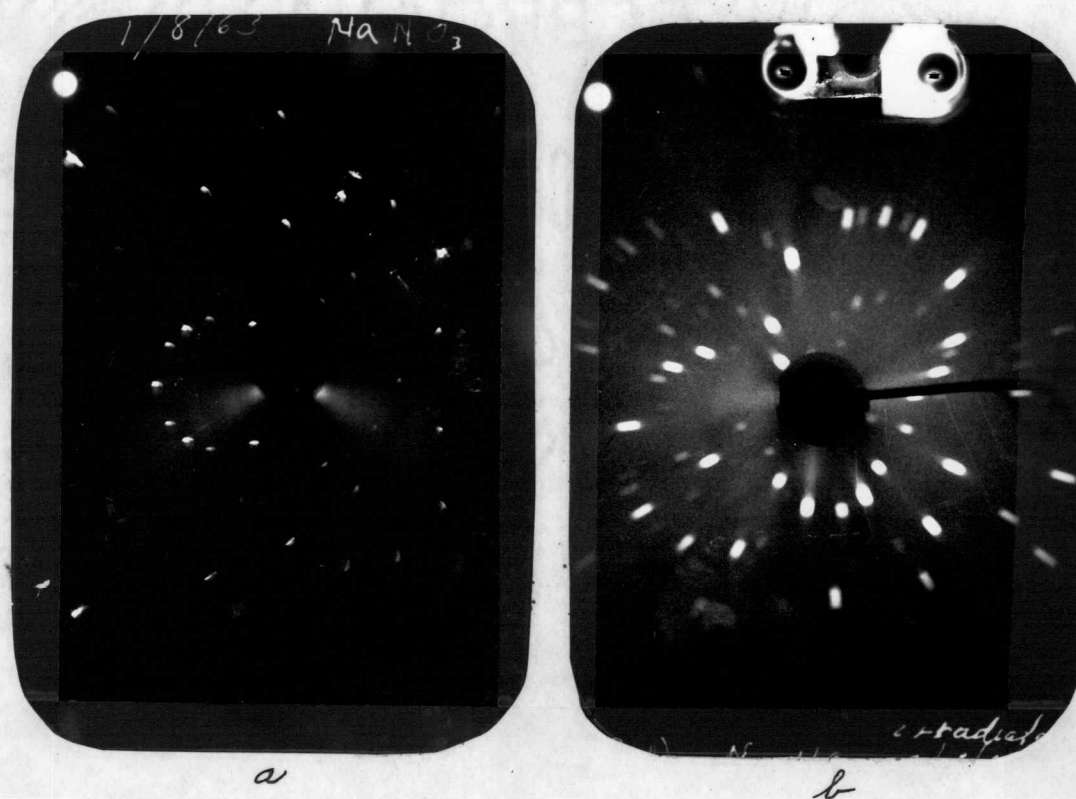


Figure 17



with minor change in configuration. However, the broad low intensity band between 1100 millimicrons and 1900 millimicrons increase in intensity relative to the other absorption bands in that region by approximately a factor of 2. The end absorption in that visible region broadened also, starting at approximately 1000 millimicrons rather than at 600 millimicrons as in the unirradiated specimen. The development of color center based upon absorption measurements could also be observed when the crystal was inspected visually. The crystal had a yellow color after irradiation. As with all of the samples spectrophotometer measurements were recorded under dark room conditions to prevent optical bleaching. Physical inspections were made after they were taken from the dark room and examined under fluorescent light. With the exception of color change no other physical macroscopic changes could be noted from visual inspection. The crystal was then subjected to Laue x-ray transmission photography. Figure 18 shows the Laue x-ray transmission patterns before and after irradiation. A significant change can be seen between the two patterns. As in the case of  $\text{NaClO}_3$  marked asterism has developed in the Laue pattern of the irradiated sample. As mentioned previously, this asterism is evidence of crystal lattice distortion. This pattern and the  $\text{NaClO}_3$  Laue pattern possess the same general characteristics. There is not only an elongation and broadening in the spots but also shows a general disruption of the entire crystal lattice. Higher angle

Figure 18

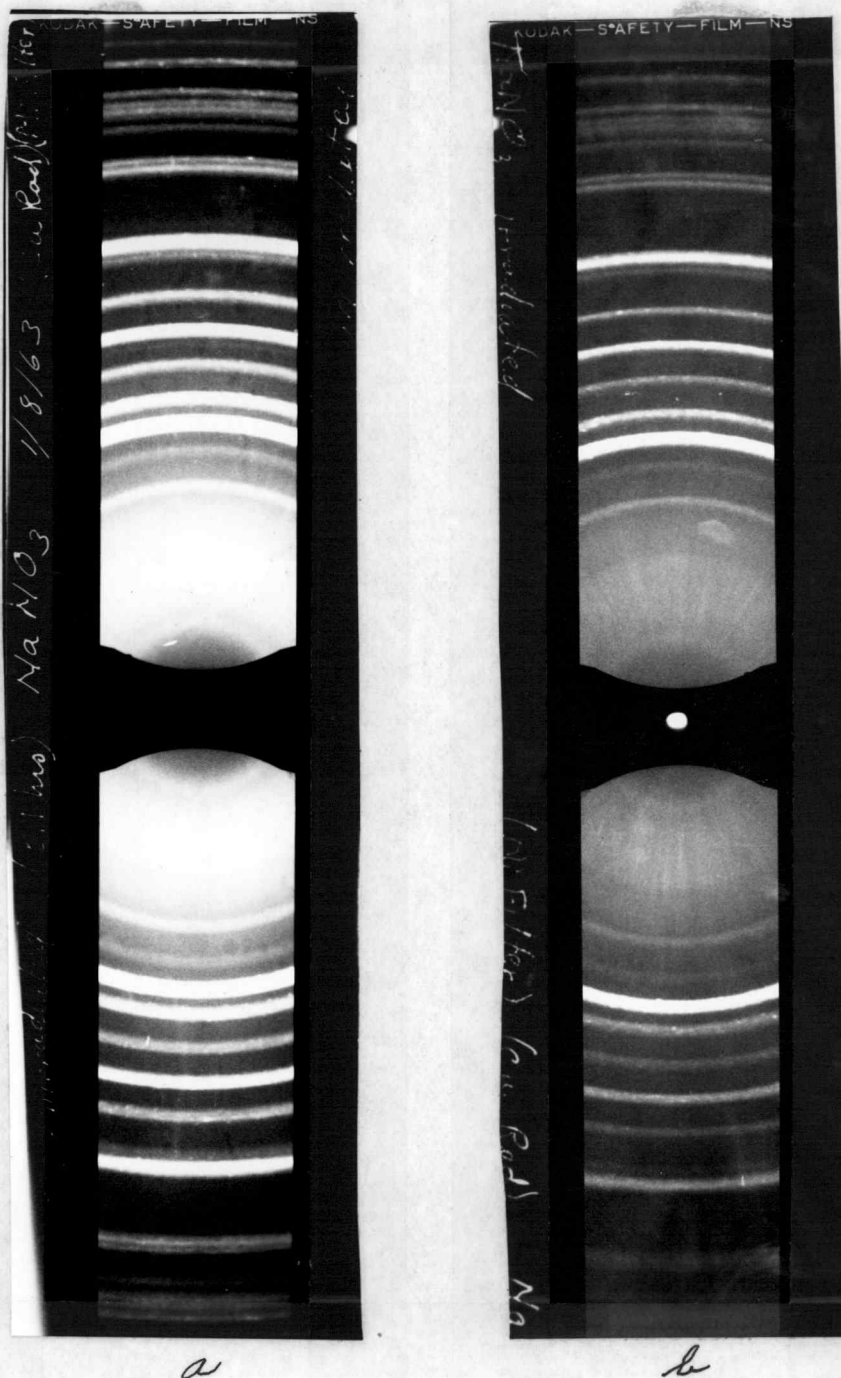


Laue X-Ray Transmission Photograph  
Single Crystal of  $\text{NaNO}_3$

- (a) Unirradiated, and  
(b) Irradiated with  $\text{Co}^{60}$  gamma rays.

reflections have moved to the edge of the photograph and some have disappeared altogether. The low angled inner reflection shows a general broadening with extra reflections becoming visible in this region. These extra reflections are produced by new planar orientation which could be caused by a mosaic or polygonized lattice structure. Vacancies and interstitial could provide the dynamic force for this new crystallographic pattern. However, whatever produced this change must have been widely distributed throughout the crystal. Isolated atomic centers of strain could not adequately explain this change. Unfortunately, x-ray data is not sufficient to determine the precise structural changes which exist in this crystal or the  $\text{NaClO}_3$  previously discussed. Density data, electronic data, electron spin resonance and other new laboratory techniques are needed to supplement this data to provide a more precise evaluation of damage. As before, additional x-ray evidence was gathered to add to the preceding information by taking powder diffraction photographs. The powder specimens before and after irradiation were photographed and are shown in Figure 19, and the data sheet used is shown in Table XI. These patterns provide further substance to the previous evidence which suggest widespread lattice disruption. Although the line positions are identical in both photographs, the line intensities are markedly different. The line intensity in the irradiated sample from the transmitted peaks are less and show a narrower line width. In the back reflection region, the intensity is

Figure 19



### X-Ray Diffraction Powder Pattern of $\text{NaNO}_3$

- (a) Powder sample unirradiated, and
- (b) Same powder sample irradiated with gamma rays.



Table XI

## X-RAY LABORATORY DATA

|  |  |
|--|--|
| Target: Cu                             | Camera: Debye - Scherrer   |
| KV: 35                                 | Specimen: $\text{NaNO}_3$  |
| MA: 18                                 |  |
| Time: 2.1 hrs.                         | Sample Prep: Mortar and pestle<br>crushed powder of $\text{NaNO}_3$ , mixed<br>with Duco cement thinned with<br>acetone. |
| Camera Constant                        | Condition: Unirradiated and<br>irradiated were the<br>same pattern,  |
| Right Zero = 319.70                    | Lattice Type: Hexagonal  |
| Left Zero = 92.70                      |  |
| $r = 227.00$                           | Lattice Parameter  |
| Corrected R = $\frac{224.94}{\pi r}$ R |  |
| = 0.992 R                              |  |

| Relative<br>Intensity | Reading<br>mm | Net<br>R<br>mm | Corrected<br>R<br>mm | Sin $\theta$ | Planar<br>Spacing<br>"d" A. |
|-----------------------|---------------|----------------|----------------------|--------------|-----------------------------|
| VW                    | 103.55        | 10.85          | 10.75                | 0.07463      | 10.3001                     |
| VW                    | 113.50        | 20.80          | 20.60                | 0.14332      | 5.3635                      |
| W                     | 121.10        | 28.40          | 28.20                | 0.19560      | 3.9300                      |
| W                     | 125.85        | 33.15          | 32.80                | 0.22699      | 3.3865                      |
| VS                    | 129.45        | 36.75          | 36.40                | 0.25139      | 3.0578                      |
| S                     | 132.65        | 39.95          | 39.60                | 0.27295      | 2.8163                      |
| M                     | 136.95        | 43.90          | 43.50                | 0.29904      | 2.5706                      |
| S                     | 141.60        | 48.90          | 48.50                | 0.33216      | 2.3142                      |
| M                     | 146.00        | 53.30          | 52.80                | 0.36032      | 2.1334                      |
| VW                    | 151.10        | 58.40          | 57.90                | 0.39330      | 1.9545                      |
| S                     | 152.85        | 60.15          | 59.70                | 0.40482      | 1.8989                      |
| M                     | 162.55        | 69.85          | 69.30                | 0.46515      | 1.6526                      |
| M                     | 163.85        | 71.15          | 74.50                | 0.49697      | 1.5468                      |
| M                     | 169.95        | 77.25          | 76.60                | 0.50964      | 1.5083                      |
| M                     | 170.30        | 77.60          | 76.90                | 0.51144      | 1.5030                      |
| M                     | 171.40        | 78.70          | 78.00                | 0.52220      | 1.4720                      |
| M                     | 172.80        | 80.10          | 79.40                | 0.52636      | 1.4604                      |
| M                     | 176.60        | 83.90          | 83.10                | 0.54815      | 1.4024                      |
| M                     | 179.20        | 86.50          | 85.70                | 0.56324      | 1.3648                      |

significantly reduced to the point of line extinction. This change is indicative of numerous vacancies and interstitials as mentioned previously. All of the evidence to this point implies the same general lattice disorders. Both the  $\text{NaClO}_3$  and  $\text{NaNO}_3$  have provided predictable results of a uniquely similar nature. The reader is also directed to research conducted by Pringsheim (44) on this material.

#### E. Effect of Irradiation on Potassium Ferricyanide

The Potassium Ferricyanide,  $\text{K}_3\text{Fe}(\text{CN})_6$ , is the only crystal which does not enjoy any geometric similarity with any of the other specimens, except that it is essentially an ionic crystal. Figure 20 shows the optical absorption measurements before irradiation. This specimen was red in its natural unirradiated form when observed visually. The absorption spectra shows a narrow high intensity peak at 2375 millimicrons followed by a low intensity but noticeable peak at 2150 millimicrons. The remainder of the spectra assumes a uniform variation up to the end absorption band which starts at approximately 700 millimicrons. Figure 21 shows the optical density as a function of wave length for the same crystal after exposure to gamma irradiation. The specimen had darkened considerably which required thinning it from its original 3 millimeter thickness to 1.25 millimeter before absorption measurements could be recorded. The absorption pattern repeated the high intensity peak at 2375 millimicrons which was noted

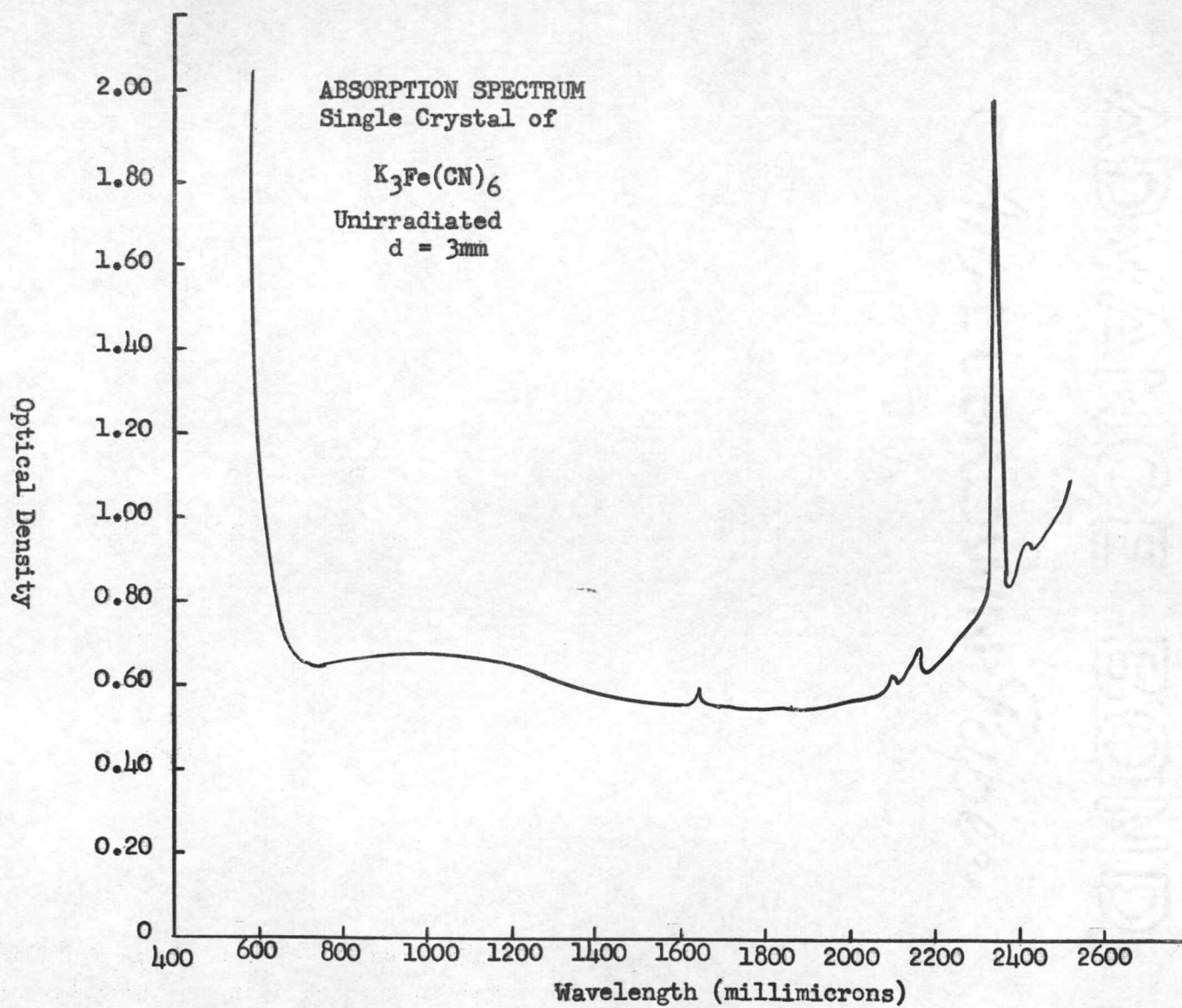


Figure 20

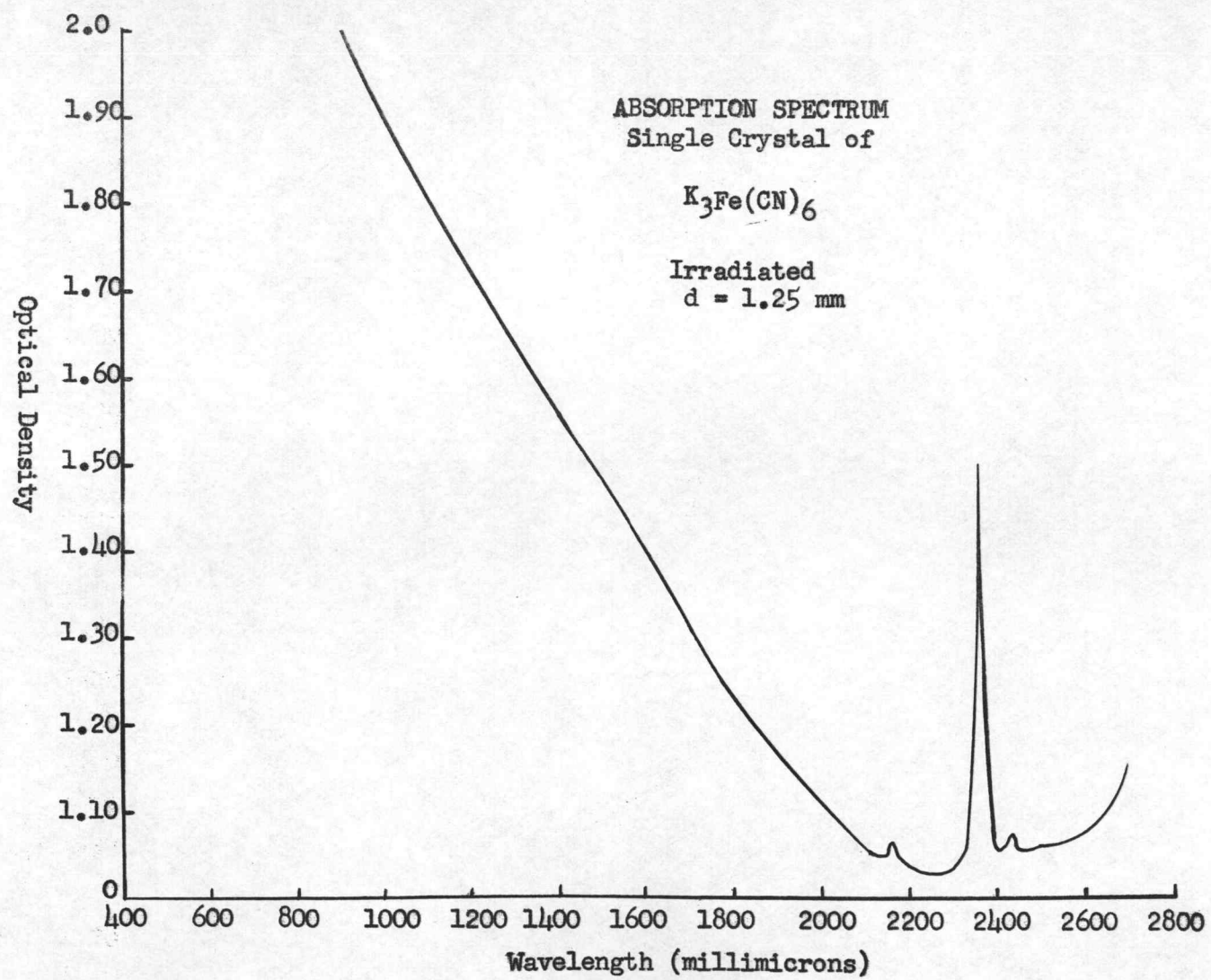


Figure 21

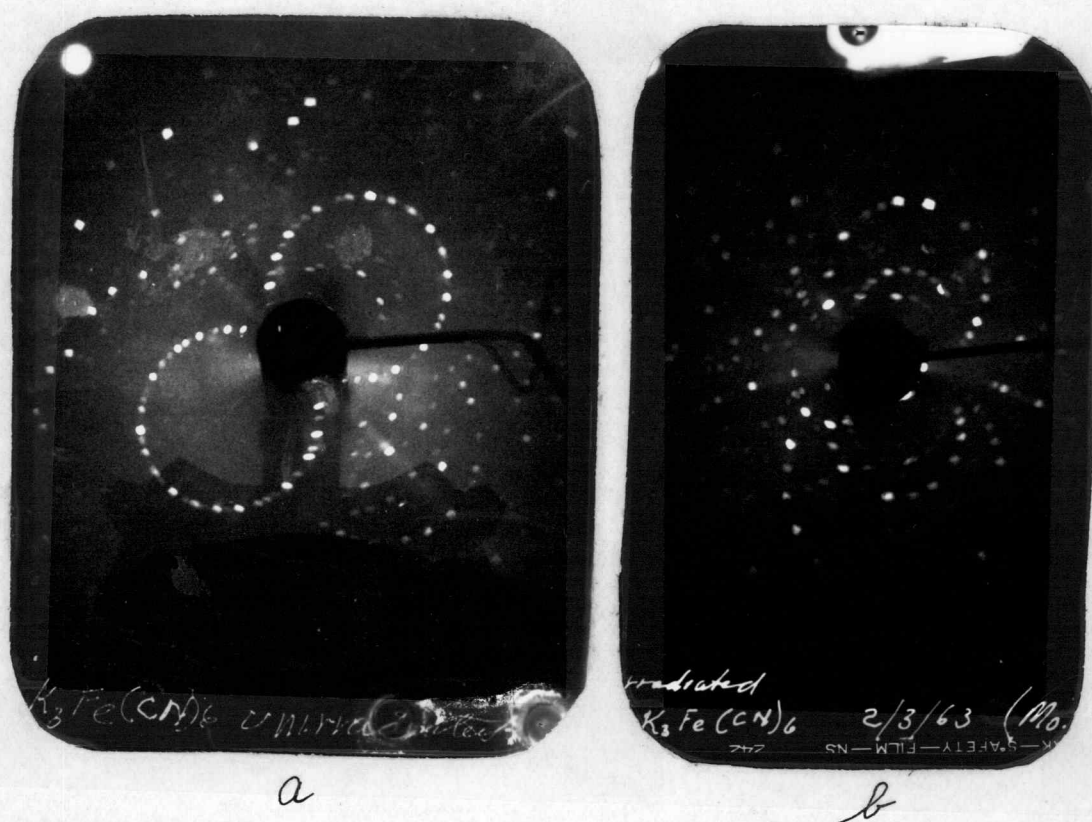


in the unirradiated sample. The small peak at 2150 millimicrons was also reproduced. However, the end absorption band was considerably broadened by starting at approximately 2100 millimicrons. As in the other specimens color center had been developed after exposure to gamma rays. The crystal was examined under normal fluorescent lights. The specimen appears black but otherwise showed no other observable physical changes. Laue x-ray patterns are shown in Figure 22 for the  $K_3Fe(CN)_6$  crystal before and after irradiation. Again, a slight change in crystal orientation relative to the x-ray beam can be recognized, but there is no lattice damage suggested by the irradiated sample pattern. The data in Table XII and the photograph in Figure 23 show no change before or after irradiation. The optical absorption data confirms color centers have been developed. However, the x-ray data does not show the existence or extent of such damage.

#### F. Effect of Irradiation on Potassium Aluminum Sulfate Decahydrate

The last crystal to be discussed is the Potassium Aluminum Sulfate Dodecahydrate,  $KAl(SO_4)_2 \cdot 12H_2O$ . The effects of gamma irradiation on this essentially ionic specimen is both remarkable and unexpected. There was no observable change in the optical absorption measurement, the Laue transmission patterns or the powder diffraction patterns. Additional visual inspection of the crystal showed no change in color, shape or general appearance. The original crystal

Figure 22



Laue X-Ray Transmission Photographs  
Single Crystal of  $K_3Fe(CN)_6$

- (a) Unirradiated, and
- (b) Irradiated with gamma rays from  $Co^{60}$ .

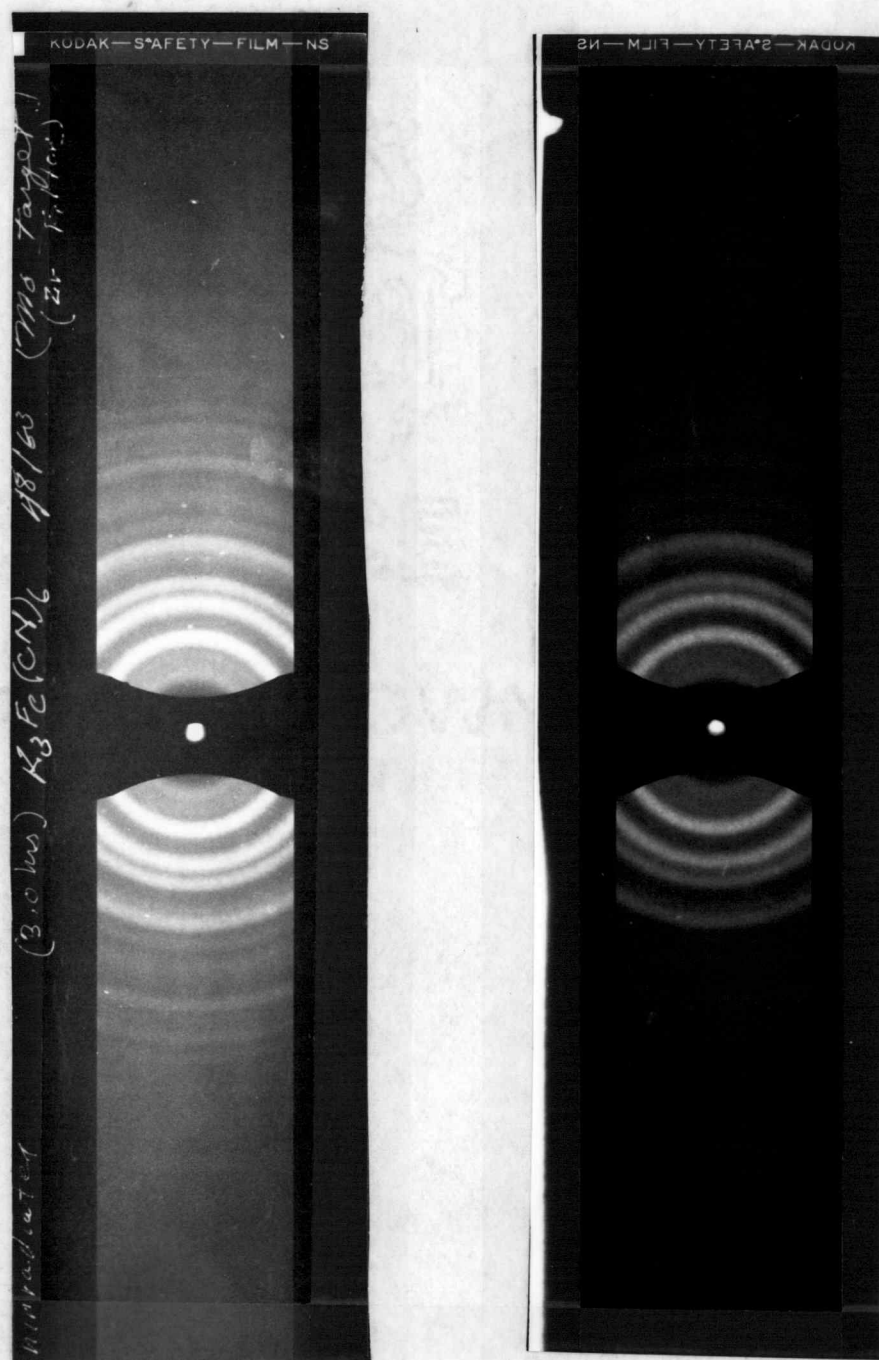
Table XII

## X-RAY LABORATORY DATA

|  |  |
|--|--|
| Target: MO                             | Camera: Debye - Scherrer   |
| KV: 35                                 | Specimen: $K_3Fe(CN)_6$  |
| MA: 18                                 |  |
| Time: 3.0 hrs.                         | Sample Prep: Mortar and pestle<br>crushed powder of $K_3Fe(CN)_6$ ,<br>mixed with Duco cement thinned<br>with acetone. |
| Camera Constant                        | Condition: Unirradiated and<br>irradiated have the same pattern.   |
| Right Zero = 320.15                    |  |
| Left Zero = 93.35                      |  |
| $r = 226.80$                           |  |
| Corrected R = $\frac{224.94}{\pi r}$ R | Lattice Type: monoclinic   |
| = 0.992 R                              | Lattice Parameter  |
|  | $a = 7.04 \text{ \AA.}$  |
|  | $b = 10.44 \text{ \AA.}$   |
|  | $c = 8.40 \text{ \AA.}$  |
|  | $\beta = 107 \frac{1}{2}$  |

| Relative Intensity | Reading mm | Net R mm | Corrected R mm | Sin $\theta$ | Planar Spacing "d" A. |
|--------------------|------------|----------|----------------|--------------|-----------------------|
| M                  | 85.45      | 7.90     | 7.84           | 0.05443      | 6.5019                |
| VS                 | 80.55      | 12.80    | 12.70          | 0.08855      | 3.9966                |
| S                  | 76.00      | 17.35    | 17.20          | 0.11979      | 2.9543                |
| S                  | 73.30      | 20.05    | 19.90          | 0.13848      | 2.5556                |
| S                  | 68.20      | 25.15    | 24.90          | 0.17296      | 2.0461                |
| VW                 | 65.45      | 27.90    | 27.60          | 0.19149      | 1.8481                |
| W                  | 57.90      | 35.45    | 35.20          | 0.24328      | 1.4547                |
| VW                 | 53.00      | 40.35    | 40.00          | 0.27564      | 1.2839                |
| VW                 | 50.50      | 43.85    | 43.50          | 0.29904      | 1.1835                |

Figure 23



Powder Patterns of  $K_3Fe(CN)_6$

- (a) Shows powder sample unirradiated,
- (b) Same powder sample irradiated with  $Co^{60}$  gamma rays.



was a colorless transparent material and the final crystal showed exactly the same properties. This was the only material tested which showed a total absence of any kind of change. Figure 24 shows the optical absorption data before and after irradiation. All features of both curves before and after irradiation were identical. It will be noted that the irradiated absorption curve has a uniformly higher optical density throughout the spectrum. This does not change the relative position of the intensity peaks which are identical for both curves. The components of a spectrophotometer that may affect the results are:

1. the way in which the light strikes the surface being measured,
2. the way in which the reflected light is picked up by the instrument,
3. the wave length sensitivity of the receptor,
4. the absolute sensitive of the receptor, and
5. the physical condition of the surfaces of the specimen.

Regardless of the reason for the shift in the curve, there is no change which is indicative of the production of new absorption peaks or valleys.

Figure 25 shows the Laue patterns, Table XIII is the x-ray powder data, and Figure 26 are powder diffraction photographs. The line positions and intensities in the powder patterns were compared with Frevel (41, p. 81) and showed identical agreement. The most

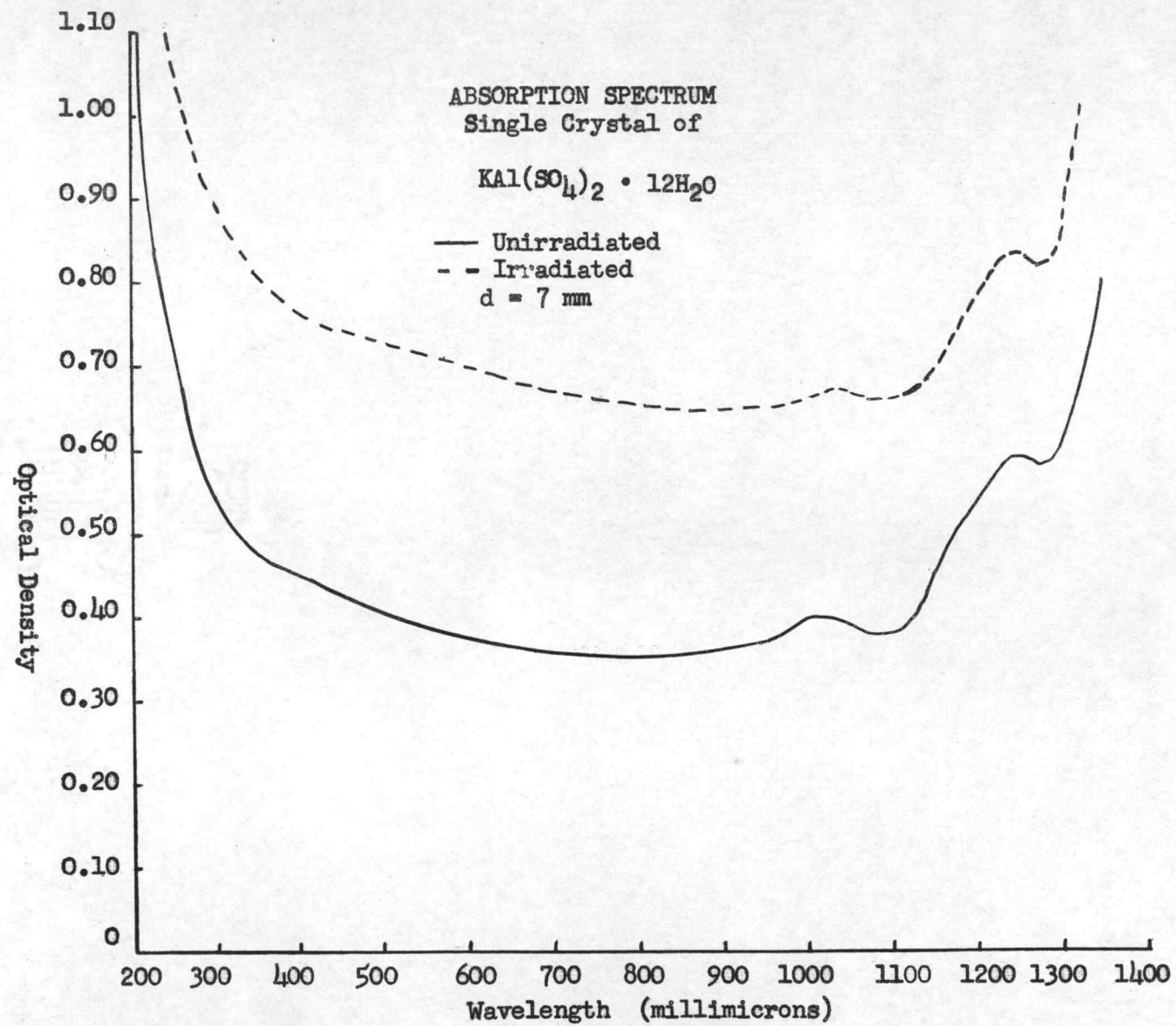
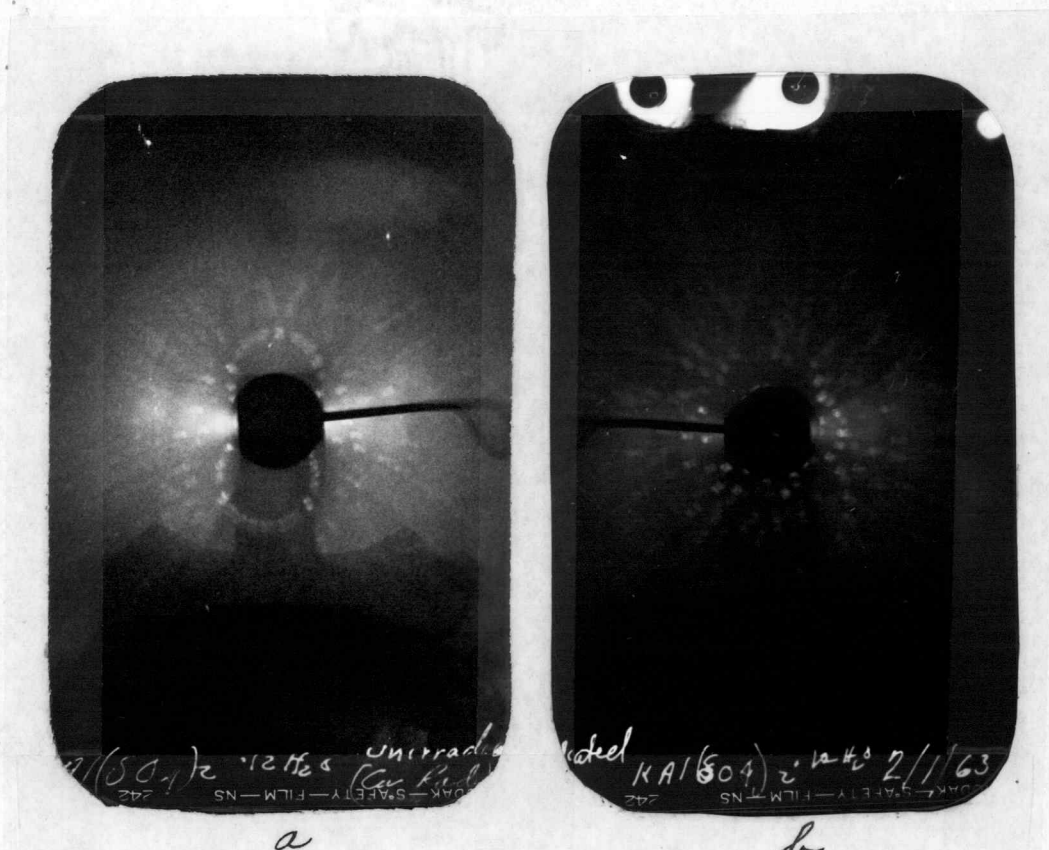


Figure 2h

Figure 25



Laue X-Ray Transmission Photographs  
Single Crystal of  $\text{KAl}(\text{SO}_4)_2 \cdot 12\text{H}_2\text{O}$

- (a) Unirradiated, and  
(b) Irradiated with gamma rays from  $\text{Co}^{60}$ .

Table XIII

## X-RAY LABORATORY DATA

Target: CU

KV: 35

MA: 18

Time: 2.0 hrs.

Camera Constant

Right Zero = 317.35

Left Zero = 90.35

 $r = 227.00$ 

Camera: Debye-Scherrer

Specimen:  $\text{KAl}(\text{SO}_4)_2 \cdot 12\text{H}_2\text{O}$ Sample Prep: Mortar and pestle  
crushed powder of  $\text{KAl}(\text{SO}_4)_2 \cdot 12\text{H}_2\text{O}$ , mixed with Duco

cement thinned with acetone.

Condition: Unirradiated and

irradiated have same pattern.

Corrected R =  $\frac{224.94}{r}$  R $= 0.992$  R

Lattice Type: Cubic

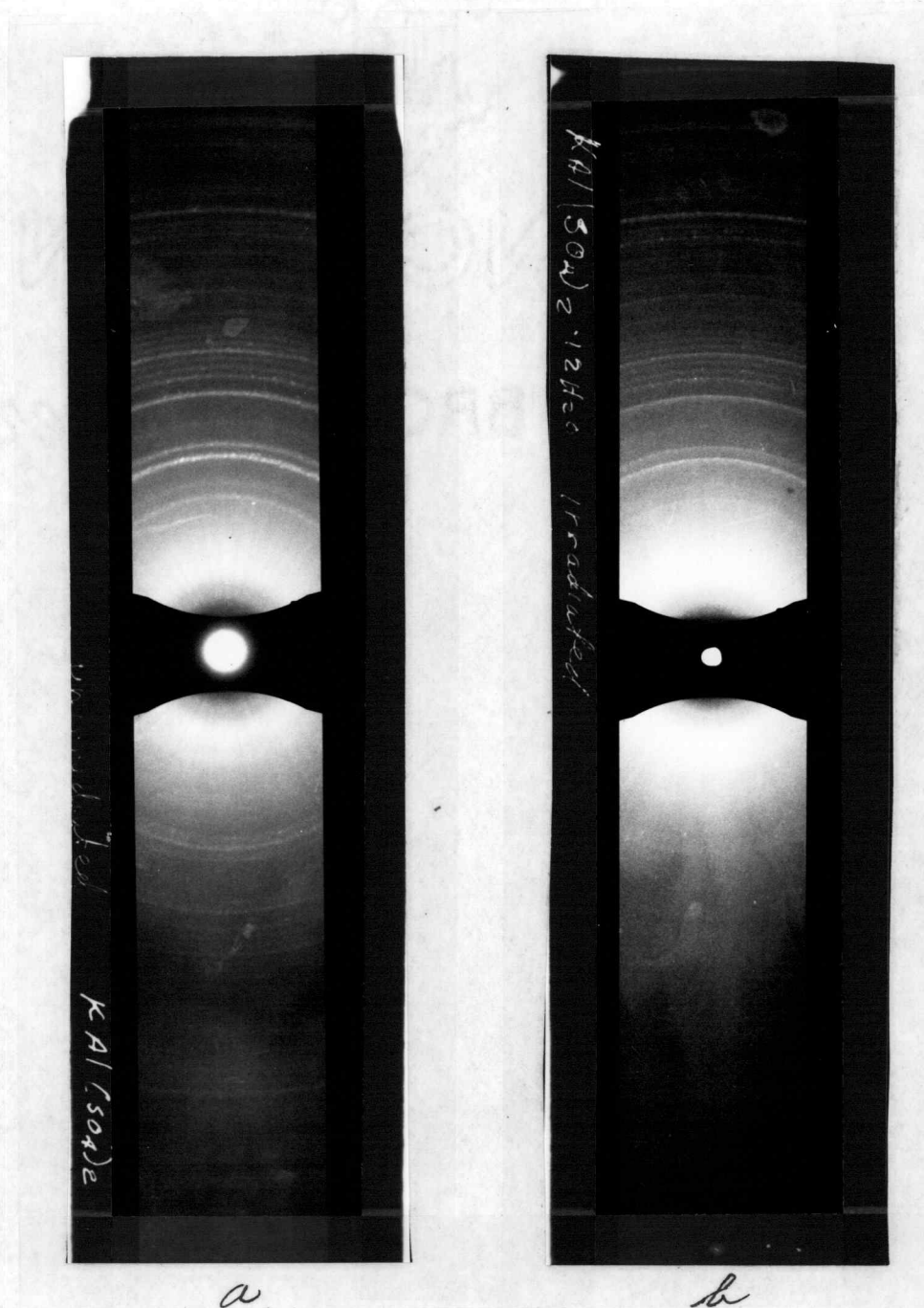
Lattice Parameters

 $a = 12.133$  A.

| Relative<br>Intensity | Reading<br>mm | Net<br>R<br>mm | Corrected<br>R<br>mm | $\sin \theta$ | Planar<br>Spacing<br>"d" A. |
|-----------------------|---------------|----------------|----------------------|---------------|-----------------------------|
| M                     | 69.30         | 2.105          | 20.85                | 0.14470       | 5.3124                      |
| W                     | 67.15         | 23.20          | 23.00                | 0.13988       | 4.8080                      |
| S                     | 63.65         | 26.70          | 27.45                | 0.18327       | 4.2102                      |
| S                     | 61.95         | 28.40          | 28.18                | 0.19492       | 3.9437                      |
| S                     | 55.10         | 35.25          | 34.95                | 0.24124       | 3.1865                      |
| M                     | 52.60         | 37.75          | 37.40                | 0.25814       | 2.9778                      |
| W                     | 51.50         | 38.85          | 38.55                | 0.26556       | 2.8946                      |
| W                     | 50.25         | 40.10          | 39.75                | 0.27362       | 2.8094                      |
| M                     | 49.20         | 41.15          | 40.70                | 0.28100       | 2.7421                      |
| W                     | 48.20         | 42.15          | 41.80                | 0.28769       | 2.6720                      |
| VW                    | 46.95         | 43.40          | 43.00                | 0.29571       | 2.5995                      |
| VW                    | 46.00         | 44.35          | 43.95                | 0.30171       | 2.5479                      |
| VW                    | 44.10         | 46.25          | 45.85                | 0.31432       | 2.4456                      |
| VW                    | 42.25         | 48.19          | 47.65                | 0.32623       | 2.3563                      |
| VW                    | 41.30         | 49.05          | 48.65                | 0.33282       | 2.3097                      |
| VW                    | 39.40         | 50.95          | 50.50                | 0.34530       | 2.2262                      |
| VW                    | 38.40         | 51.95          | 51.50                | 0.35184       | 2.1848                      |
| VW                    | 35.90         | 54.45          | 54.00                | 0.36812       | 2.0882                      |
| VW                    | 33.35         | 57.00          | 56.50                | 0.38430       | 2.0003                      |
| VW                    | 31.90         | 58.45          | 57.50                | 0.39073       | 1.9673                      |
| W                     | 30.15         | 60.20          | 59.70                | 0.40482       | 1.8989                      |
| VVW                   | 28.10         | 62.25          | 61.70                | 0.41755       | 1.8410                      |
| VVW                   | 18.50         | 71.85          | 71.20                | 0.47685       | 1.6120                      |
| VVW                   | 10.25         | 80.10          | 79.40                | 0.52636       | 1.4604                      |
| VVW                   | 7.70          | 82.85          | 81.80                | 0.54053       | 1.4221                      |



Figure 26



Powder Patterns of  $\text{KAl}(\text{SO}_4)_2$

- (a) Shows powder sample unirradiated,
- (b) Same powder sample irradiated with  $\text{Co}^{60}$  gamma rays.

significant result of exposure to gamma irradiation was the totally unexpected absence of change.

The author has searched the literature which reports on the effects of radiation on materials but he could not find a report of any essentially ionic material undamaged by ionizing radiation. There is no explanation for this result offered at this time. Further research is planned on these crystals and this material by the author.

## SECTION VI

### GENERAL SUMMARY

This section will include the conclusions reported in the literature reviewed for this thesis and the experimentation conducted by the author.

It is generally agreed gamma rays cause reproducible and measurable changes in essentially ionically bonded single crystals. Their most significant effect is to cause ionization which releases high energy electrons which in turn produces secondary electronic excitation. Since ionic crystals rely upon electronic forces to maintain structural harmony, the gamma rays disturb their equilibrium and produce lattice defects. These defects are vacancies, interstitials or combinations of them within regions of disorders and trapped particles. As a consequence of these dynamic changes in the lattice

equilibrium electrons become trapped in a variety of crystal defects. These traps cause the optical absorption peaks which absorb light to produce color centers. The optical absorption data presented in this thesis provides further evidence color centers are produced in single crystals of semi-ionic bonding similar to those centers reported in monovalent alkali halides. The single crystal which did not show color center production was  $\text{KAl}(\text{SO}_4)_2 \cdot 12\text{H}_2\text{O}$ . The complete absence of any measureable or observable change in this crystal makes it unique among ionically bonded materials studied thus far. This effect would be expected in metal where the "electron cloud" theoretically anneals ionizing damage. However, this cannot be expected in the alum crystal. The author cannot provide a reasonable explanation for this result; however, further research is intended as stated previously.

In addition to the optical absorption data, another index of gamma irradiation damage in ionic crystals can be measured by electrical conductivity. Only one specimen was checked for ionic conductivity that was the  $\text{NaClO}_3$  crystal. Contrary to report of others, the ionic conductivity increased. It was mentioned earlier in this thesis that ionic conductivity in ionic crystals is directly related to a specific lattice defect, the positive ion vacancy. The results of the Laue x-ray diffraction photograph suggests there were numerous atom displacements and a general warping of the lattice which could be

caused by vacancies and/or interstitials. If these defects shown by the x-ray diffraction photographs were positive ion vacancy then the increase in ionic conductivity is not surprising. On the other hand, this contradicts previous research made by others. This difference of results emphasizes the need for further research on this topic.

For completeness, mention should be made of the other electronic property generally report in literature as a unique property in ionic solids with F centers, namely, photoconductivity. Photoconductivity is related to excitons which increases the photocurrent in ionic crystals which contain F centers. The bleaching of ionic crystals is attributed to the ionization of the F center and is accompanied by photoconductivity. This in essence states that crystal with F centers have photoconducting peaks during irradiation with wave length which are in resonance with the energy of the electron bound in the anion vacancy.

Although no tests were conducted in this project to evaluate the photoconductivity the probability of its behavior similar to the alkali halides is assumed. This could serve as a fruitful area of further investigation to strengthen the theory of similar electron models of the F center configuration.

Based upon the Varley mechanism, one important aspect of his multiple-ionization displacement process suggests the probability of atomic displacement in an ionic lattice by relatively low energy "x" or



gamma radiation. Five of the six specimens used in this research showed evidence of atomic displacement. These atomic displacements create lattice vacancies, interstitials and imperfections as shown by x-ray photographs and the absorption data. The x-ray data presented provides a wealth of information which aided in supporting the current concept of damage in solids. The decomposition of the Rochelle Salt coupled with the change in the powder diffraction pattern support previous reports. All of the other x-ray data pointed to the ionizing, ion displacement, lattice defects and electron trappings proposed by Seitz and Varley. Ionic and ionic-covalent crystal which rely on their ionic features for lattice geometry are highly susceptible to ionizing radiations. The irradiation causes lattice structure changes and also decomposes molecules which cause property changes in the crystal. It has been reported by others (1, 44, 10, 16, 18) that this has occurred in various salts. Based upon these reports, it can be assumed the same event occurred in the specimen reported upon in this research. Again this becomes another area of future inquiry.

The proven sensitivity of ionic crystal to ionizing radiations provides researchers with a convenient material to relate radiation damage to microscopic and macroscopic phenomena in solids.

## BIBLIOGRAPHY

1. Allen, A. O. and J. A. Ghormley. Decomposition of solid barium nitrate by fast electrons. *Journal of Chemical Physics* 15:208-209. 1947.
2. Berman, R., E. L. Foster, and H. M. Rosenberg. The thermal conductivity of irradiated dielectric crystals at low temperatures. In: *Report of the Conference on Defects in Crystalline Solids*, University of Bristol, 1954. London, The Physical Society, 1955. p. 321-327.
3. Billington, Douglas S., and James H. Crawford, Jr. *Radiation damage in solids*. Princeton, New Jersey, Princeton University Press, 1961. 450 p.
4. Borie, B. X-ray diffraction effects of atomic size in alloys. *Acta Crystallographica* 10:89-96. 1957.
5. Buckley, H. E. *Crystal growth*. New York, John Wiley and Sons, 1951. 571 p.
6. Cochran, W. Scattering of x-rays by defect structures. *Acta Crystallographica* 9:259-262. 1956.
7. Cohen, A. J. Anisotropic color centers in alpha quartz. 1. Smoky quartz. *Journal of Chemical Physics* 25:908-914. 1956.
8. Crawford, J. H., Jr., and M. C. Wittels. A review of investigations of radiation effects in covalent and ionic crystals. *Proceedings of the International Conference on the Peaceful Uses of Atomic Energy*, Geneva, 1955. vol. 7. New York, United Nations, 1956. p. 654-665. (Paper No. 753)
9. Cullity, B. D. *Elements of x-ray diffraction*. Reading, Mass., Addison-Wesley Publishing Company, 1956. 514 p.
10. Dienes, G. J. and G. H. Vineyard. *Radiation effects in solids*. New York, Interscience, 1957. 226 p.
11. Delbecq. C. J., B. Smaller and P. H. Yuster. *Physical Review* 104:599-604.

12. Eshelby, J. D. Distortion of a crystal by point imperfections. *Journal of Applied Physics* 25:255-261. 1954.
13. Esterman, I., W. J. Leivo, and O. Stern. *Physical Review* 75:627-633. 1949.
14. Ewald and Herman. *Strukturbericht. Akademische Verlagsgesellschaft. Leipzig* (1916 ff). 6 vols.
15. Griffiths, J. H. E., J. Owen and I. M. Ward. Magnetic resonance in irradiated diamond and quartz. In: *Report of the Conference on Defects in Crystalline Solids, University of Bristol, 1954. London, The Physical Society, 1955. p. 88-91.*
16. Gilliland, J. W., Jr., and H. P. Yockey. Thermoluminescence studies of the gamma ray irradiated ferroelectrics rochelle salt and guanidine aluminum sulfate hexahydrate. *Journal of Physics and Chemistry of Solids* 23:367-374. 1962.
17. Heal, H. G. The chemical effects of ionizing radiation in solids. *Atomic* 6:205-208. 1955.
18. Hennig, G., R. Lees and M. S. Matheson. The decomposition of nitrate crystals by ionizing radiations. *Journal of Chemical Physics* 21:664-668. 1953.
19. Herman, R. C., M. C. Wallis and R. F. Wallis. Intensities of  $R_1$  and  $R_2$  bands in KCl crystals. *Physics Review* 103:87-93. 1956.
20. Holden, Alan and Phyllis Singer. *Crystals and crystal growing. New York, Anchor Books - Doubleday, 1960. 320 p.*
21. Huang, K. X-ray reflections from dilute solid solutions. *Proceedings of the Royal Society (London)* 190A:102-116. 1947.
22. Kaenzig, W. Electron spin resonance of  $V_1$ -centers. *Physical Review* 99:1890-1891. 1955.
23. Kanzaki, H. Point defects in face-centered cubic lattice. 1. Distortions around defects. *Journal of Physics and Chemistry of Solids* 2:24-36. 1957.
24. Kaplan, Irving. *Nuclear physics. Reading, Mass., Addison-Wesley Co, 1955. 609 p.*

25. Kats, A. and J. M. Stevels. The effect of ultraviolet and x-ray radiation on silicate glasses, fused silica and quartz crystals. Philips Research Reports 11:115-156. 1956.
26. Levy, M. and J. H. O. Varley. Radiation induced color centers in fused quartz. Proceedings of the Physical Society (London) 68B:223-233. 1955.
27. Levy, P. W. and G. J. Dienes. Colour centers induced in  $\text{Al}_2\text{O}_3$  by reactor and gamma ray irradiation. Report of the Conference on Defects in crystalline Solids, University of Bristol, 1954. London, The Physical Society, 1955. p. 256-260.
28. Levy, P. W. Reactor and gamma-ray induced coloring in crystalline quartz and corning fused silica. Journal of Chemical Physics. 23:764-765. 1955.
29. Mapother, Dillon. Effect of x-ray irradiation on the self-diffusion coefficient of Na in NaCl. Physical Review 89: 1231-1232. 1953.
30. Mason, Warren P. Piezoelectric crystals and their application to ultrasonics. New York, D. Van Nostrand, 1950. 508 p.
31. Matsubara, T. J. Theory of diffuse scattering of x-rays by local lattice distortions. Journal of the Physical Society of Japan 7:270-274. 1952.
32. McClelland, J. D. and J. J. Donoghue. The effect of neutron bombardment upon the magnetic susceptibility of several pure oxides. Journal of Applied Physics 24:963. 1953.
33. Megaw, Helen D. Ferroelectricity in crystals. London, Methuen, 1957. 220 p.
34. Mitchell, E. W. J. and E. G. S. Paige. On the formation of color centers in quartz. Proceedings of the Physical Society (London) 67B:262-264. 1954.
35. Mitchell, E. W. J. and E. G. S. Paige. The anisotropic absorption of the visible bands in irradiated gamma quartz. Philosophical Magazine 46:1353-1361. 1955.



36. Mitchell, E. W. J. and E. G. S. Paige. The optical effect of radiation induced atomic damage in quartz. *Philosophical Magazine* 1:1085-1115. 1956.
37. National Aeronautics and Space Administration Technical Note D-1523. Optical properties of satellite materials -- The theory of optical and infrared properties of metals. Washington, NASA, March 1963. 253 p.
38. Nelson, C. M., R. L. Sproull, and R. S. Caswell. Conductivity changes in KCl produced by gamma and neutron irradiation. *Physical Review* 90:364. 1953.
39. O'Brien, M. C. M. The structure of the color centers in smoky quartz. *Proceedings of the Royal Society (London)* 231A:404-414. 1955.
40. O'Brien, M. C. M. and M. H. L. Pryce. Paramagnetic resonance in irradiated diamond and quartz: Interpretation. In: *Report of the Conference on Defects in Crystalline Solids*, University of Bristol, 1954. London, The Physical Society, 1955. p. 88-91.
41. Parrish, W., M. G. Ekstein, and B. W. Irwin. Data for x-ray analysis. New York, Philips Technical Library, 1953. 81 p.
42. Primak, W. Gamma-ray dosage in inhomogeneous nuclear reactors. *Journal of Applied Physics* 27:54-62. 1956.
43. Primak, W., L. H. Fuchs, and P. Day. Radiation damage in insulators. *Physical Review* 92:1064-1065. 1953.
44. Pringsheim, P. Absorption spectrum of  $\text{NaNO}_3$  exposed to ionizing radiation. *Journal of Chemical Physics* 23:369-375. 1955.
45. Richtmyer, F. K. and E. H. Kennard. *Introduction to modern physics*. 4th ed. New York, McGraw-Hill, 1947. 759 p.
46. Rosenwasser, Hyman, Russell W. Dreyfuss and Paul W. Levy. Radiation induced coloring of sodium azide. *Journal of Chemical Physics* 24:184-190. 1956.
47. Scott, Allen B., William A. Smith and Mihon A. Thompson. Alkali halides colored by colloidal metal. *Journal of Physical Chemistry* 57:757-761. 1953.

48. Scott, Allen B., and Lamar P. Bupp. The equilibrium between F-center and higher aggregates in CKl. *Physical Review* 79:341-346. 1950.
49. Seitz, Frederick. *The modern theory of solids*. New York, McGraw-Hill, 1940. 698 p.
50. Seitz, Frederick. Color centers in alkali halide crystals. *Reviews of Modern Physics* 18:384-408. 1946.
51. Seitz, Frederick. Color centers in alkali halide crystals 2. *Reviews of Modern Physics* 26:7-94. 1954.
52. Seitz, Frederick and David Turnbull. *Solid state physics*. vol. 10. New York, Academic Press, 1960. 516 p.
53. Simmons, R. and R. Balluffi. X-ray study of deuteron irradiated copper at 12°K. *Bulletin of the American Physical Society* 2:151. 1957.
54. Smoluchowski, R. Effect of nuclear irradiation on ionic crystals. *Proceedings of the International Conference on the Peaceful Uses of Atomic Energy*, Geneva, 1955. vol. 7. New York, United Nations, 1956. p. 676-681. (Paper No. 748).
55. Stevels, J. M. and A. Kats. The systematics of imperfections in silicon-oxygen networks. *Philips Research Reports* 2:103-114. 1956.
56. Stevels, J. M. and A. Katz. The effect of ultraviolet and x-ray radiation on silicate glasses, fused silica and quartz crystals. *Philips Research Reports* 2:115-156. 1956.
57. Theisen, Floyd E. and Allen B. Scott. Rate of coagulations of F-center in KCl. *Journal of Chemical Physics* 20:529. 1952.
58. Tucker, C. W. and P. Senio. X-ray scattering effects due to localized static lattice defects. *Physical Review* 99:1777-1780. 1955.
59. Varley, J. H. O. A mechanism for the displacement of ions in an ionic lattice. *Nature* 174:886-887. 1954.
60. Varley, J. H. O. A new interpretation of radiation-induced phenomena in alkali halides. *Journal of Nuclear Energy* 1:130-143. 1954.

61. Weeks, R. A. Paramagnetic resonance of lattice defects in irradiated quartz. *Journal of Applied Physics* 27:1376-1381. 1956.
62. Wilson, A. J. C. (ed). *Structure Reports for 1942-1944.* vol. 9. Utrecht, Netherlands, International Union of Crystallography, 1955. 448 p.
63. Wyckoff, Ralph W. G. *The structure of crystals.* 2d ed. New York, Reinhold, 1935. 240 p.
64. Wyckoff, Ralph W. G. *Crystal structures.* New York, Interscience, 1960. 5 vols.